

**Applications of Multi Sensor Satellite Data and Generalized
Additive Model (GAM) for Open Ocean Tuna Habitat and
Precipitation Studies**

(複数センサ多時期衛星データおよび GAM を用いたリモートセンシング
のマグロ生態系解明および降雨予測問題への適用)

平成 27 年 9 月

山口大学大学院 理工学研究科

Martwi Diah Setiawati

博士論文

Applications of Multi Sensor Satellite Data and Generalized Additive Model (GAM) for Open Ocean Tuna Habitat and Precipitation Studies

(複数センサ多時期衛星データおよび GAM を用いたリモートセンシング
のマグロ生態系解明および降雨予測問題への適用)

Martiw Diah Setiawati

Department of Environmental Science and Engineering

Graduate School of Science and Engineering

Yamaguchi University

September 2015

A dissertation submitted in partial fulfillment of the requirements
for the degree of Doctor of Engineering

Committee members:

Prof. Fusanori Miura (supervisor)

Prof. Hideaki Nakamura

Prof. Masahiko Sekine

Prof. Tasuku Tanaka

Prof. Koji Asai

Assoc.Prof. Koichi Yamamoto

SUMMARY

Integration of time series data, multi sensor analysis and statistical models are important for accurate mapping for open ocean tuna habitat and precipitation studies. In this study, habitat characteristics of bigeye tuna were investigated as a representative for open ocean tuna habitat studies and validation and correction of Global Satellite Mapping Precipitation (GSMaP) were performed as representative for precipitation studies. Tuna habitat is an important issue to study because global tuna catches have increased steadily from a half million tonnes in 1950 to almost 4 million tonnes in 1999. In addition, validation and correction of GSMaP is necessary to study because GSMaP precipitation amount generally has been underestimated and it will cause high bias for flood forecasting. Historical data of open ocean tuna habitat and precipitation studies were derived by open access multi sensor satellite remote sensing data and were conducted in the two study areas: Southern Waters off Java-Bali in Indonesia for open ocean habitat studies and Kyushu Island in Japan for precipitation studies.

The aims of this research are to introduce the simple method to analyze the relationship between bigeye tuna and environmental variable by using linear regression, to introduce Generalized Additive Model (GAM) for dealing with nonlinear data, to determine the best model for bigeye tuna habitat in the study area, to evaluate the ability of GSMaP data as satellite precipitation during rainy season and to reduce the bias of GSMaP product during heavy rainfall.

This study was divided into two main parts. First is the introduction and explanation of the analysis method, and second is the application of multi-sensor satellite data for open ocean tuna habitat and precipitation studies. In the first application for open ocean tuna habitat studies, scatterplot smoother method was used to analyze a relationship between environmental variables and fisheries data. Then, simple predicted map can be determined.

The second application, GAM was conducted to measure the relationship between environmental variables and fisheries data and then to build the habitat suitability index.

In the first application for open ocean tuna habitat studies, satellite remote sensing data of sea surface temperature (SST), sea surface chlorophyll (SSC) and sea surface height deviation (SSHD) as environmental data variables and daily fish catch data from PT Perikanan Nusantara, Bali during 2006-2010 were used. To determine the relationship between environmental variables and bigeye tuna, scatterplot smoother were conducted. The results clearly showed that SST, SSC, SSHD which derived from satellite observation, confirmed a strong relationship with the abundance of bigeye tuna. However, the parameters which give the dominant effect bigeye tuna cannot be distinguished.

In the second application, GAM as the recent development of regression model was applied. By GAM, the data did not force to be linear and parameters which give the dominant effect bigeye tuna can be distinguished. In this study, seven models were constructed from the simplest form by using only one independent variable (i.e., SST, SSC, SSHD) and combination of all the variables (i.e., SST+SSC, SST+SSHD, SSC+SSHD and SST+SSC+SSHD). Then, GAM and geographic information system (GIS) method were combined to determine the spatial distribution of bigeye tuna habitat. The results showed that SST was the most important habitat predictor for bigeye tuna migration in the Southern Waters off Java and Bali, followed by SSHD and SSC. The spatial pattern of bigeye tuna habitat characteristic gave typical low SST, negative to low SSHD and extreme value of SSHD and low to moderate SSC.

For precipitation studies, we evaluated and corrected GSMaP_MVK at daily time scales with a spatial resolution of 0.1° latitude/longitude. The reference data came from thirty four rain gauges over Kyushu Island, Japan. This study focused on the GSMaP_MVK ability to detect heavy rainfall pattern that may lead to flooding. Statistical analysis was used

to evaluate the GSMaP_MVK data both quantitative and qualitative. The statistical analysis included the relative bias (B), the mean error (E), the Nash-Sutcliffe (C_{NS}), the Root Mean Square Error (RMSE) and the correlation coefficient (r). In addition, GAM was conducted for GSMaP_MVK data correction. The results of these analyses indicate that GSMaP_MVK data have lower values than observed data and have serious underestimate during heavy rainfall. By applying GAM for bias correction, GSMaP_MVK ability was improved to detect heavy rainfall. In addition, GAM for bias correction is well applied for serious underestimate of GSMaP_MVK (i.e., bias more than 55%). Thus, GAM is a promising way to predict the rainfall amount for flood and landslide monitoring, especially in the area where rain gauge data are limited.

The advantage of this research is all the satellite remote sensing data which we used are open access and it can be applied in the developing countries. For the future research for tuna habitat, developing a method which measures the interaction of predictor variables to the fish catch data is necessary to develop. In precipitation studies, correction of GSMaP_MVK data product is the first step to make a model for flood prediction map more accurate.

TABLE OF CONTENT

SUMMARY	4
CHAPTER 1. INTRODUCTION	14
1.1 Background	14
1.2 Research Motivation.....	16
1.3 Research Problem	17
1.4 Research Scope and Objective.....	17
1.5 Research Outline.....	18
1.6 Overview of the study area	21
1.6.1 Southern waters off Java-Bali, Indonesia	21
1.6.2 Kyushu island, Japan	23
CHAPTER 2. ANALYSIS METHODS	25
2.1 Multi sensor of satellite remote sensing.....	25
2.2 Multi sensor images for Open Ocean Tuna habitat studies.....	27
2.2.1 Open Ocean Ecosystem	27
2.2.2 Bigeye Tuna Characteristics.....	28
2.2.3 Satellite Remote Sensing Characteristics for Bigeye tuna Habitat	30
2.3 Multi sensor images for precipitation studies	34
2.3.1 Global Satellite Mapping Precipitation (GSMaP).....	35
2.4 Generalized Additive Model (GAMs).....	39
2.4.1 A framework for use of statistical models.....	39
2.4.2 GAM	39
CHAPTER 3. APPLICATION FOR OPEN OCEAN TUNA HABITAT 1	43
Utilization of Scatterplot smoothers to Understand the Link Between Bigeye Tuna Catches And Remote Sensing Environmental Data in The Southern Waters Off Java–Bali.....	43

3.1 Introduction.....	43
3.2 Study area.....	45
3.3 Materials and Methods.....	46
3.3.1 Fisheries data and remotely sensed environmental data.....	46
3.3.2 Classification of fisheries data.....	48
3.3.3 Scatterplot Smoothers.....	49
3.3.4 Generating the optimum range of environmental variables.....	51
3.3.4 Generating a simple predicted map.....	52
3.4 Results.....	52
3.4.1. Distribution of number of bigeye tuna caught and environmental data.....	49
3.4.2 Classification of fisheries data.....	54
3.4.3 Scatterplot smoothers.....	56
3.4.4 Relationship between environmental factors and bigeye tuna caught.....	58
3.5 Relationship between ocean dynamics and preferred habitat for bigeye tuna.....	64
3.6 Conclusions.....	66
CHAPTER 4. APPLICATION FOR OPEN OCEAN TUNA HABITAT 2	68
Characterization of Bigeye Tuna Habitat in the Southern Waters Off Java-Bali Using Remote Sensing Data	68
4.1 Introduction.....	68
4.2 Materials and Methods.....	69
4.2.1 Study Area.....	69
4.2.2 Fisheries data and classification.....	71
4.2.3 Remote sensing data.....	71
4.2.4. Application of Generalized Additive Model (GAM).....	71
4.2.5 Habitat Suitability Index.....	76
4.3 Results.....	77
4.3.1 Analysis of habitat characteristics for bigeye tuna by using GAM.....	77
4.3.2 Model validation and bigeye tuna habitat prediction.....	79

4.4 Discussion	81
4.5 Conclusions	90
CHAPTER 5. APPLICATION FOR PRECIPITATION STUDIES	91
Evaluation and Bias Correction of GSMaP Daily Rainfall Satellite Data for Flood Monitoring In Kyushu Island, Japan by Generalized Additive Model Approach	91
5.1 Introduction	91
5.2 Materials and Methods	93
5.2.1 Study Area	93
5.2.2 Rain Gauge Data	94
5.2.3 GSMaP Data	95
5.2.4 Validation and Intercomparison	96
5.2.5 Determining a bias correction by power function	99
5.2.6 Determining a bias correction by Generalized Additive Models (GAM)	99
5.3 Results and Discussion	100
5.3.1 General comparison of daily rain gauges with GSMaP_MVK data	100
5.3.2 Validation and correction of GSMaP_MVK in the highland and lowland	102
5.3.3 Validation and correction of GSMaP_MVK in the eastern part and western part of Kyushu	105
5.3.4 Validation and Correction of GSMaP MVK during rainy days	108
5.3.5 Validation and Correction of GSMaP MVK during heavy rainfall	109
5.4 Conclusions	112
CHAPTER 6. CONCLUSIONS	114
ACKNOWLEDGEMENT	116
REFERENCES	117

LIST OF FIGURES

Figure 1.1 Outline of the dissertation	20
Figure 1. 2 (A) Map of the Indonesian seas, with the inset box representing the study area. (B) Map of the study area in the eastern Indian Ocean (EIO) off Java (Syamsudin et al., 2013).	22
Figure 1.3 Map of Kyushu Island.....	23
Figure 2.1 Data collection by remote sensing (Joseph, 2005).....	25
Figure 2.2 An Example of multi sensor analysis which distinguishes habitat suitability index (Mugo et al., 2011)	26
Figure 2.3 Food web in open ocean (www.studyblue.com)	28
Figure 2.4 Tuna fishing methods (WWF, 2014)	29
Figure 2.5 The electromagnetic spectrum (https://engineering.purdue.edu).....	31
Figure 2.6 How altimetry measures SSHD (http://www.aviso.altimetry.fr)	33
Figure 2.7 Flow chart of the GSMaP algorithm (Ushio et al., 2009)	36
Figure 2.8 Schematic illustration combining the precipitation field forward and backward in time. The white belts denote the coverage of the microwave sensor.	37
Figure 3.1 Study area	45
Figure 3.2 The relation between number of tuna and hook rate	47
Figure 3.3 Data illustration	50
Figure 3.4 Histograms of number of bigeye tuna and environmental data: (a) distribution of number of bigeye tuna, (b) distribution of log-transformed number of bigeye tuna, (c) SST, (d) SSC, (e) SSHD.	53
Figure 3.5 Frequency of fishing days in relation to (a) SST, (b) SSC, (c) SSHD and (d) month from 2006 to 2010. They were grouped according to the way used by Andrade and Garcia (1999).....	55

Figure 3.6	Number of bigeye tuna in relation to SST during 2006-2010.....	56
Figure 3.7	Number of bigeye tuna in relation to SSC during 2006-2010	57
Figure 3.8	Number of bigeye tuna in relation to SSHD during 2006-2010	57
Figure 3.9	Average number of bigeye tuna SST from 2006-2010.....	58
Figure 3.10	Average number of bigeye tuna in relation to SSC from 2006-2010.....	59
Figure 3.11	Average number of bigeye tuna in relation to SSHD from 2006-2010.....	60
Figure 3.12	Empirical cumulative distribution frequencies for (a) SST, (b) SSC and (c) SSHD as weighted by bigeye tuna catch during the period of 2006-2010.....	62
Figure 3.13	Spatial distribution of longline fisheries in July from 2006 to 2010 overlaid with simple prediction map generated from combination of SST, SSC and SSHD	63
Figure 4.1	The study area in the Southern Waters off Java-Bali. This area has been passed by five dominant waves and current systems, namely, South Java Current (SJC), Indonesia Through Flow (ITF), Indian Ocean Kelvin Waves (IOKW), Rossby Waves (RW), and the Indian Ocean South Equatorial Current (SEC). (Modified from Syamsudin et al., 2013)	70
Figure 4.2	Effect of three oceanographic variables on the number of bigeye tuna (a) SST, (b) SSC and (c) SSHD. Tick marks at abscissa axis represent the observed data points. Full line is the GAMs function. Dashed dot lines indicate the 95% confidence level.	79
Figure 4.3	(a) A Scatter plot between the average observed values and GAM model predicted ones. (b) A Scatter plot between all ranges observed values and GAM model predicted ones.	80
Figure 4.4	Habitat suitability index for bigeye tuna from January to December 2009 overlaid with bigeye tuna fishing location (continue to the next page).....	83

Figure 4.4 Habitat suitability index for bigeye tuna from January to December 2009 overlaid with bigeye tuna fishing location (from the previous page)	84
Figure 4.5 The spatial distribution of SSC and bigeye tuna catches in Southern Waters off Java-Bali in 2009 (continue to the next page).....	88
Figure 4.5 The spatial distribution of SSC and bigeye tuna catches in Southern Waters off Java-Bali in 2009 (from the previous page)	89
Figure 5.1 The study area, Kyushu Island, and its topography. Black triangle indicates the rain gauge locations	94
Figure 5.2 Scatter plot of daily rain gauge data versus GSMaP_MVK product during rainy season from 2005 to 2007.....	101
Figure 5.3 Long term mean of daily rainfall measured by AMEDAS and GSMaP_MVK for three years during rainy season. Daily rainfall is spatially averaged over 34 rain gauges.	102
Figure 5.4 Comparison of the performance GSMaP_MVK in the highland (a), lowland (b), corrected highland (c), corrected lowland (d)	104
Figure 5.5 Smoothing function of GSMaP_MVK	105
Figure 5.6 The wind direction of southern part of Japan in June 2006 (source: ASCAT, 2014).....	107
Figure 5.7 Comparison of the performance GSMaP_MVK in the Eastern part (a), western part (b), corrected Eastern part (c), corrected western part (d)	108
Figure 5.8 The performance of GSMaP_MVK during rainy days (a), corrected by GAM (b)	109
Figure 5.9 Heavy rainfall measurement by AMEDAS, GSMaP and corrected by GAM for three years.....	111
Figure 5.10 Extreme rainfall, which caused flood in Miyazaki 2006 (a), Kagoshima 2006 (b), Kumamoto 2006 (c), Kumamoto 2007 (d)	112

LIST OF TABLES

Table 1.1 Climatological (1961-1990) annual precipitation totals and percentage of precipitation during each season for four stations on Kyushu Island (Uvo et al., 2001).....	24
Table 2.1 Coefficient for SST MODIS band 31 and 32 (Brown and Minnet., 1999).....	32
Table 2.2 Characteristic of microwave radiometer of GSMaP data product35_Toc427146772	
Table 3.1 The full matrix of high catches data	48
Table 4.1 Data structure of environmental variables and fish catch	72
Table 4.2 Iteration process.....	74
Table 4.3 GAM models used in this study and obtained values for P-value, percent DE, AIC value, and DF, respectively (N=7751).	76
Table 5.1 Contingency table of yes or no events/ with rain or no rain.	98
Table 5.2 Validation statistics of daily GSMaP_MVK product during rainy season from 2005 to 2007.....	102
Table 5.3 Validation statistics over the highland and lowland before and after corrected by GAM.....	104
Table 5.4 Validation statistics over the eastern part and western part part before and after corrected by GAM	107
Table 5.5 Validation statistics during rainy days	109
Table 5.6 Validation statistics during heavy rainfall.....	111

CHAPTER 1

INTRODUCTION

1.1 Background

Remote sensing offers the ability to observe and collect data for large areas relatively quickly, and is an important source of improving natural resources management, land use and protection of the environment. In this study, open ocean tuna habitat and precipitation were concerned for remote sensing application because open ocean is the largest area of marine ecosystem which is the main resources for human being and precipitation plays a primary role in the global water and energy cycle. Integration of time series data, multi sensor analysis and statistical models are important for accurate mapping for open ocean tuna habitat and precipitation studies. One of the common situations we deal with in ecological data and precipitation pattern is that the relationship between response variables (Y) and predictor variables (X) are nonlinear. One of the methods for dealing with nonlinearity in regression problem is Generalized Additive Models (GAM) which fits a smoothing curve through the data and keeps the requirements of independence, normal errors and constant variance (Hastie and Tibshirani, 1990).

In this study, habitat characteristics of bigeye tuna in the Southern Waters off Java-Bali, Indian Ocean were investigated as a representative for open ocean tuna habitat studies. It is an important issue to study because global tuna catches have increased steadily from a half million tonnes in 1950 to almost 4 million tonnes in 1999 (Miyake et al., 2004). In addition, the Pacific Ocean has the highest proportion of catches (65%) then the second rank of the proportion of catches (20%) is the Indian Ocean (Miyake et al., 2004). Bigeye tuna is one of the tuna species which widely traded and fully exploited in the Indian Ocean (IOTC, 2006a) and overfishing in the Atlantic (ICCAT, 2006a) and in the Pacific Ocean (WCPFC, 2006a). Without swift and effective management action, the status of bigeye tuna stocks is likely to

deteriorate in the same way as stocks of Atlantic Bluefin Tuna (*Thunnus thynnus*) and Southern Bluefin Tuna (*Thunnus macoyii*), which are now considered by the world conservation union to be critically endangered or endangered (WWF, 2007). By combining multi-sensor satellite data and statistical analysis, the habitat models can be built with the certain error values. In the first application for open tuna habitat studies, the scatter smoothers method to analyze a relationship between environmental variables and fisheries data was introduced. Then, simple predicted map can be determined. The second application, according to scatter smoothers concept, GAM was conducted by adding smoothing function to measure the relationship between environmental variables and fisheries data and then to build the habitat suitability index.

In precipitation studies, validation and correction of Global Satellite Mapping Precipitation (GSMaP) were conducted. Satellite precipitation data contribute significantly to the improvement of meteorological reanalysis products that are widely used for climate change, agriculture, and disaster prevention research (Saha et al., 2010). The suitability of satellite data for monitoring therefore should be considered (Trenberth and Hurrell., 1997) because satellite data often contain uncertainties caused by biases in sensors and retrieval algorithms, as well as inconsistencies between continuing satellite missions with the same sensors. In other words, satellite precipitation observations should be calibrated /validated to provide adequate temporal and spatial sampling over a long period of time (Karl et al., 2010). The GSMaP data, as the highest temporal and spatial resolution satellite data, can detect a precipitation event with the same trend as rain gauge data, but the precipitation amount generally has underestimated (Fukami 2010, Kubota et al. 2009, Makino 2012, Seto et al. 2009, Shrestha et al. 2011). Underestimated precipitation can cause underestimated discharge and it cause high bias for flood forecasting (Kabold and Suselj 2005, Pauwels and Lannoy 2005). Hence, validation and correction of GSMaP data are necessary. Because of

the nonlinear pattern of precipitation data, GAM model was introduced to reduce the bias of GSMaP data in this study.

1.2 Research Motivation

Historical data of open ocean tuna habitat and precipitation studies over a wide area are necessary to distinguish the dynamic change of them. Satellite imagery is the best source of such data, because observations need to be extensive, regular and consistent to establish baseline and trends. In many cases, satellite data are restricted and charged for, but for ocean and atmospheric observation, satellite data are open-access (i.e., NASA, precipitation satellite, altimetry satellite). In this study open access satellite data are used to analyze the characteristic of bigeye tuna habitat in case of open ocean ecosystem studies and to correct GSMaP satellite precipitation product in case of precipitation studies.

Open-access remote sensing data have three significant impacts for tracking and understanding the environmental and climate change studies, namely “continuity”, “affordability”, and “access” (Turner et al., 2014). “Data continuity” relates to the maintenance of long-term satellite data products. It will give a knowledge of how the environmental variables have changed and why. “Data affordability” arises from the cost of imagery, but some of them are free of charge like data from ocean color and altimetry satellite to monitor the environmental parameter in the ocean and the GSMaP satellite precipitation product to monitor the rain rate with high temporal resolution. “Data access” means the ability of the researchers to discover, retrieve, manipulate, and extract value from satellite imagery as well as link it with other types of information. Thus, open access satellite with long term records are necessary to be processed in interdisciplinary application (i.e habitat studies and satellite data product correction for flood monitoring). Due to data continuity records of satellite data, validation and calibration is important step which requires insitu data information as a reference.

Nonlinearity is another problem of ecological data and precipitation data. For that reason, the modern regression analysis was introduced which called GAM. This statistical method does not force data into unnatural scales, and allow for non-linearity and non-constant variance structures in the data (Hastie and Tibshirani, 1990). In addition, GAM has the ability to handle a large data sample which is very useful for open ocean tuna habitat and precipitation studies.

1.3 Research Problem

The research was conducted to use open access global coverage of satellite data by long term analysis for some environmental problems. Problems were found as follows:

- 1) Both of open ocean tuna habitat and precipitation studies have typical nonlinear data.
- 2) Southern Waters off Java and Bali is known as spawning area for tuna species and the habitat characteristic studies in that area are very limited.
- 3) The rain gauge availability is limited in the isolated area or in developing countries. Thus satellite precipitation data is necessary. GSMaP is one of the satellite precipitation data, however, it has error value in its system.
- 4) GSMaP has a serious underestimate during heavy rainfall. In addition, the heavy rainfall amount which close to rain gauge data is important to predict the accurate flood occurrence.

1.4 Research Scope and Objective

The objectives of this research are:

- 1) To introduce scatter smoothers method to analyze the relationship between bigeye tuna habitat and environmental variables in the study area by using linear regression.
- 2) To determine the best model for bigeye tuna habitat in the study area by introducing GAM for dealing with nonlinear data.

- 3) To evaluate the ability of GSMaP data as satellite precipitation data during rainy season.
- 4) To reduce the bias of GSMaP product during heavy rainfall.

1.5 Research Outline

This research is divided into two parts. First is the introduction and explanation of satellite remote sensing and GAM and second is the application of multi sensor satellite data and GAM for open ocean tuna habitat and precipitation studies. Figure 1.1 describes the outline of the dissertation. The dissertation is constructed by six chapters, as follows:

Chapter 1

Introduction of the research is described in this chapter. The chapter discusses the general introduction and basic motivation of this research. The research problem and research scope are listed and the research objectives are given

Chapter 2

This chapter explains the concept of multi sensor of remote sensing data, GAM and the theoretical background of research topic and the application for open ocean tuna habitat studies and precipitation.

Chapter 3

This chapter describes the application of multi sensor satellite data for open ocean tuna habitat study “part one”. Relationship studies between environmental data derived from satellite remote sensing and bigeye tuna using scatterplot smoothers method were selected as representative of this case. The background, method, technical process, result and discussion, and conclusion were explained.

Chapter 4

This chapter discusses about the application of multi sensor satellite data and GAM for open ocean tuna habitat study “part two” and bigeye tuna characterization was chosen as

representative of this case. The background, method, technical process, result and discussion, and conclusion were explained.

Chapter 5

This chapter discussed about the application of multi sensor satellite data and GAM for precipitation studies. Validation and bias correction of GSMaP was chosen as representative of this case. The background, method, technical process, result and discussion, and conclusion are explained.

Chapter 6

Chapter 6 presents the conclusions and the future work of the research.

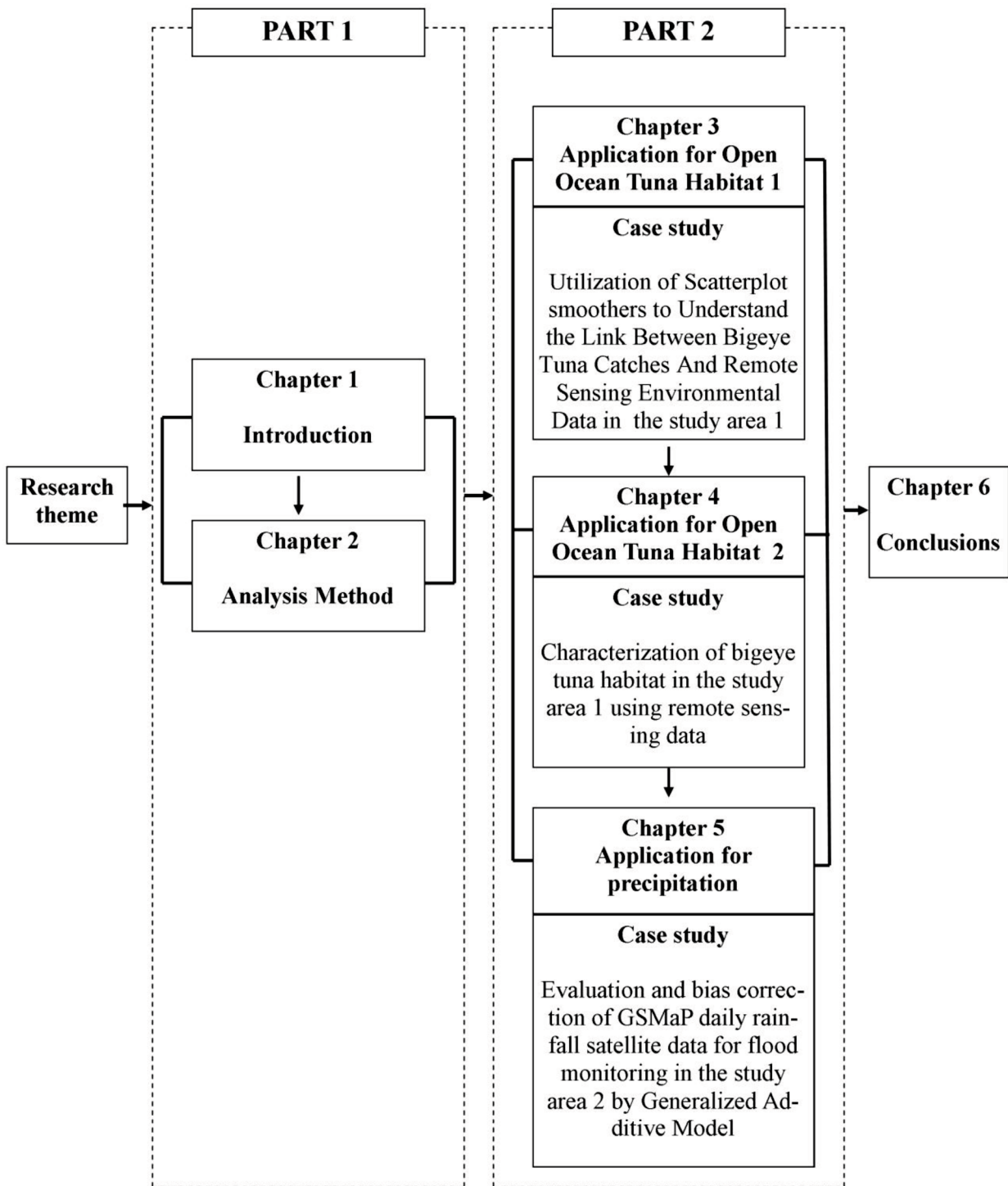


Figure 1.1 Outline of the dissertation

1.6 Overview of the study area

The research was conducted in two study areas: Southern waters off Java-Bali in Indonesia and Kyushu Island in Japan. These areas were selected for open ocean tuna habitat studies and precipitation studies.

1.6.1 Southern waters off Java-Bali, Indonesia

As explained in the outline of dissertation, Southern waters off Java-Bali is the representative for study area 1. Southern waters off Java-Bali as part of the Indian Ocean which locates between Indonesia and Australia. This area is the unique water because of its geography influenced by water masses in the Western Indian Ocean (WIO) and the outflow water masses from the Pacific Ocean. Both of these water masses affect the variability of oceanographic conditions in this area. In addition, the location of its waters is in a monsoon wind system, causing conditions of oceanographic which is affected by monsoon winds system (Wyrcki, 1961). Winds over the Indonesian maritime continent and the position of the Intertropical Convergence Zone (ICZ) are dominant features of strong monsoon signatures in this area. During the southeast monsoon (May to October), southeasterly winds from Australia generate upwelling along the southern coasts of Java and Bali. Upwelling events lead to the concentration of chlorophyll-a increase that causes the primary productivity (Wyrcki, 1962; Purba, 1995). These conditions are reversed during the northwest monsoon (November to April) (Gordon, 2005). This area has complex dynamic currents and wave systems (Syamsuddin et al, 2013). The dominant current and wave features consist of are shown in Figure 1.2 : 1) Indonesia throughflow (ITF), outflow water from the Pacific Ocean (Molcard et al., 2001; Gordon et al., 2010); 2) the seasonally reversing South Java Current (SJC) along the southern coast of the Indonesian Sea (Sprintall et al., 2010); 3) the Indian Ocean South Equatorial Current (SEC) flows from the southern Indian Ocean to an area off southern Java (Zhou et al., 2008); 4) downwelling Indian Ocean

Kelvin Waves (IOKW) that propagate to the east along the coasts of west Sumatra, Java, and the Lesser Sunda Islands (Syamsudin et al., 2004); and 5) westward Rossby Waves (RW) propagation at 12–15°S (Gordon, 2005; Sprintall et al., 2009). Besides these current and wave systems, winds over the Indonesian maritime continent and the position of the ICZ are dominant features of strong monsoon signatures.

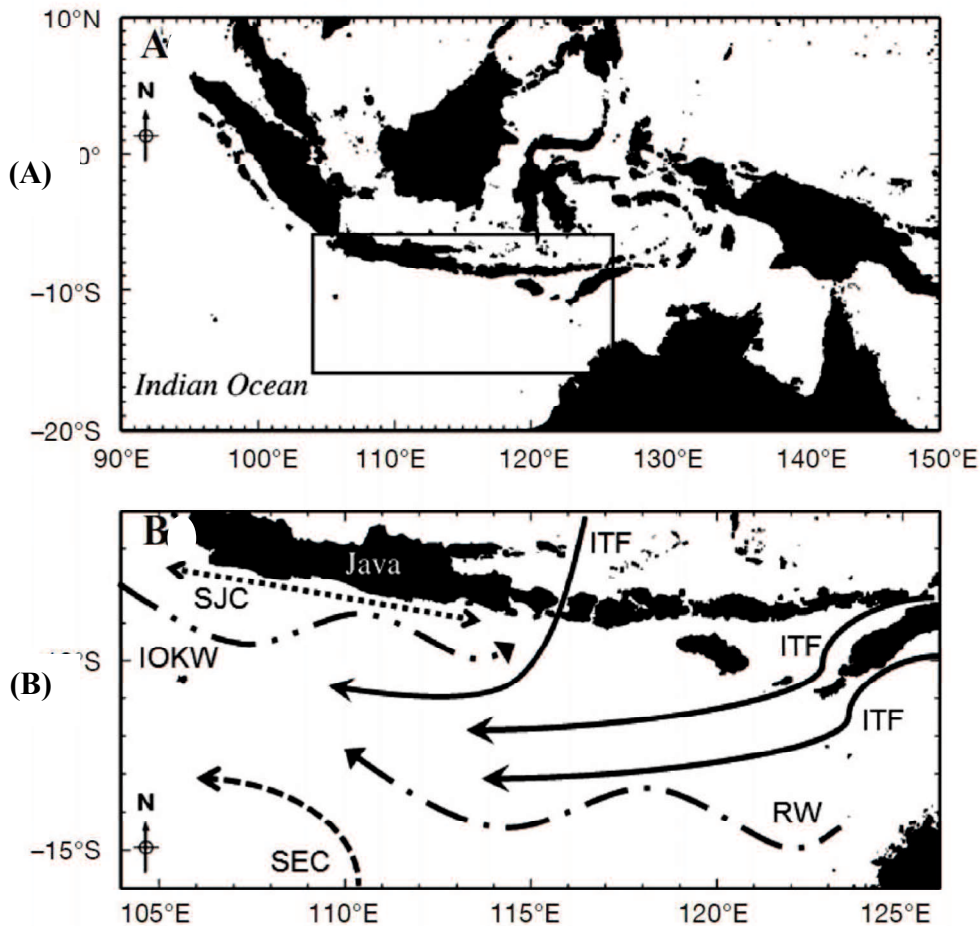


Figure 1. 2 (A) Map of the Indonesian seas, with the inset box representing the study area. (B) Map of the study area in the eastern Indian Ocean (EIO) off Java (Syamsudin et al., 2013).

In Figure 1.2B, the wave and current systems in the Eastern Indian Ocean (EIO) off Java are indicated by the dotted line for the South Java Current (SJC), solid lines for ITF, the line with dashes and 2 dots for IOKW, the line with dashes and 1 dot for the Rossby Waves (RW), and the dashed line for SEC.

1.6.2 Kyushu island, Japan

As explained in the outline of dissertation, Kyushu island is the representative for study area 2. Kyushu is the third largest island of Japan and was located in the southwesternly of its four main island (Fig 1.3).

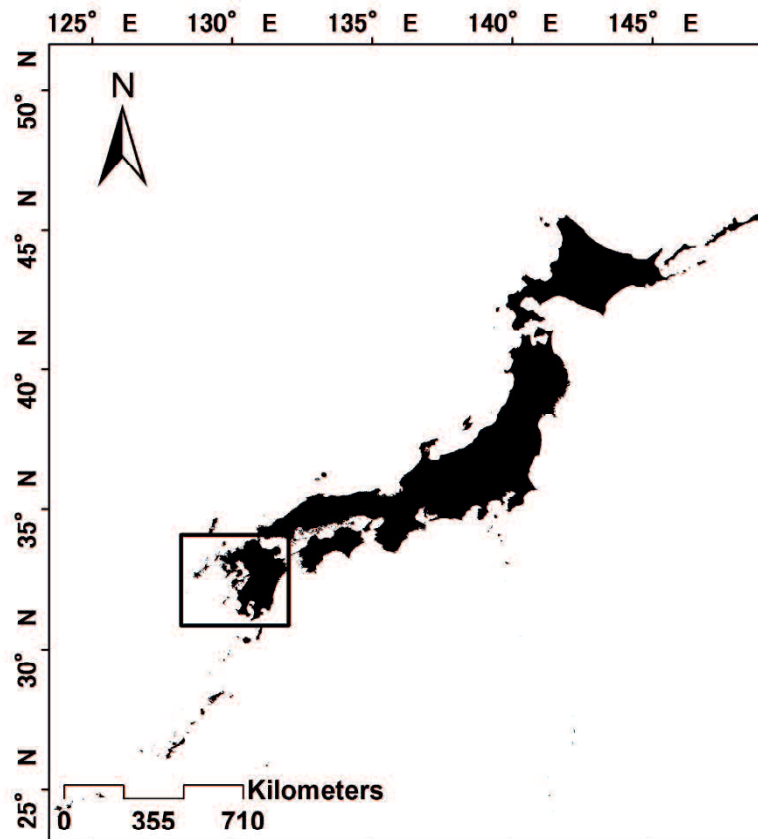


Figure1.3 Map of Kyushu Island

This island has an area of 35,640km² from latitude 31° N to 34°N and longitude 129°30'E to 132°E. The most important topographic feature of Kyushu Island is the Kyushu mountains aligned in a north-south direction at the centre of the island. The spatial distribution of precipitation depends largely on the direction of prevailing winds relative to the orientation of this mountain range. The annual precipitation and its seasonal distribution at four meteorological stations are shown in Table 1.1. According to Table 1.1, the highest annual precipitation occurred during summer season, which mostly caused flood and debris flow. Since it is in southern Japan, Kyushu has a subtropical climate and its inhabitants

produce a variety of agricultural products. In addition, most of Kyushu's population is concentrated along the northwest, in the cities of Fukuoka and Kitakyushu.

Table 1.1 Climatological (1961-1990) annual precipitation totals and percentage of precipitation during each season for four stations in Kyushu Island (Uvo et al., 2001)

<i>Name</i>	<i>Location</i>	<i>Annual Prec.</i>	<i>Spring</i>	<i>Summer</i>	<i>Autumn</i>	<i>Winter</i>
Fukuoka	33.6N 130.2E	1604.3 mm	23.0%	42.4%	21.9%	12.7%
Kumamoto	32.8N 140.3E	1967.7 mm	24.6%	50.0%	16.3%	9.5%
Miyazaki	31.9N 131.4E	2434.6 mm	26.9%	39.4%	25.6%	8.0%
Kagoshima	31.6N 130.6E	2236.8 mm	29.0%	41.0%	18.3%	11.7%

CHAPTER 2

ANALYSIS METHODS

2.1 Multi sensor of satellite remote sensing

Remote sensing is the science to get the information about the Earth's feature using instruments which are remote to the Earth's surface (Joseph, 2005). To denote identification of earth features, the characteristic of electromagnetic radiation, which is reflected/emitted by the earth system is distinguished. A device to detect the electromagnetic radiation reflected or emitted from an object is called a sensor which is located on the platform (e.g, satellite, aircraft, etc). These explanations are described in Figure 2.1.

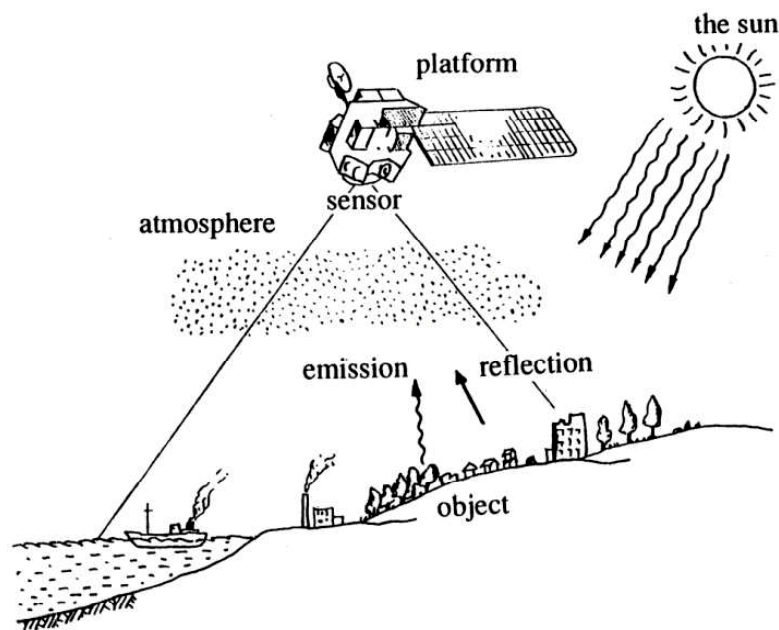


Figure 2.1 Data collection by remote sensing (Joseph, 2005)

The output of this technique can be an image/ binary data which displays in the digital format. For some remote sensing instruments, the distance between the target being imaged and the platform, plays a large role in determining the detail of information obtained and the total area imaged by the sensor. The detail information of an image depends on the spatial resolution of the sensor and refers to the size of the smallest possible feature that can be

detected. In addition, the temporal resolution is also important for the satellite remote sensing system, which refers to the period of the satellite passes on the same territory.

Remote sensing offers the ability to observe and collect data for wide areas relatively quickly, and is an important source of improving natural resources management, land use and protection of the environment. An increased utilization of satellite remote sensing data will increase the demand for harmonizing heterogenous data by using multi sensor analysis approach (Mergey and Mockness., 2009). Figure 2.2 shows an example of multi sensor analysis.

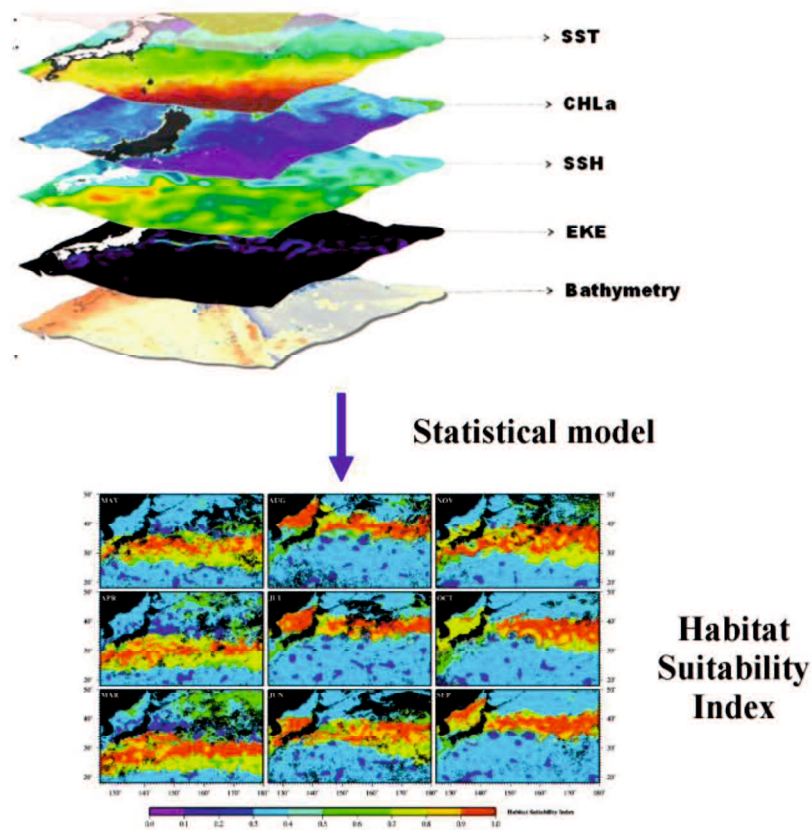


Figure 2.2 An Example of multi sensor analysis which distinguishes habitat suitability index (Mugo et al., 2011)

Multi-sensor analysis is often used to determine a certain phenomenon/ characteristics by combining some multi-sensor image. The advantage of this approach is multi-sensor analysis may provide increased interpretation capabilities and more reliable results since

data with different characteristics are combined and can achieve improved accuracies, better temporal coverage, and better inference about the environment than could be achieved by the use of a single sensor alone (Von and Huang., 2005). In addition, multi-temporal analysis is an underway methodology for handling and analyzing the time series of data (e.g. time series of sea surface temperature (SST) image observed from satellite). This approach is able to characterize the dynamic change during a certain period. A combination of multi-sensor image data may also be used to examine large-scale spatial patterns on the earth's surface.

2.2 Multi sensor images for Open Ocean Tuna habitat studies

2.2.1 Open Ocean Ecosystem

The interaction between animal, plant and the environment is known as ecosystem. Marine ecosystems cover an area greater than 70 percent of the Earth's surface. They contain some of the most diverse organisms and least known habitats of our planet. The open ocean consists of water column (pelagic) and sea floor (the benthic realm) in international waters that is beyond 200 miles from a nation coastline (Mills and Carlton, 1998). Food web in the open ocean is shown in Figure 2.3. It describes that phytoplankton as primary producer and tuna as the third level of carnivore. From the point of view of conservation, the declined pelagic fisheries has been recognized, especially for tuna fisheries (Mills and Carlton, 1998).

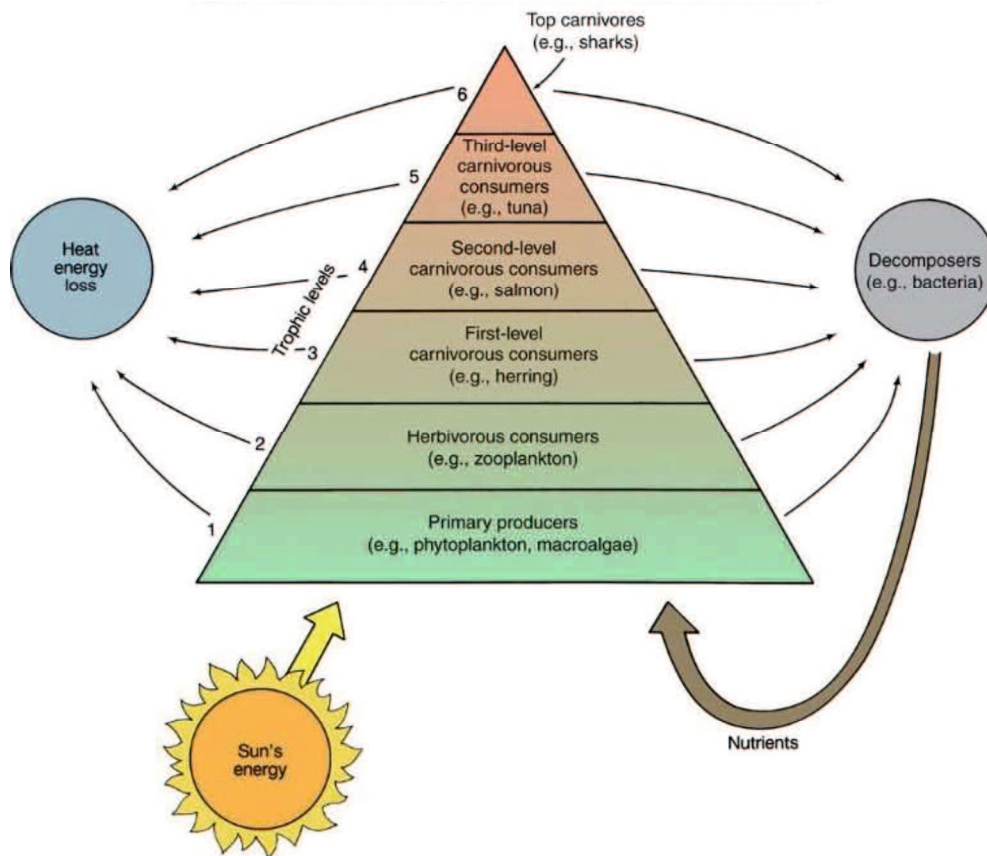


Figure 2.3 Food web in open ocean (www.studyblue.com)

2.2.2 Bigeye Tuna Characteristics

Bigeye tuna is one of the tuna species which widely traded and fully exploited in the Indian Ocean (IOTC, 2006a) and overfished in the Atlantic Ocean (ICCAT, 2006a) and in the Pacific Ocean (WCPFC, 2006a). Bigeye tuna mostly are caught by purse seine and long line fleets (Figure 2.3). Juvenile bigeye tuna are taken by purse seine fleets for canning industry, while adult bigeye tuna are taken by longline fleets for sashimi and sushi market. Even though longline fleets only catch adult bigeye tuna, it also has an impact on a range of bycatch species (i.e., sharks, marlin, swordfish, turtle, marine mammals, finfish, and seabirds). In addition, by longline fleets methods, the proportion of the bycatch reached 76% in 2005 in the Indian Ocean and it was the highest bycatch proportion of all (Oceanic Fisheries Programme, 2006).

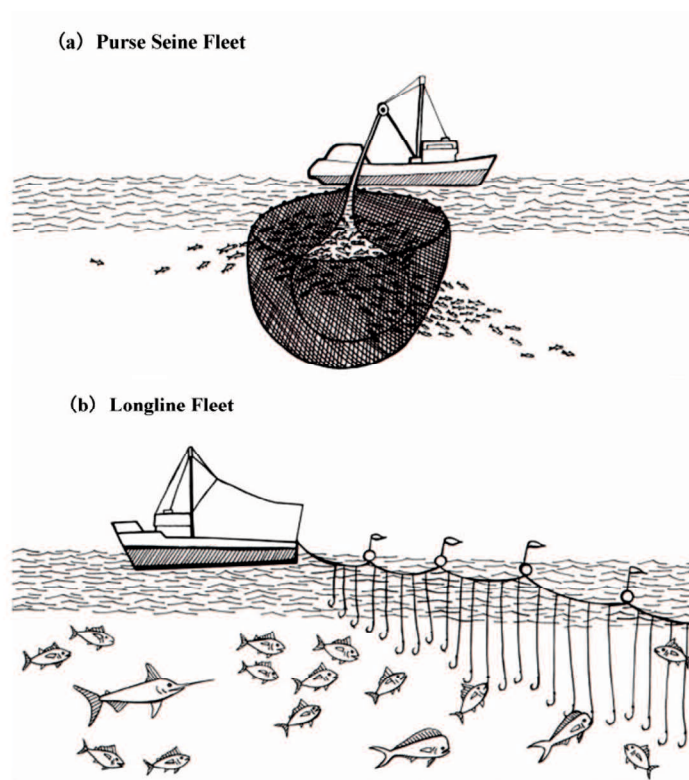


Figure 2.4 Tuna fishing methods (WWF, 2014)

Bigeye tuna is a member of the Scombridae Family in the Order Perciformes and it is classified as a highly migratory species which spread globally. Bigeye tuna is relatively long lived species, later to spawn and of lower biological productivity compared with other tuna species (Froese and Pauly, 2007). As a result, bigeye tuna is more vulnerable to overfishing than species such as skipjack tuna and yellow fin tuna. Bigeye tuna fisheries have not only impacted to bycatch species, but also have the impact for the food webs and habitat (WWF, 2007). Bigeye tuna, like other tuna species, is a high level predator in the marine food chain, while there is a little research on the role of bigeye tuna explicitly in the food webs (Kitchell et al., 1999). Purse seine fishing method which is used to catch bigeye tuna have the impact for bigeye tuna existence and have some localised impacts on benthic habitats (MRAG Americas Inc., 2002).

Bigeye tuna periodically stay near the surface pelagic environment (Brill et al., 2005), hence satellite data provide appropriate observations for their horizontal habitats. Bigeye tuna are known to associate with the temperature conditions (Brill et al., 2005 and Howell et al., 2010), thermocline layer (Brill et al., 2005) and water clarity (Sund et al., 1981; Blackburn et al., 1968; and Bertrand et al., 2002) which are features that can be distinguished from satellite remotely-sensed SST, ocean color and altimetry data. Studying bigeye tuna's habitat from remotely-sensed environmental data provides a scientific basis for understanding their response to externalities such as climate change and fishing pressure. Habitat models based on remotely-sensed data can facilitate fishery forecasting, effort control or design of dynamic marine protected areas. To build a habitat model, multi-sensor satellite data, time series data and statistical model are needed.

2.2.3 Satellite Remote Sensing Characteristics for Bigeye tuna Habitat

In this study, Aqua MODIS (Moderate Resolution Imaging Spectroradiometer) sensor and altimeter sensor (NRA and SSALT) were used. Aqua MODIS sensor has spectral coverage from 405nm to 14385nm (IOCCG, 2014) and altimeter sensor has spectral coverage from 1cm to 1m (Aviso, 1996). By Aqua MODIS sensor, SST and Sea Surface Chlorophyll (SSC) can be obtained and by altimeter sensor Sea Surface Height Deviation (SSHD) can be obtained. In relation with bigeye tuna habitat parameter, SST, SSC, and SSHD were used as a representative for temperature, water clarity and thermocline layer.

By Aqua MODIS sensor, SST and SSC observation can be measured in the near infrared band (750nm - 950nm) and visible band (450 nm – 690 nm), while altimeter sensor can be measured in the microwave band (Figure 2.5). Due to the difference of the electromagnetic spectrum, Aqua MODIS data and altimeter data have a different spatial resolution.

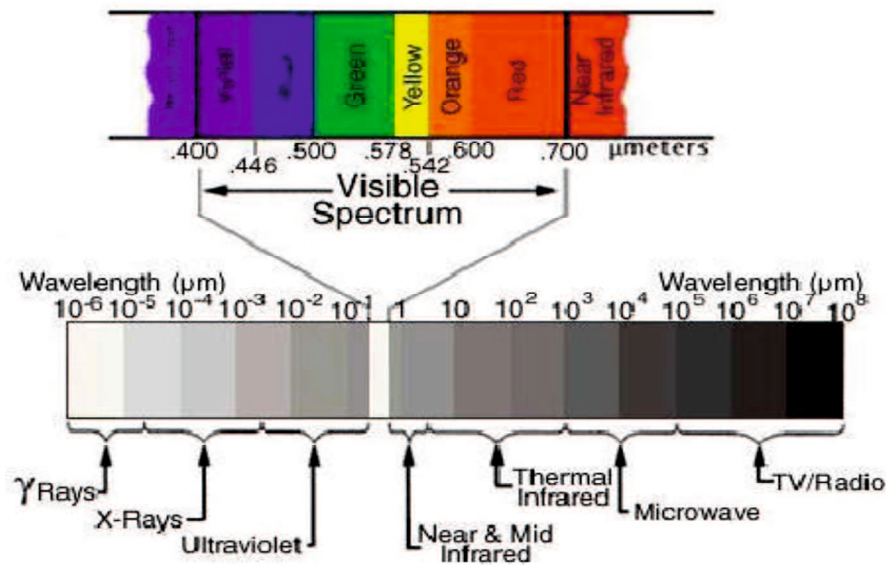


Figure 2.5 The electromagnetic spectrum (<https://engineering.purdue.edu>)

Ocean properties are always changing, so temporal resolution is more important than spatial resolution. Thus, time series data were applied. In addition, time series data is important to build the habitat models for bigeye tuna. Time series data cause large numbers of data, therefore the higher level data of Aqua MODIS sensor (level 3) and altimeter sensor (4) were selected for efficiency data processing. Higher level data were defined as the conversion of raw data to physical property data, i.e., SST ($^{\circ}\text{C}$), SSC (mg/m^3) and SSHD (cm). The raw data of SST and SSC are radiance ($\text{w}/\text{m}^2/\text{cm}^4/\text{sr}$) and SSHD is telemetry data record (m). The conversion algorithm of SST, SSC and SSHD are described as follows:

To obtain SST, two algorithms were conducted, first conversion from radiance to brightness temperature ($^{\circ}\text{K}$) and second conversion from brightness temperature to SST (Brown and Minnet., 1999).

$$T = \frac{h \cdot c}{(L \cdot k \cdot (\ln(\frac{2h \cdot c^2}{L^5 \cdot R}) + 1))} \quad (2.1)$$

Where, T is the brightness temperature ($^{\circ}\text{K}$), h is Plank constant ($6.6260755 \times 10^{-34}$ J s), c is speed of light (2.99792458×10^8 m/s), L is wavelength (cm), k is Boltzmann constant (1.380658×10^{-23} J/K), and R is the radiance value ($\text{w/m}^2/\text{cm}^4/\text{sr}$). After brightness temperature was obtained, SST can be calculated as follow:

$$\text{SST} = C_1 + C_2 * T_{31} + C_3 * T_{3132} + C_4 * (\sec(\theta) - 1) * T_{3132} \quad (2.2)$$

Where T_{31} is brightness temperature of band 31, T_{3132} is brightness temperature difference of band 32 and band 31 (band 32 - band 31) and C_1, C_2, C_3, C_4 are coefficient for MODIS band 31 and 32 which are listed in Table 2.1.

Table 2.1. Coefficient for SST MODIS band 31 and 32 (Brown and Minnet., 1999)

Coefficient	$T_{32}-T_{31} \leq 0.7 \text{ }^{\circ}\text{K}$	$T_{32}-T_{31} \geq 0.7 \text{ }^{\circ}\text{K}$
C_1	1.228552	1.692521
C_2	0.976555	0.9558419
C_3	0.1182196	0.0873754
C_4	1.774631	1.199584

To obtain SSC, OC3M algorithm was applied (Werdell and Bailey., 2005) as follows:

$$\log(\text{SSC}) = a_0 + a_1 * X + a_2 * X^2 + a_3 * X^3 + a_4 * X^4 \quad (2.3)$$

where

$$X = \log \left(\frac{\text{Max}(R_s(443)*R_s(489))}{R_s(555)} \right) \quad (2.4)$$

Where a_0, a_1, a_2, a_3 and a_4 are the coefficients with the value of 0.283, -2.753, 1.457, 0.659 and -1.403. $R_s(443), R_s(489)$ and $R_s(555)$ are remote sensing reflectance in the wavelength 443nm (band 9), 489nm (band10) and 555nm (band 11). The R_s values can be obtained by the following equation:

$$R_s = \frac{L_w(\lambda)}{E_s(\lambda)} \quad (2.5)$$

Where L_w is water leaving radiance, E_s is downwelling surface irradiance which derived from buoys measurements and λ is wavelength.

Figure 2.6 shows how altimetry measures SSHD. First, altimeters emits signals to the earth and receive the echo from the sea surface, after its reflection. The sea height is represented by the distance satellite minus the surface and the satellite's position relative to an arbitrary reference surface (the reference ellipsoid).

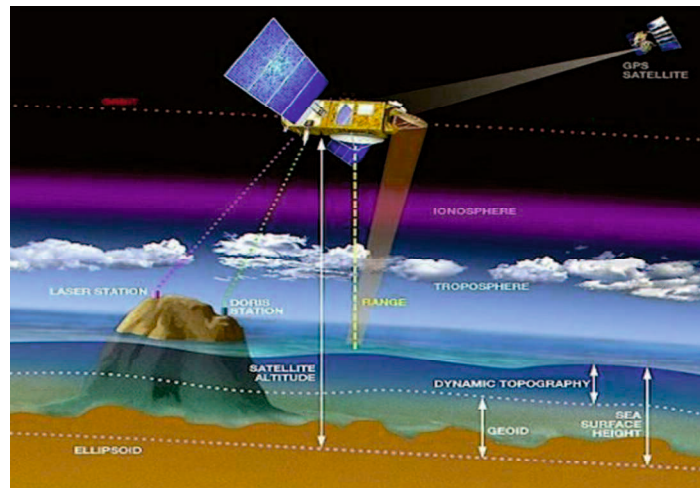


Figure 2.6 How altimetry measures SSHD (<http://www.aviso.altimetry.fr>)

To obtain SSHD, the algorithms were applied as follows:

$$SSHD = SSH - MSS \quad (2.6)$$

Where MSS is the mean sea surface height with 20 years reference, SSH is sea surface height which can obtained by following equations:

$$SSH = \text{Geoid} + \text{surface echo} - R - \text{bias} \quad (2.7)$$

Where, geoid is equal to -0.3mm , surface echo is the value from telemetry data (m), R is the range between satellite position and surface (2 cm) and bias is the error value after calibration.

To build the model, time series data of SST, SSC and SSHD were integrated by using statistical analysis, such as empirical cumulative distribution function (EDF) and GAM (Generalized Additive Models). It is explained in Chapter 3 and 4. To create spatial distribution of habitat map, habitat suitability index (HSI) was applied as explained in the Chapter 4. By applying this method, habitat characteristic of bigeye tuna can be recognized during a certain time.

2.3 Multi sensor images for precipitation studies

There are many climate parameters, which are measured by satellite remote sensing such as SST, aerosol, precipitation, sea ice, mean sea level, and solar radiation and so forth. In this study, precipitation is concerned because it plays a primary role in the global water and energy cycle (Yang et al., 2013). The spatial and temporal variability of precipitation on the global scale can be obtained from observations made by satellite precipitation. Although studies using longer satellite time series produced smaller rate of precipitation increase, these results are still regarded as unconfirmed result due to the shortness of the series (Liepert et al., 2009). A survey of available satellite-based long-term precipitation products showed mostly no trend in global precipitation (Grubber et al., 2008). These divergent findings represent the problems of detecting a robust global mean trend of precipitation, which lead to high variability of precipitation, systematic biases associated with instruments, and inadequate interpretation of the surface and atmospheric properties in the retrieval algorithms (Liu et al., 2012). Hence, validation and correction of satellite precipitation data is necessary. Although there is still uncertainty regarding a general trend, satellite

observations have greatly enhanced our understanding of the climate processes that control the variability of precipitation.

2.3.1 Global Satellite Mapping Precipitation (GSMaP)

The Global Satellite Mapping of Precipitation (GSMaP) is a recent addition to the repository of satellite-based high-resolution precipitation estimates which supported by Japan Science and Technology Agency (JST) and Japan Aerospace Exploration Agency (JAXA). GSMaP seeks to produce a high-precision, high resolution precipitation map using satellite data. For that reason, GSMaP combined two main sensors that are microwave radiometer (MWR) sensor from low orbit satellite and infrared radiometer (IR) sensor from geostationary satellite (Ushio et al., 2009). The MWR sensor consists of special sensor microwave/ imager (SSM/I), Tropical Rainfall Measuring Mission (TRMM) microwave imager (TMI) and advanced microwave scanning radiometer (AMSR-E) for Earth Observing System (EOS), which characteristic are listed in Table 2.2. In addition, SSM/I sensors consist of three platform namely, Defense Meteorological Satellite Program Satellite F13 (DMSP-F13), DMSP-F14 and DMSP-F15

Table 2.2 Characteristic of microwave radiometer of GSMaP data product (Aonashi et al., 2009)

Name	Altitude (km)	Sensor	Frequency (GHz)
TRMM	402	TMI	10, 19, 21, 37, 85
AQUA	705	AMSRE	7, 10, 19, 24, 37, 89
DMSP-F13	803	SSM/I	19, 37, 85
DMSP-F14	803	SSM/I	19, 37, 85
DMSP-F15	803	SSM/I	19, 37, 85

The MWR sensors emit brightness temperature, then converts into surface precipitation according to the algorithm of Aonoshi et al. (1996) and Kubota et al. (2007). In contrast, infrared radiometer sensor from geostationary satellite do not measure directly the precipitation, but their measurements are located in the cloud height top which directly correlate with surface precipitation by large variance (Ushio et al., 2009). Thus, Kalman filter was used to provide better feedback information for temporal variations. The original spatial resolution of infrared sensor is 0.036 degrees and the limited spatial resolution for microwave radiometer is 0.1 degrees. So, by integrating algorithm between MWR sensor and infrared sensor based on morphing technique, 0.1 degrees/1 hour resolution is produced (Joyce et al., 2004). This product was called GSMaP_MVK and it was used for this study. More detail about the algorithm is shown in Figure 2.7.

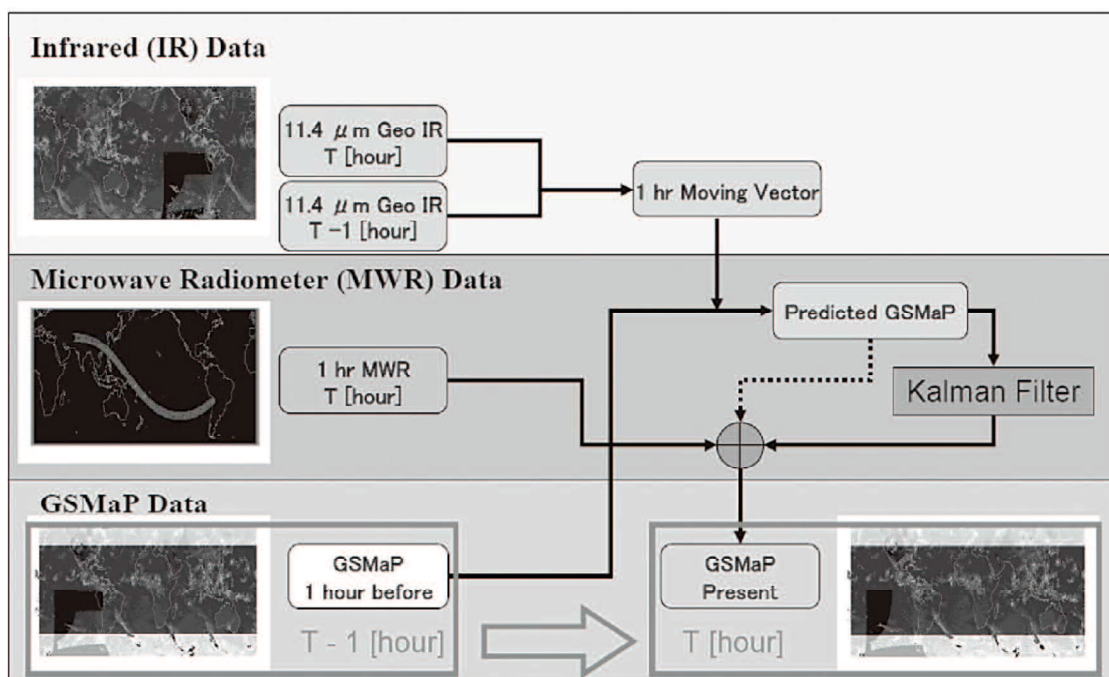


Figure 2.7 Flow chart of the GSMaP algorithm (Ushio et al., 2009)

GSMaP algorithm contains two main processes, namely advection system and rainfall propagation and Kalman filter. There are two processes to determine the advection vector. First, two dimensional cross correlation coefficient of images of IR brightness temperature

with one hour resolution at $t = 0$ and $t = 1$ is calculated. Second, if the image at $t = 1$ is lagged to $t = 0$ image spatially in longitude and latitude direction, the correlation is calculated for given spatial offset. By repeating this procedure for various offset and searching for horizontal offset which generates a maximum correlation and advection vector was determined. After maximum correlation was determined, the rainfall area from MWR is propagated forward in time by the advection vector derived from infrared image. In addition, the rainfall area is spatially propagated backward using the same advection vector. And then, the optimum estimates of rainfall rate are computed by calculating the weighted average from backward and forward propagation rainfall rates as explained in Figure 2.8 called as Kalman filter processes. This algorithm is used because in the previous one, the rain rate of surface precipitation has large variance and this algorithm can improve the accuracy of temporal variation of precipitation system (Ushio et al., 2009).

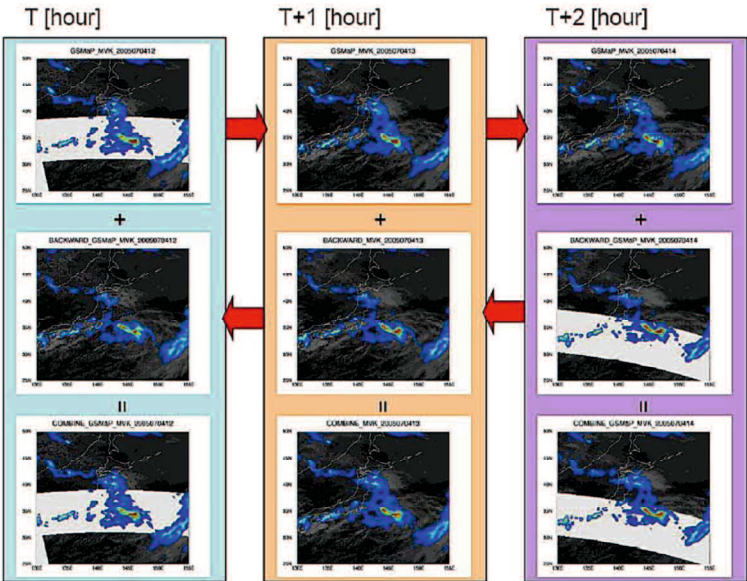


Figure 2.8 Schematic illustration combining the precipitation field forward and backward in time. The white belts denote the coverage of the microwave sensor.

The description about advection system, rainfall propagation and Kalman filter equation can be explained as follows:

$$X_{k+1} = X_k + w \tag{2.8}$$

Where, X_k is precipitation rate at time k which is propagated precipitation rate forward in time and w is called system noise. After a pixel propagated along with moving vector, the predicted the precipitation rate at time $k+1$ is not necessary as same as the actual rain rate at the time. If its uncertainty is represented as w which is called as system noise. In addition, the actual relationship between the infrared brightness temperature and surface precipitation rate is quite nonlinear (Ushio et al., 2009) with large variance. To apply Kalman filter into a linear basis, the linearization approximation is needed as explained in equation (2.9).

$$Y_k = HX_k + v \quad (2.9)$$

Where Y_k is brightness temperature at the time k , X_k is precipitation rate at the time k , v is noise and H is coefficient constant. After applying the kalman filter to the propagated rainy pixel stated above, the same propagation and Kalman filter is applied to the rainy pixel backward propagation (Figure 2.7). To obtain the optimal rain rate, the weighted average equation is applied:

$$\widehat{R}_t = R_{t,i}^f \frac{\sigma_j}{\sigma_j + \sigma_i} + R_{t,j}^b \frac{\sigma_i}{\sigma_j + \sigma_i} \quad (2.10)$$

Where \widehat{R}_t is optimal rainfall at the time t , $R_{t,i}^f$ is the forward refines precipitation rate by Kalman filter after i hours, $R_{t,j}^b$ is the backward refines precipitation rate by Kalman filter after j hours and σ is the root mean square of the uncertainty estimates after i and j hours from microwave radiometer overpass.

GSMaP as multi sensor satellite, which tends to underestimate values especially when heavy rainfall occurs. In addition, the ability of GSMaP to observe heavy rainfall is necessary to predict the probability of flood occurrence. For that reason, validation of GSMaP data is important to estimate the error value (i.e., root mean square and bias) which is necessary to improve the GSMaP algorithm. In addition, bias correction is necessary to

reduce the underestimate value during heavy rainfall. Long term analysis is necessary to obtain the error value and to create the solution for its correction. Thus, multi satellite data were used.

2.4 Generalized Additive Model (GAMs)

2.4.1 A framework for use of statistical models

The purpose of the statistical model is to provide a mathematical basis for interpretation, examining such parameters as ‘fit’ (Do the measured predictors adequately explain the response?), ‘strength’ of association (Is the relationship between the response and the predictors significant?), and to ascertain the contributions and roles of the different variables. Regression analyses have been broadly applied in ecology to determine the relationship between response and explanatory variables. Linear regression (LR) is one of the oldest statistical techniques, and has long been used in biological research. However, LR has limitation of its assumption. Then, one field where the use of modern regression (i.e. Generalized linear model (GLM) and Generalized Additive Model (GAM)) approaches has proven particularly useful is the modeling of the spatial distribution of species and communities (Guisan and Zimmermann, 2000; Scott et al., 2002). In addition, GLM is more flexible than LR and GAM is the wider generalization of GLM. That is;

$$LR \subset GLM \subset GAM \quad (2.11)$$

2.4.2 GAM

GAMs are semi-parametric extensions of GLMs (Generalized Linear Models) which do not force data into unnatural scales, and thereby allow for non-linearity and non-constant variance structures in the data (Hastie and Tibshirani, 1990). GAM has the ability to handle a larger class of distributions for the response variable Y. Data may be assumed to be from

several families of probability distributions, including the normal, binomial, Poisson, negative binomial, or gamma distribution, many of which better fit the non-normal error structures of most ecological data (Guissan et al., 2002). Thus, GAMs are more flexible and better suited for analyzing ecological relationships, which can be poorly represented by classical Gaussian distributions (Austin, 1987). In addition, the underlying assumption made is that the functions are additive by “smooth” function. GAM uses a link function to establish a relationship between the mean of the response variable and a ‘smoothed’ function of the explanatory variable(s). The strength of GAMs is their ability to deal with highly non-linear and non-monotonic relationships between the response and the set of explanatory variables. GAMs are sometimes referred to as data- rather than model driven. This is because the data determine the nature of the relationship between the response and the set of explanatory variables rather than assuming some form of parametric relationship (Yee and Mitchell, 1991). The ability of GAM to handle nonlinear data structures can aid in the development of ecological models that better represent the underlying data, and hence increase our understanding of ecological systems.

Generalized Additive Model (GAM) can be summarized by the following components:

$$g(\mu) = \alpha + \sum_{i=1}^p f_i(X_i) \quad (2.12)$$

Where, g is link function (i.e., log link, inverse link and identity link), μ is a response variable, α is a constant value, f_i are spline smooth function that summarize the data’s tendencies, and X_i is the predictor variables. A smoothers is a tool for summarizing the trend of a dependent variable μ as a function of one or more independent variables X_1, X_2, \dots, X_p . In addition, smoothers estimate the dependence of the mean of μ in the predictors.

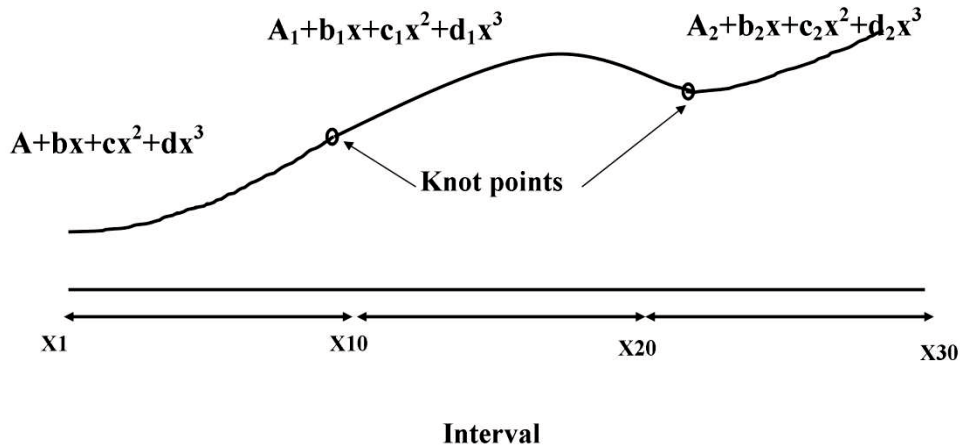


Figure 2.9. cubic spline function

To determine spline smoothers piecewise polynomial was applied. As seen in Fig.2.9 predictor variable (x) was divided into intervals. Each interval (i.e cubic polynomial) is fitted and then fitted values per segment are glue together (i.e point where the intervals connect was called by *knots*).In addition, $f(x)$ at first and second derivative are continues at each x_i , so the cubic polynomial in each intervals can be determined. After each smoother line was calculated in each predictor variables, then all predictor variables were combined using multiple regressions. The main output of GAM is partial residual plot in each predictor variables which also represents smoothing functions.

$$R_j = g(\mu) - \alpha - \sum_{k \neq j} f_k(X_k) \quad (2.13)$$

Where, R_j is partial residual, $g(\mu)$ is a response variable with link function, α is a constant value, $f_k(X_k)$ are smoothing functions of other predictor variables. In other words, partial residual means the residuals after removing the effect of all predictor variables (i.e., smoothing function in each predictor variables).

GAM was widely applied to several studies related to ecology and meteorological applications. Simon Barry and Alan Welsh (Guissan et al., 2002) present alternative flexible GAMs for predicting species distributions when observed count data include a larger

proportion of zeros than expected (i.e., zero inflated) in a Poisson distribution. Zagaglia et al. (2004), Zainuddin et al. (2008), Mugo et al. (2010), Syamsudin et al. (2013) and Setiawati et al. (2015) present the application of GAM to predict tuna distribution in oceans by environmental variables. Hastie and Tibshirani (1984) present the application of GAM by using Gaussian model for large meteorological data set.

CHAPTER 3

APPLICATION FOR OPEN OCEAN TUNA HABITAT 1

Utilization of Scatterplot smoothers to Understand the Link Between Bigeye Tuna Catches And Remote Sensing Environmental Data in The Southern Waters Off Java–Bali

3.1 Introduction

Tuna fisheries play an important role in the economic sector related to the fisheries resources utilization in Indonesia and its exports reached U.S. \$ 400 million in 2011 and continues to increase every year (MMAF, 2011). Southern waters off Java and Bali, part of Indian Ocean are identified as potential fishing grounds of tuna fisheries (Bailey et al., 1987; Osawa and Julimantoro, 2010). In addition, the waters of the Indian Ocean, between Indonesia and Australia, are known as important spawning grounds for commercial tuna and tuna-like species (Nishikawa et al., 1985). Hence, the availability of biological and environmental data around the Indian Ocean becomes an essential step to conserve and manage bigeye tuna resources.

Bigeye tuna are species highly migratory that are distributed between 40°N and 40°S, especially in the tropical waters (Laevastu and Rossa 1962, Kikawa and Ferraro 1966, Collette and Nauen 1983, Fonteneau et al., 2004). They prefer to stay at the temperature around the thermocline layers (Brill et al., 2005) and they have large tolerance of water temperature (Brill et al., 2015). The main depth of fishing activity for bigeye tuna in the Indian Ocean is between 161–280 m (Mohri and Nishida, 1999), while they can stay in the surface layer (0-100 m) in the night time (Howell et al., 2010). Moreover, bigeye tuna are considered as a visual predator which means that they favor to stay in the clear water with low chlorophyll-a concentration (Sund et al., 1981).

The biophysical environment plays an important role in controlling tuna distribution and abundance (Zainuddin et al., 2006), including those of bigeye tuna. The near real time data of biophysical environment by global coverage can be derived from satellite remote sensing. Recent decades, the satellite remote sensing has become an instrumental ecology for environmental monitoring (Chassot et al., 2011) and is used to manage fisheries sustainable levels (Klemas et al., 2013).

Satellite remote sensing data provide reliable global ocean coverage of sea surface temperature (SST), sea surface height deviation (SSHd), surface winds, and sea surface chlorophyll (SSC), with relatively high spatial and temporal resolution (Polovina and Howell, 2005). Application of satellite remote sensing in fisheries is increasing worldwide (e.g. Laurs et al., 1984; Laurs, 1986; Stretta, 1991; Lehodey et al., 1997; Santos, 2000; Zagaglia et al., 2004; Zainuddin et al., 2006; Druon, 2010; Yen et al., 2012; Perez et al., 2013; Kamei et al., 2014). Oceanographic phenomena are often used to understand preferred habitat and to estimate the potential of fishing grounds (Mohri, 1999; Mohri and Nishida, 1999; Lennert-Cody et al., 2008; Song et al., 2009; Osawa and Julimantoro, 2010). However, there have been relatively few tuna fisheries ecology studies using satellite remote sensing data in the Southern Waters off Java and Bali (Natih et al., 2010, Osawa and Julimantoro, 2010; Arief et al., 2011, Syamsuddin et al., 2013). Natih et al., (2010), Osawa and Julimantoro (2010) and Arief et al., (2011) reported that environmental variables had not significant to the abundance of bigeye tuna while Syamsuddin et al. (2013) reported that El Nino gave the significant effect to bigeye tuna abundance in the Southern waters of Java-Bali.

The aims of this study are to determine the relationship between bigeye tuna catches and environmental data derived from satellite remote sensing and to determine the optimum value of each variable. SST, SSC and SHD were used as the environmental factors in this

study. SST has been used to investigate productive frontal zones (Hanamoto, 1987; Andrade and Garcia, 1999; Lu et al., 2001), SSH can be used to infer oceanic features such as current dynamics, fronts, eddies, and convergences (Polovina and Howell, 2005), while SSC can also be used as a valuable indicator of water mass boundaries and may identify upwelling which can influence tuna distribution in the region. We applied scatterplot smoother method to analyze the relationship among the data and empirical cumulative distribution function to find the optimum value after data were classified into high catches data.

3.2 Study area

The Southern Waters off Java-Bali as a part of the eastern Indian Ocean are selected as a study area and are located between latitude from 10°S to 18°S and longitude from 110°E to 118°E as shown in Figure 3.1.

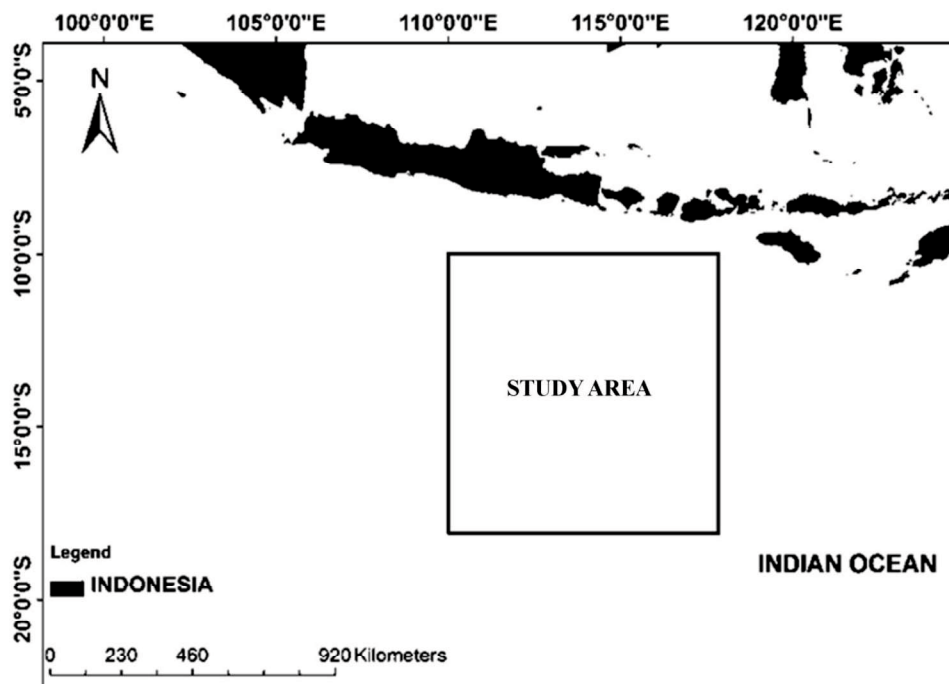


Figure 3.1 Study area

The study area has a tropical monsoon type of climate, resulting from the Asia-Australian monsoon wind systems, which change the wind direction according to the seasons. In July–September, the prevailing southeast monsoon favours upwelling along the

coast off Java-Bali and Sumatra (Du et al., 2008). These conditions are reversed during the northwest monsoon (November to April; Susanto et al., 2006). The Southern waters off Java-Bali is not only forced by intense annually reversing monsoonal winds, but also influenced by the throughflow variability (Feng and Wijffels, 2002). Physically, the study area and the surroundings have some complex dynamic currents and wave systems (Feng and Wijffels, 2002). The range value of SST depends on the seasonal monsoon (Soman and Slingo, 1997). The surface layer of the tropical ocean is warm and the annual variation of temperature is normally small (Wyrski, 1961). In addition, range of SSC inversely proportional with SST. Every year, higher concentrations of SSC occur in June to September and lower concentrations in December, January and February (Hendiarti et al., 2005; Swardika et al., 2012). These conditions directly affect the amount of fishing catches (Syamsuddin et al., 2013).

3.3 Materials and Methods

3.3.1 Fisheries data and remotely sensed environmental data

We analyzed daily catch data of bigeye tuna and remotely sensed environmental data for the period of 2006–2010. Data set for bigeye tuna catch was used to examine the link between the number of bigeye tuna caught and environmental data in the study area. The in-situ bigeye tuna catch data were obtained from nineteen longline fishing logbooks provided by PT Perikanan Nusantara, an incorporated company of the Indonesian government, at Benoa, Bali. Most of fishing operations were run by medium-sized vessels (100 gross tonnage). Each month, 19–20 vessels were operated with the same fishing gear (longline sets) and similar fishing technique (Syamsudin et al., 2013). The data sets consist of geographic positions of fishing activities (latitude and longitude), operational days, vessel numbers, and the number of tuna caught per day. We compiled and digitized them into the

monthly database. The unit of daily catch data was the number of bigeye tuna caught. Although most researchers have used catch per unit effort (CPUE) as an index of fish abundance (Zagaglia et al., 2004; Zainuddin et al., 2008; Lan et al., 2011; Mugo et al., 2010), we used number of bigeye tuna caught as an index of fish abundance due to its trend which almost same with hook rate (i.e hook rate can be referred as CPUE) data as shown in the Figure 3.2. Moreover. We assume that fish catch was caught one boat in one location. So, it is proportional to fish density in one location.

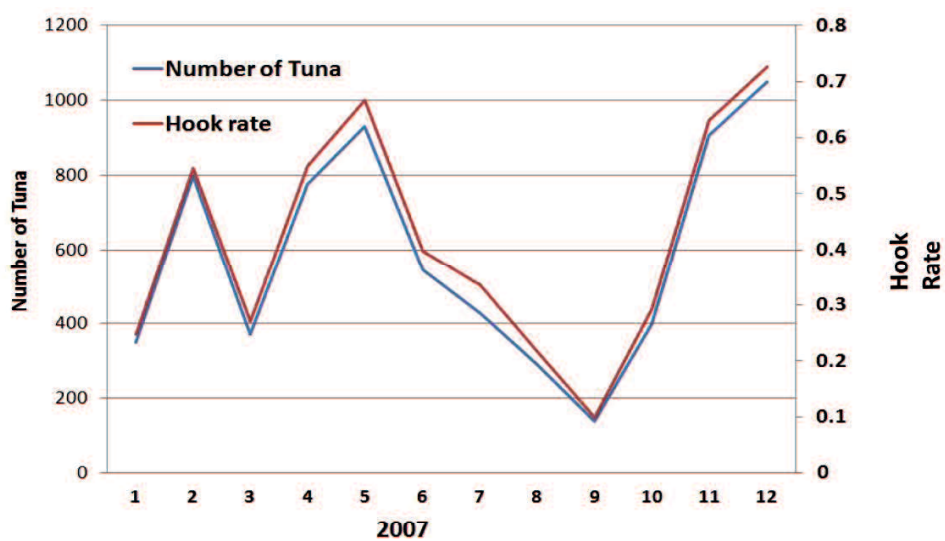


Figure 3.2 The relation between number of tuna and hook rate

SST, SSC, SSHD were used as indices for remote sensing environmental data. Monthly SST ($^{\circ}\text{C}$) and SSC (mg/m^3) Level 3 Standard Mapped Images (SMI) with 4 km spatial resolution were downloaded from Aqua MODIS satellite data (<http://oceancolor.gsfc.nasa.gov/>). The SSC data correction was carried out to remove noise which was mainly due to clouds (Maritorena et al., 2010), removing unexpected value of SSC concentration (<0 and $> 10 \text{ mg}/\text{m}^3$) (Abbott and Letelier, 1999). SSHD were downloaded from aviso homepage by using environmental data connector (EDC) which has 0.25° spatial resolution and then resampled to fit the SST and SSC spatial resolution. The EDC is compatible with ArcGIS software and can be downloaded for free from the National

Oceanic and Atmospheric Administration (NOAA) website (<http://www.pfeg.noaa.gov/products/edc/>). Monthly values of SST, SSC and SSHD data were extracted from each pixel corresponding to the location of fishing activities by using spatial analysis tool of Arc GIS software. The outcome was a full matrix of number of bigeye tuna caught and environmental variables. The full matrix was used for classification of fisheries data and for scatterplot smoothers.

3.3.2 Classification of fisheries data

Classification of fisheries data is very useful for inferring the type of fish catch data and for determining the optimum range of environmental variables and also can reduce the bias due to null catches (Andrade and Garcia, 1999; Zainuddin et al., 2008; Setiawati et al., 2015). The classification of fisheries data was divided into three groups based on Quartile method (Andrade and Garcia, 1999): (a) null catches (0); (b) positive catches (1~3); and (c) high catches (≥ 4). The high catches number of four was estimated from the lower limit of the upper quartile (Q3) of the number of bigeye tuna caught. The Q3 was obtained from 7750 observational data. The result of this analysis was the full matrix of high catches data of bigeye tuna and environmental variables. Table 3.1 is a part of the full matrix. This result was used to generate the optimum range by using ECDF (section 3.3.4)

Table 3.1 The full matrix of high catches data

Date	Month	Year	Latitude	Longitude	Number of bigeye tuna	SST	SSC	SSHD
9	2	2006	-14.333	112.167	4	28.19	0.055	-10.3
9	2	2006	-13.350	114.667	4	28.610	0.0905	0.3
10	2	2006	-14.167	113.167	4	28.8	0.085	-6.53
.
.
D_i	M_i	2010	Lat_i	Lon_i	max	SST_i	SSC_i	$SSHD_i$

3.3.3 Scatterplot Smoothers

Scatterplot smoothers method was employed to analyze the relationship between number of bigeye tuna and environmental variables (i.e SST, SSC and SSHD) according to Tibshirani and Hastie, 1986. In this method, each environmental variables as predictor variables were analyzed separately.

$$E(Y|X) = s(X) \quad (3.1)$$

Where Y is number of bigeye tuna, X is SST or SSC or SSHD and s is smooth functions of X. First, logarithmic transformation was applied (i.e $\log_{10}(\text{number of bigeye tuna} + 1)$). Transformation was conducted because the data type is integer and asymmetric. A factor 1 was added before log-transformation to account zero number of bigeye tuna. To estimate $s(x)$ from the data, we can use any reasonable estimate of $E(Y|X=x)$. One class estimates are the local average estimates:

$$\hat{s}(x_i) = \text{Ave}_{j \in N_i} \{y_j\} \quad (3.2)$$

Where, Ave represents averaging operator (mean) of y_j of N_i data. To calculate N_i , the data points are sorted by increasing x value, a formal definition is:

$$N_i = \{\min(w_1, 1), (w_2, 2), \dots, \max(w_{50}), 50\} \quad (3.3)$$

Where, the total number of class (knots) was determined that is 50, w is span/ window/ interval which has the same total points in each interval. In addition, point in each interval was determined by total number observation divided by total number of class.

Due to all data observation were used, the span size (w) is different depend on the data rank as shown in the Fig. 3.3.

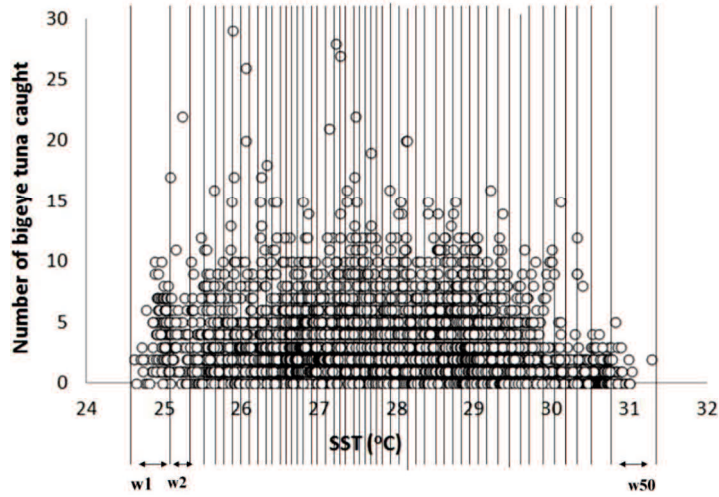


Figure 3.3 Data illustration

The span w controls the smoothness of the resulting estimate, and it is chosen according to the data distribution of each predictor variables. The Ave in eq.3.2 of this chapter stands for polynomial estimates as defined by :

$$\hat{s}(x_i) = c_1 + c_2x + c_3x^2 + \dots + c_{n+1}x^n \quad (3.4)$$

$$[ck] = \left[\sum_{k=1}^n f_i(X_k) \cdot f_j(X_k) \right]_{n \times n}^{-1} \left[\sum_{k=1}^n f_j(X_k) \cdot y_k \right]_{n \times 1} \quad (3.5)$$

Where $f_1=1$, $f_2=x$, $f_3=x^2$, $f_i=x^n$, x is the average in each w_i span and y_k the average of \log_{10} (number of bigeye tuna+1) in w_i span, the bracket symbols means all the calculation was determined by using matrix. This model was evaluated by using P_{value} (i.e the probability that our data would be at least this inconsistent with the hypothesis) and coefficient determination (R^2) was calculated to analyze the influence of predictor variables to the number of bigeye tuna as defined below:

$$R^2 = 1 - \frac{\sum_{i=1}^n (y_k - \hat{s}(x_i))^2}{\sum_{i=1}^n (y_k - \bar{y})^2} \quad (3.6)$$

Where \bar{y} is the total average of the number of bigeye tuna. High number of R^2 means high relation of both data. By applying scatter plot function, σ^2 of each span was almost same, so that the trend can be determined.

3.3.4 Generating the optimum range of environmental variables

Preferred environmental conditions were obtained by considering confidence ranges of high catches data of ECDF. The stronger association between the two environmental variables and number of bigeye tuna were analyzed using ECDF. In this analysis, three functions, $f(t)$, $l(x_i)$, $g(t)$, were used (Perry and Smith, 1994; Andrade and Garcia, 1999) as follows:

$$f(t) = \frac{1}{n} \sum_{i=1}^n l(x_i) \quad (3.7)$$

with the indicator functions

$$l(x_i) = \frac{1}{n} \begin{cases} 1 & \text{if } x_i \leq t; \\ 0 & \text{otherwise} \end{cases} \quad (3.8)$$

$$g(t) = \frac{1}{n} \sum_{i=1}^n \frac{y_i}{\bar{y}} l(x_i) \quad (3.9)$$

$$D(t) = \max|f(t) - g(t)| \quad (3.10)$$

Where $f(t)$ is empirical cumulative distribution function of the environmental variables (i.e. SST, SSC, SSHD), t signifies an index ranking the ordered observations from the lowest to highest value of the environmental variables, n represents the number of fishing trips, $l(x_i)$ is indication function, and x_i denotes the measurement for satellite-derived environmental variables in a fishing trip i . The relationship between the number of bigeye tuna caught and environmental variables was characterized by catch weighted cumulative distribution function which was denoted as $g(t)$, where y_i is the number of bigeye tuna caught in a

fishing trip i , and \bar{y} is the estimated mean value of the number of bigeye tuna for all fishing trips. Furthermore, $D(t)$ is the absolute value of the difference between the two curves $f(t)$ and $g(t)$ at any point t , and assessed by the standard Kolmogorov–Smirnov test. The coordinate labeled ‘max’ represents the specific value of the variables at which the difference between the two curves $|f(t) - g(t)|$ was maximum. In this approach, the optimum range was determined if the $D(t)$ value is larger than $D_{critical}$ (i.e. $D_{critical}$ was obtained from the Kolmogorov-Smirnov Table).

3.3.4 Generating a simple predicted map

The optimum range of environmental variables from ECDF were considered to determine the preferred habitat of bigeye tuna. A simple predicted map was computed by combining both environmental variables range (SST, SSC and SSHD) into a single map with the same spatial and temporal resolution using spatial analyst toolbox in Arc.GIS software. This map was composed by two binary output in which white color indicates a predicted area of preferred habitat and blue color indicates low probability area (non potential habitat). Catch data were then overlaid on the map.

3.4 Results

3.4.1 Distribution of number of bigeye tuna caught and environmental data

The distribution of number of bigeye tuna caught and the three environmental variables in the Southern Waters off Java and Bali from 2006 to 2010 are shown in Figure 3.4. The distribution of the number of bigeye tuna caught was asymmetrical (Figure 3.4a). A log transformation of the number of bigeye tuna caught indicated Poisson distribution (Figure 3.4b). Bigeye tuna were caught at SST between 24.6 and 30.8°C, with the highest frequency at 28.5°C (Figure 3.4c). The range of SSC for the fishing sets was 0.02 – 0.46 mg m⁻³ and the preferable concentration ranged from 0.05 to 0.17 mg m⁻³ (Figure 4.3d). The SSHD

ranged from -20 to 30 cm and values of -5 to 15 cm were preferable for the fishing sets, with the peak at 10 cm (Figure 4.3e). The preferable environmental factors for fishing sets can be distinguished using these histograms of Figure 3.4

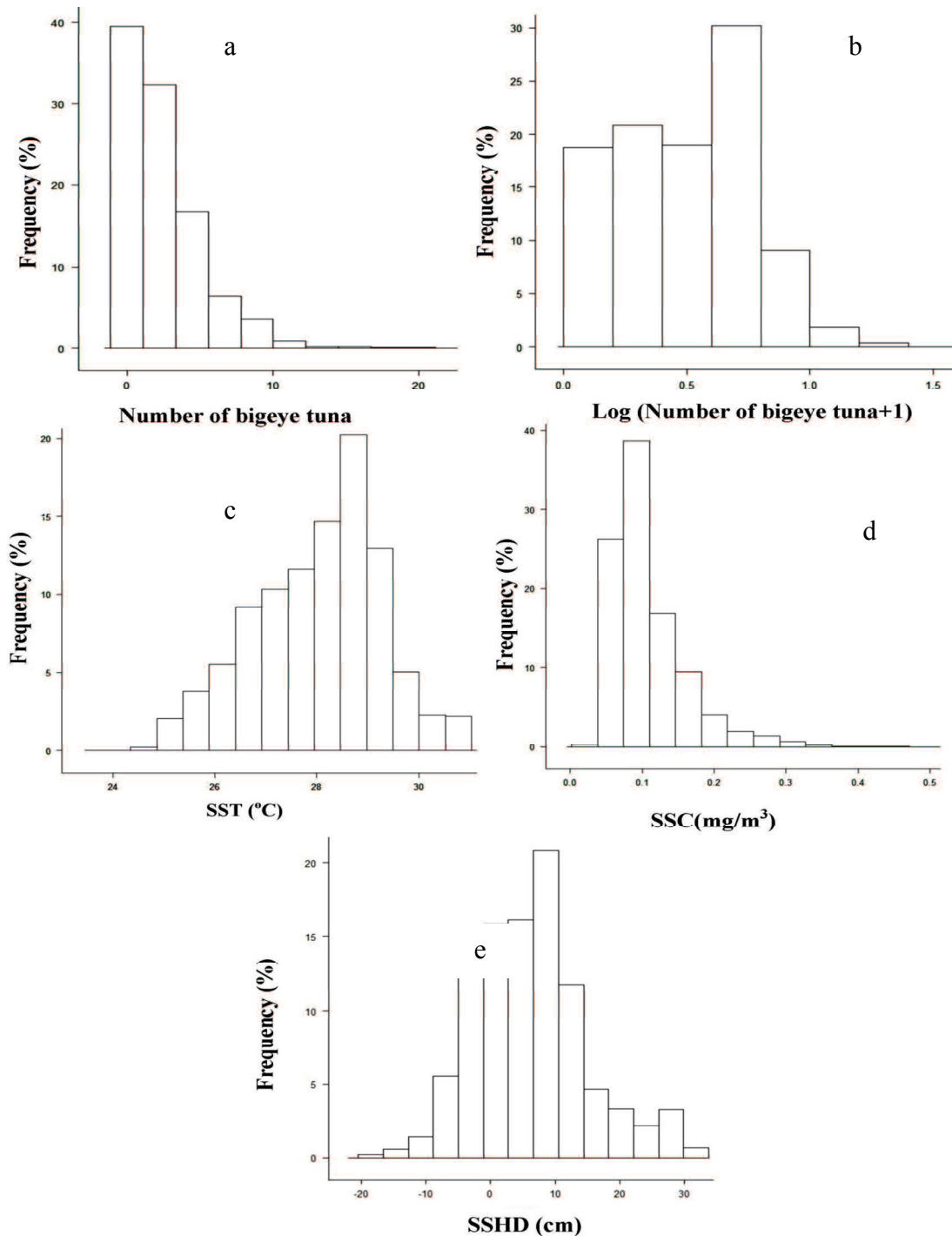


Figure 3.4 Histograms of number of bigeye tuna and environmental data: (a) distribution of number of bigeye tuna, (b) distribution of log-transformed number of bigeye tuna, (c) SST, (d) SSC, (e) SSHD.

3.4.2 Classification of fisheries data

The frequency of fishing days in relation to SST, SSC, SSHD and month is shown in Figure 3.5. For the SST, SSC and SSHD, high catches, positive catches and null catches had similar patterns, except that positive catch was the predominant group of bigeye tuna catch in the Southern Waters off Java and Bali from 2006 to 2010. The average null catch during this 5-year period was almost 19% and the highest was approximately 30% in 2010. The average positive catch frequency was approximately 53% and the frequency of high catches was approximately 28%. The average SST values for the null, positive and high catches were 28.4 ± 1.3 , 28.1 ± 1.3 , and $27.8 \pm 1.2^\circ\text{C}$, respectively; the average SSC values for the null, positive and high catches were 0.1 ± 0.06 , 0.11 ± 0.05 , and $0.11 \pm 0.05 \text{ mg/m}^3$, respectively. In addition, the average SSHD values of the null, positive and high catches were 8 ± 6 , 8 ± 7 and $8 \pm 8 \text{ cm}$, respectively. Judging from the distribution of high catches data the optimum ranges of SST, SSC and SSHD were $26.6\text{--}29^\circ\text{C}$, $0.06\text{--}0.16 \text{ mg/m}^3$ and $0\text{--}16 \text{ cm}$, respectively.

By using high catches data, the preferable time to catch bigeye tuna can be determined. High catches can be found from January to December (i.e., year round), with the highest frequency in July and the lowest in March (Figure 3.5d). The distribution of high catches data is significantly different from that of the other distributions (positive and null catches), which was confirmed using a Student's *t*-test with significance level of 95%.

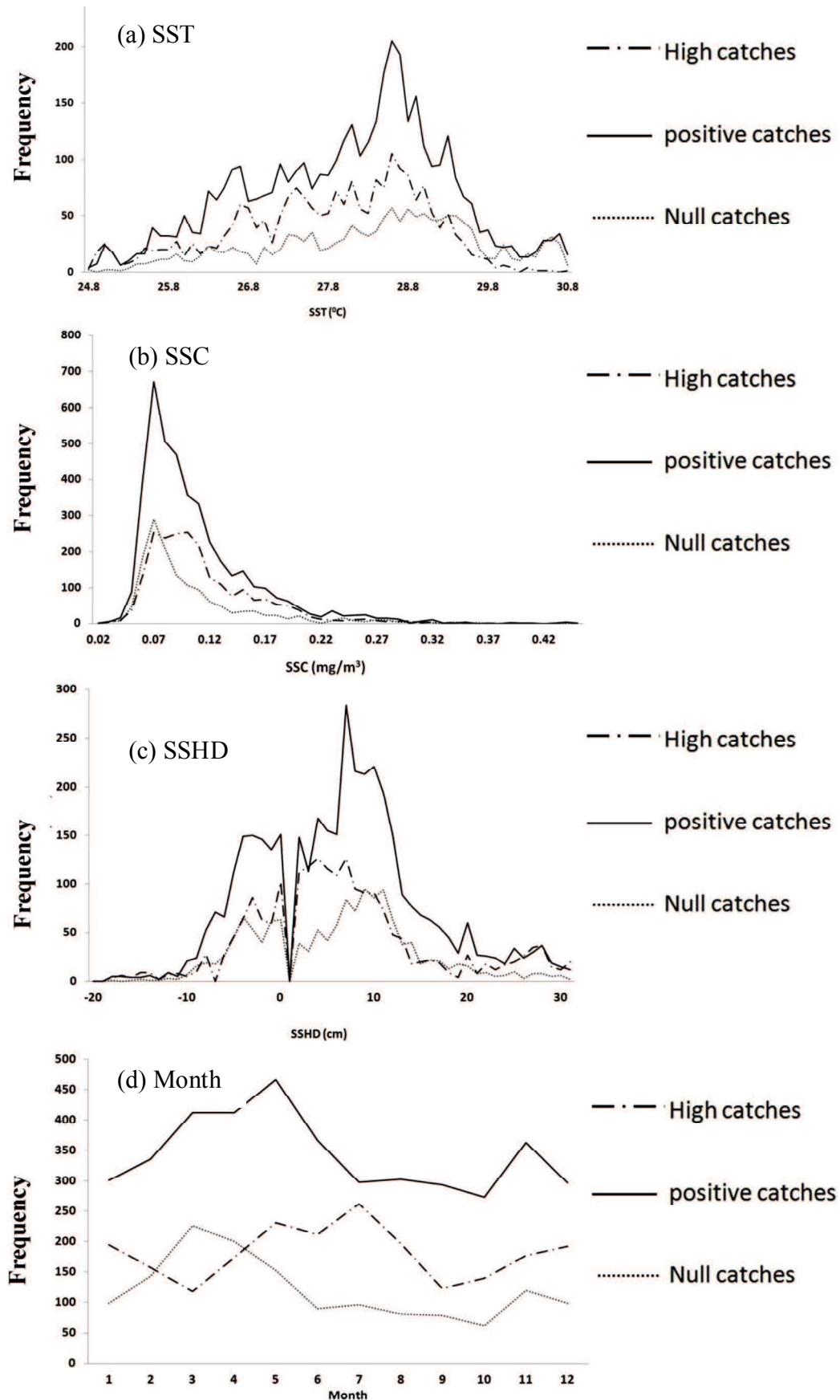


Figure 3.5 Frequency of fishing days in relation to (a) SST, (b) SSC, (c) SSHD and (d) month from 2006 to 2010. They were grouped according to the way used by Andrade and Garcia (1999).

3.4.3 Scatterplot smoothers

The relationship between the average, variance (σ^2), maximum value of bigeye tuna and SST in are shown in Figure 3.6. The average, variance and maximum value of Y axis is the transformation of number of bigeye tuna into $\log_{10}(\text{BE} + 1)$, where BE indicates number of bigeye tuna caught. The average and variance value were conducted by scatterplot smoother method (i.e by averaging the value of BE in each interval/span) in this figure. The solid line represents the average of BE in each span w, the dash line represents σ^2 (variance) and dot dash line represents maximum value in each span. This figure indicates that bigeye tuna exist in the area when SST was from 24.6°C to 30.8°C. Moreover, as the variance value is almost constant so that the trend of bigeye tuna caught is reliable. According Figure 3.6 bigeye tuna tend to decrease when SST is increased, especially when SST is higher than 29.4°C.

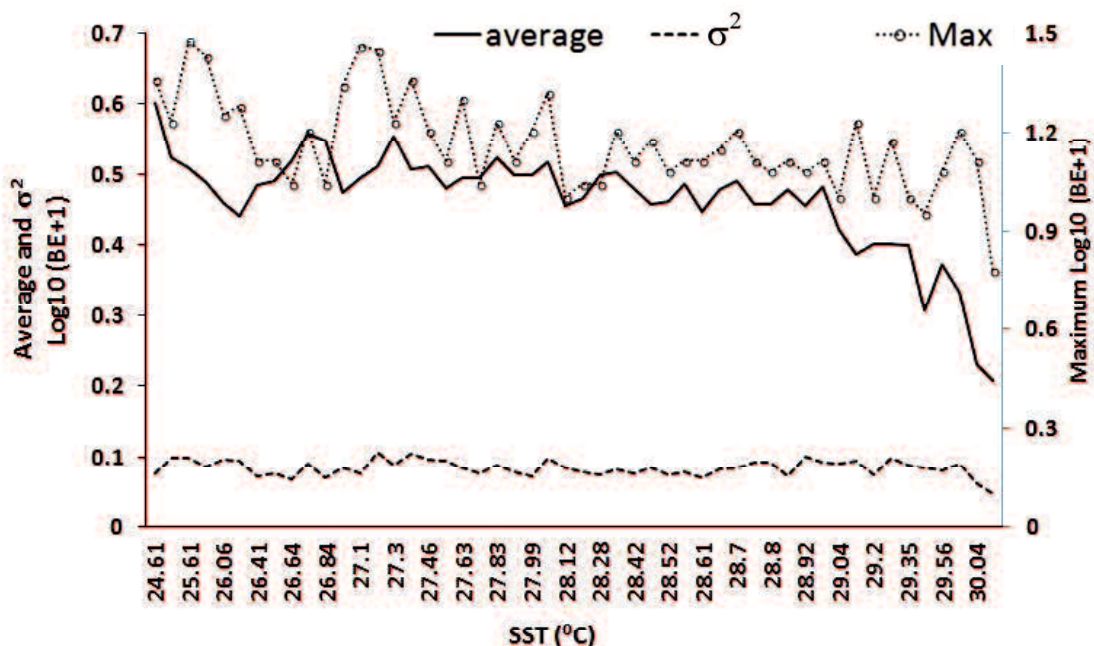


Figure 3.6 Number of bigeye tuna in relation to SST during 2006-2010

Figure 3.7 describe the relationship between SSC and number of bigeye tuna. This figure indicates that bigeye tuna exist in the area where SSC was from 0.02-0.34 mg/m^3 .

Because we used the same sample number in each span, variance is constant as shown in the dash line, so that the trend can be observed. Moreover, bigeye tuna tend to increased as SSC is increases until 0.151 mg/m³, but more than it number of bigeye tuna tend to decrease. However, generally speaking, the maximum value tend to increase when SSC increases.

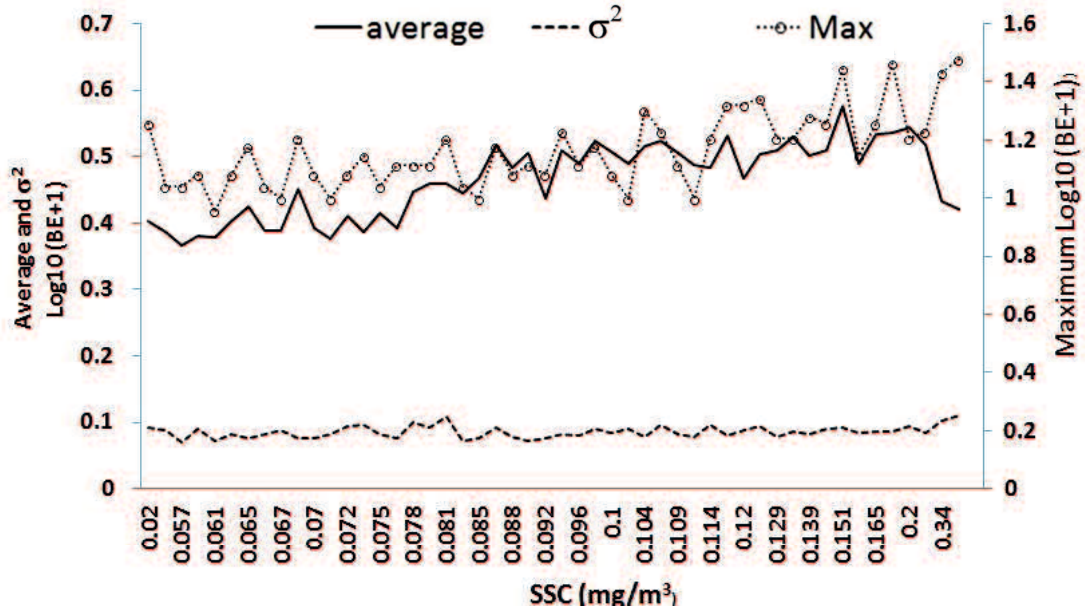


Figure 3.7 Number of bigeye tuna in relation to SSC during 2006-2010

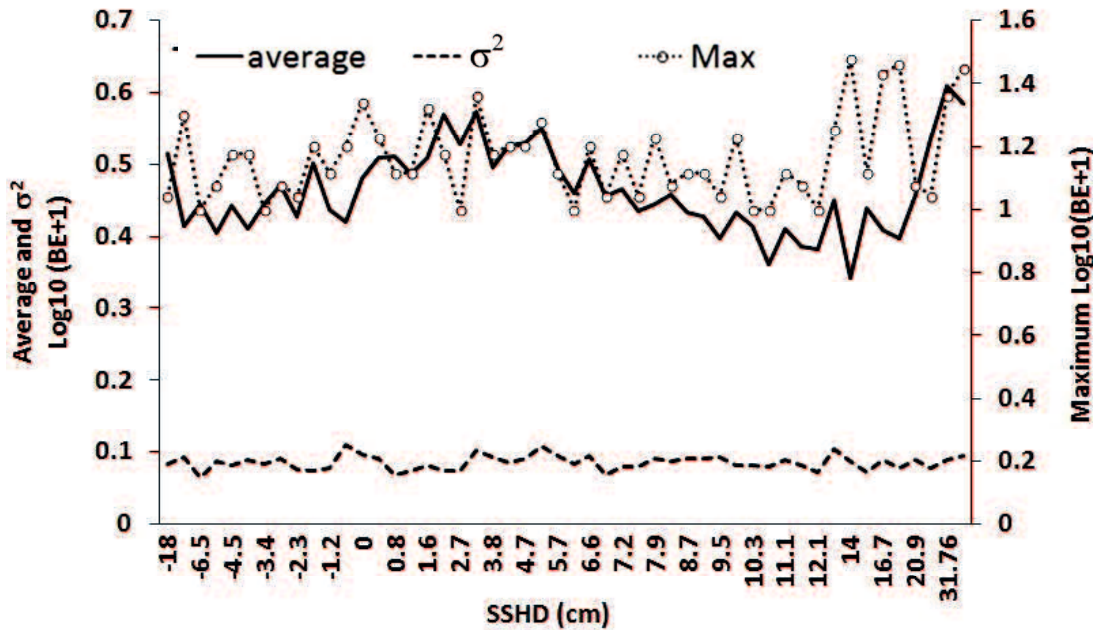


Figure 3.8 Number of bigeye tuna in relation to SSHD during 2006-2010

Figure 3.8 shows the relationship between the number of bigeye tuna and SSHD. Bigeye tuna were found in the area that had the SSHD range from -18.46 to 31.76 cm. In addition, the variance is also constant as shown in the dash line with the average of SSHD is fluctuated as shown in the solid line and maximum value is high when it reach extreme positive of SSHD.

3.4.4 Relationship between environmental factors and bigeye tuna caught

Figure 3.9 shows the relationship between the average number of bigeye tuna caught and SST in each span w. The average number of bigeye tuna in each span was explained in the section 3.3.3. From Fig 3.9, it can be said that SST has strong relationship with bigeye tuna with the R^2 is 0.85. In addition, the number of bigeye tuna tends to decrease when SST increases, especially when SST is equal and more than 29°C . In other words, bigeye tuna increases when SST is less than 29°C . That is bigeye tuna prefer to remain in the low SST in the study area.

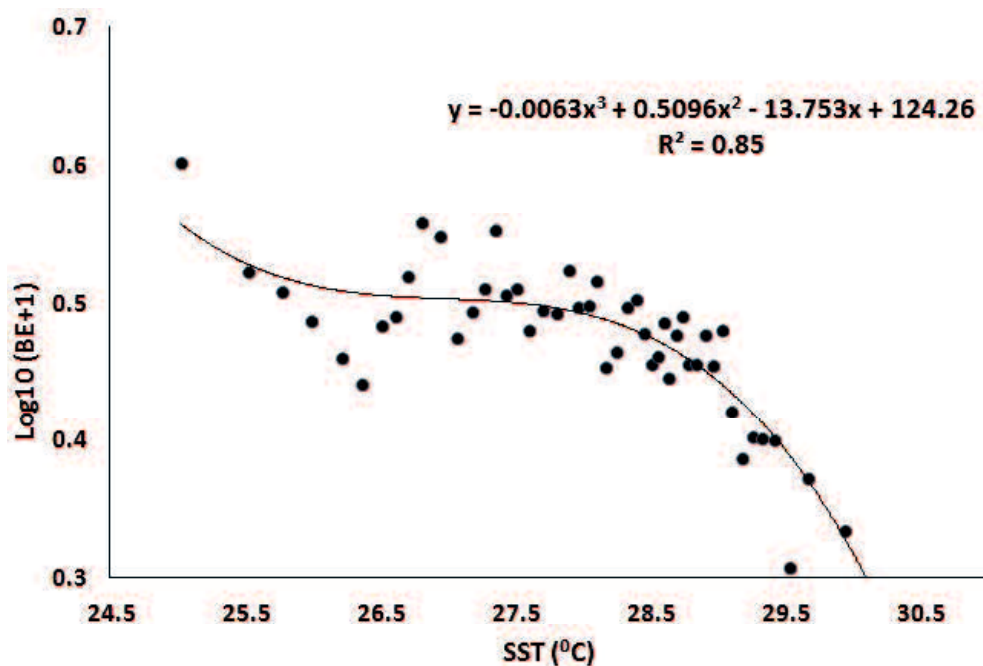


Figure 3.9 Average number of bigeye tuna SST from 2006-2010.

Figure 3.10 shows the relationship between the average number of bigeye tuna caught and SSC in each span w. It can be seen that SSC has strong relationship with bigeye tuna with the R^2 is 0.78. In addition, the number of bigeye tuna tend to increased when SSC is increased until $0.16\text{mg}/\text{m}^3$, but number of bigeye tuna gradually decreases when SSC concentration is more than $0.17\text{mg}/\text{m}^3$.

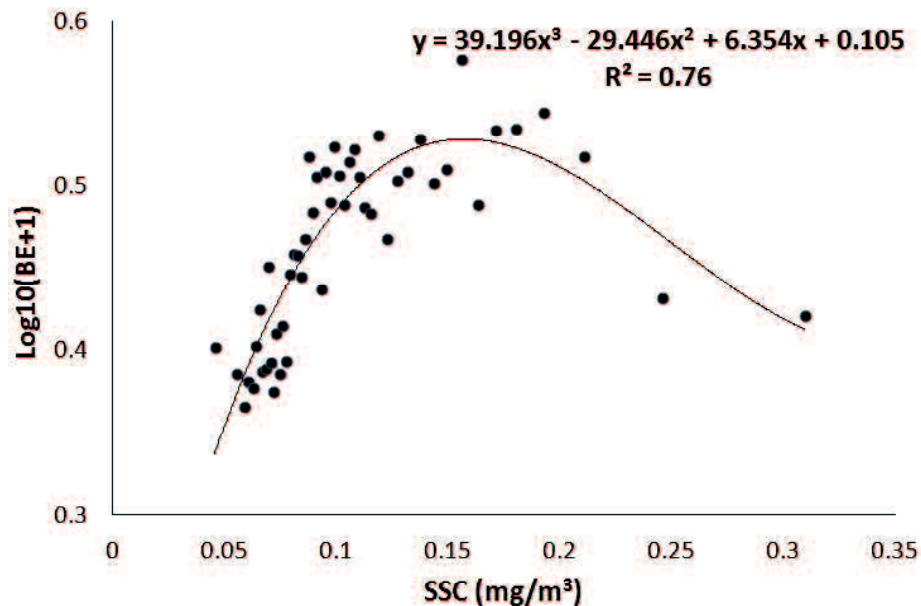


Figure 3.10 Average number of bigeye tuna in relation to SSC from 2006-2010

Figure 3.11 shows the relationship between the average number of bigeye tuna caught and SSHD in each span w. This figure states that SSHD has strong relationship with bigeye tuna with R^2 of 0.72. From this figure, we can see that the number of bigeye tuna is fluctuated. Number of bigeye tuna is high when SSHD is in the extreme negative value, low positive value and extreme positive value. However in the both side of extreme negative and positive value, the standard error of SSHD is also high (i.e., it is related with wide span size in the extreme values).

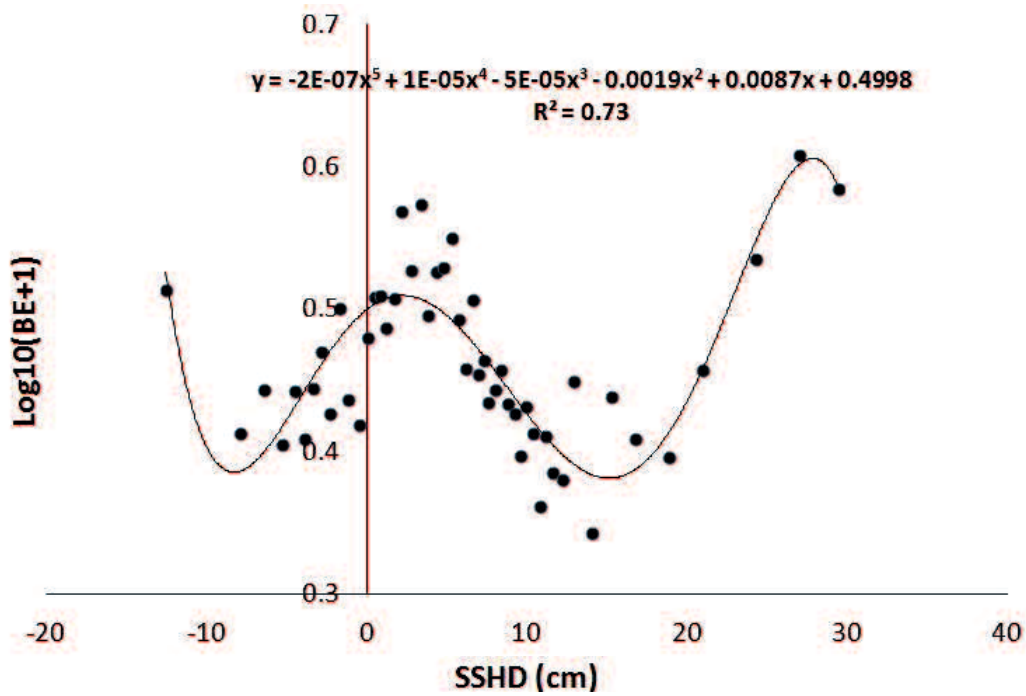


Figure 3.11 Average number of bigeye tuna in relation to SSHD from 2006-2010

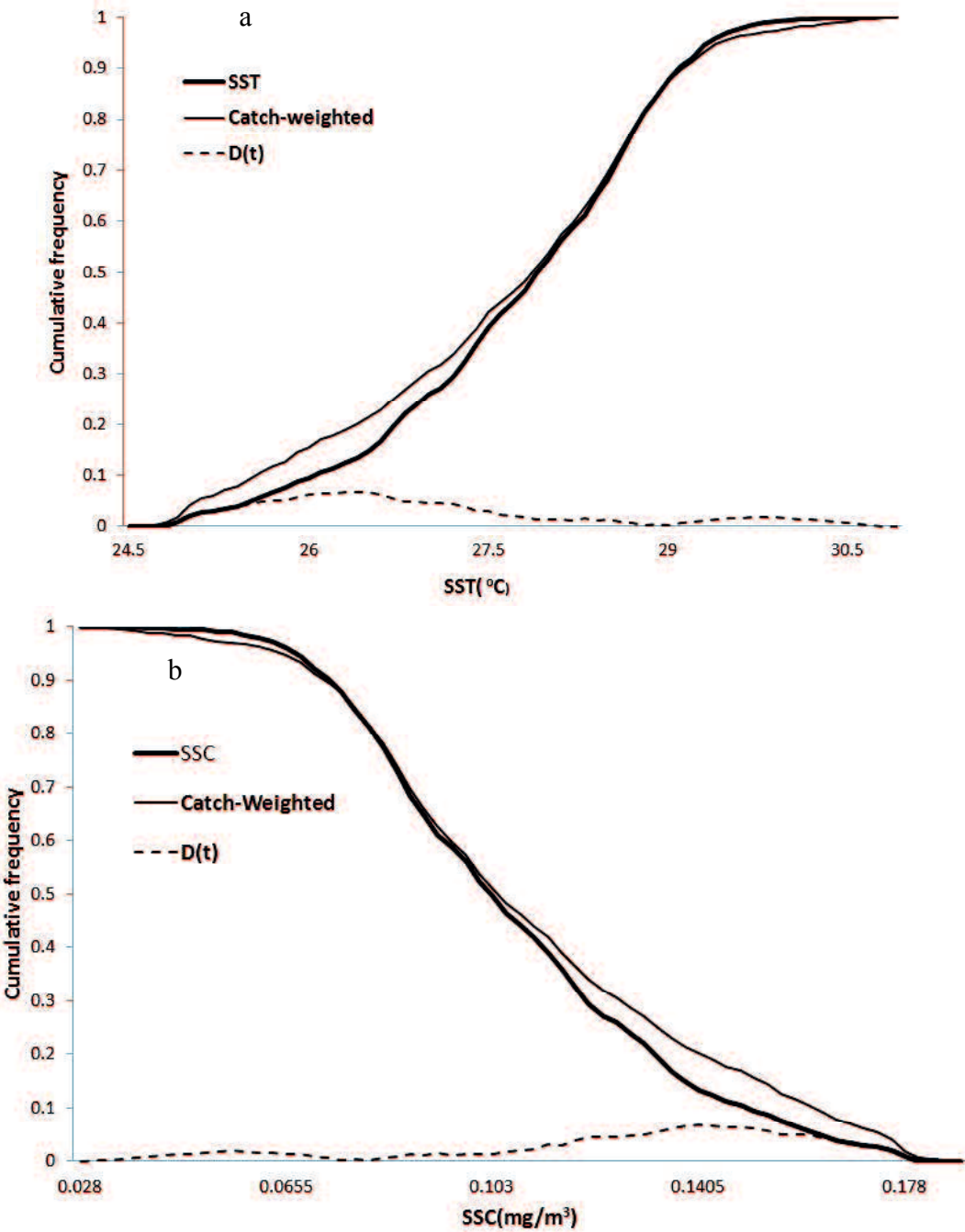
The result of the polynomial regression analysis using scatter smoothers function is summarized in Table 3.2. In this chapter, we analyzed each parameter separately.

Table 3.2 Regression analysis result

Model	P-value	R ²
SST	3.7x10 ⁻¹⁹	0.85
SSC	3.12x10 ⁻¹⁴	0.78
SSHD	1.53x10 ⁻¹¹	0.73

According to Table 3.2, three parameters (SST, SSC, SSHD) were highly significant as shown with low P-value (P-value < 0.01). Furthermore, SST, SSC, SSHD influenced the number of bigeye tuna caught with the range of R² equal to 73 to 82 % which means the strong relationships.

Polynomial regression can estimate how important the impact of environmental variables to the number of bigeye tuna, but it has difficulty to estimate the optimum value of environmental variables for bigeye tuna preference. Hence, ECDF was applied by using high catches data groups. Using the ECDF, the relationship between bigeye tuna and the three environmental variables were obtained. The results are shown in Figure 3.12



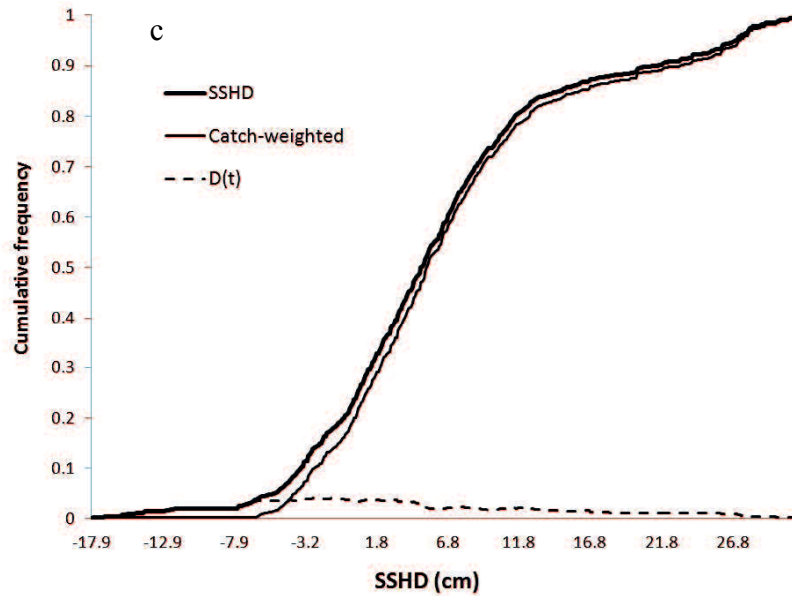


Figure 3.12 Empirical cumulative distribution frequencies for (a) SST, (b) SSC and (c) SSHD as weighted by bigeye tuna catch during the period of 2006-2010.

The cumulative distribution curves of the variables are different and the degrees of the difference ($D(t)$) between two curves (i.e., SSHD-catch-weight) are highly significant ($P < 0.01$). The results showed a stronger association between the number of bigeye tuna caught and the variables, with SST ranging from 25.2 to 27.5 °C (Figure 3.11a), SSC ranging from 0.11 to 0.17 mg/m³ (Figure 3.12b) and SSHD ranging from -6.7 cm to 4.8 cm (Figure 3.12c). The optimum ranges were obtained from the ranges when calculated $D(t)$ is bigger than critical $D(t)$ (i.e., Kolmogorov-Smirnov Table). The strongest associations between the number of bigeye tuna caught and the variables occurred at 26.4°C of SST, 0.14 mg/m³ of SSC and -1.1 cm of SSHD, respectively (i.e. the strongest associations means the highest value of $D(t)$). The number of bigeye tuna caught tended to decrease in the ranges of outside these preferable ones. Based on these results, the preferred environmental conditions for bigeye tuna can be in the areas of SST: 25.2 to 27.5 °C, SSC: 0.11 to 0.17 mg/m³, and SSHD: -6.7 cm to 4.8 cm.

Then, those preferred environmental conditions of bigeye tuna were plotted into simple predicted map as shown in Figure 3.12.

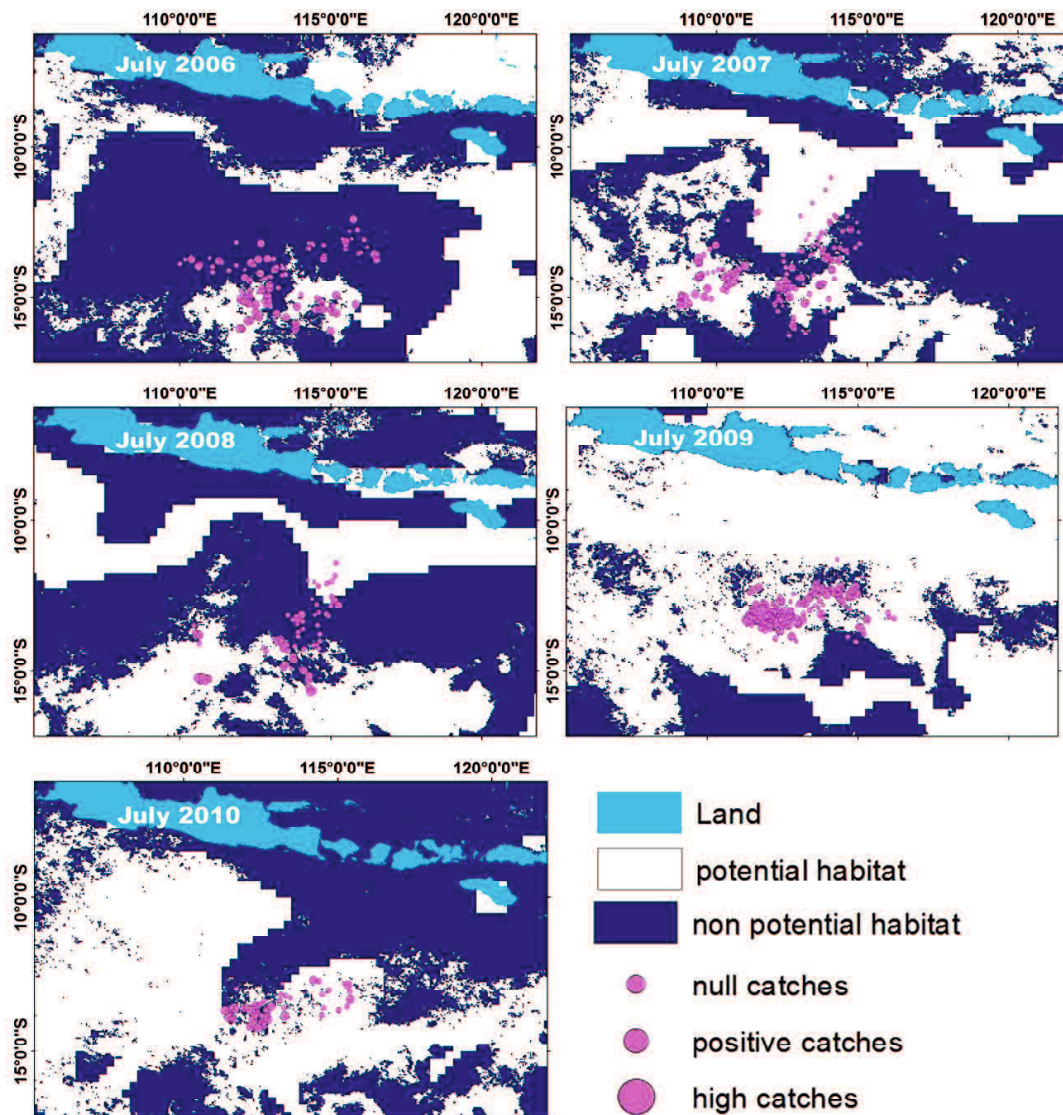


Figure 3.13 Spatial distribution of longline fisheries in July from 2006 to 2010 overlaid with simple prediction map generated from combination of SST, SSC and SSHD

The figure describes the preferred location of bigeye tuna in July from 2006 to 2010. July was selected for predicted map due to the highest frequency of high catches data as shown in Figure 3.5d. The simple predicted map and the spatial distribution of bigeye tuna were not same. Bigeye tuna mostly found in the area around 12°S to 15°S and in the western part of the study area. The predicted area of occurrence (i.e., potential habitat) was the

widest in July 2009 and it associated with the El-Nino phenomenon in the Indian Ocean (Kim et al., 2011). In addition, the El-Nino phenomenon affected oceanographic condition in the southern waters of Java and Bali and the El-Nino had a positive effect on catch rate of bigeye tuna (Syamsuddin et al., 2013).

3.5 Relationship between ocean dynamics and preferred habitat for bigeye tuna

Combining observations of ocean dynamics from satellite and in-situ observations related to the fisheries abundant is necessary because they are complimentary types of data each other. In this study, we combined remote sensing data and catch data of bigeye tuna in the southern waters off Java-Bali in order to examine the relevance between the number of bigeye tuna and environmental variables. The availability of bigeye tuna catch data from one of the biggest tuna fishing industry in Indonesia helped much in providing the fish catch data in the southern waters off Java-Bali. According to the distribution of fishing activity, the fishing effort of the tuna longliner was distributed in 10°S - 18°S and 110°E - 118°E and it had not changed significantly for 5 years. Hence, the change of environmental variables is important to evaluate bigeye tuna existence in the study area.

Bigeye tuna catch rate varied as time and environmental variables changed (Figure 3.5). The highest fishing activity was from June to October because of low null catches and rich high catches (Figure 3.5d). Most of the null catches occurred during the northwest monsoon season, especially from February to April (Figure 3.5d). This condition imposed high costs on fishermen. According to the classification of fisheries data, the average frequency of null catches over five years was 19% and it reached almost 30% in 2010, when a strong La Nina event was observed (Feng et al., 2013).

Like other pelagic species, bigeye tuna has their preferred living environment. Then bigeye tuna catch statistics should have some correlation with the ocean environmental parameters, such as SST, SSC and SSHD. According to the SST, SSC and SSHD trend line

which were described in Figure 3.9, Figure 3.10 and Figure 3.11 stated that bigeye tuna has high correlation with environmental variables and tend to stay low of SST, low SSC and low positive of SSHD and extreme SSHD. These conditions are related to bigeye tuna behavior. Bigeye tuna prefer to stay in low SST to prevent overheating (Brill et al., 1994), thus it would need to curtail heat retention to avoid thermal limits of activity and distribution (Neill et al., 1976). This condition mostly occurs in the tropical waters which has almost same of SST.

The other environmental variable which influenced bigeye tuna distribution is SSC. Bigeye tuna is a visual predator which depends on the water clarity to forage their prey (Sund et al., 1981). They remain to stay in the clear water to increase the efficiency of prey foraging. Clear water means poor of nutrient which can be reworded as low SSC concentration. Hence, most of the fishing activities were found in the low SSC. Even though fishing data was not free from bias based on the fishermen's choice of fishing locations, it was the low cost of bigeye tuna distribution data sets which available to fishery scientists (Mugo et al., 2010).

SSHD also influence bigeye tuna behaviour, because bigeye tuna migration was influenced by the thermocline layer and its can be measured by calculating SSHD (Syamsudin et al., 2013). According to Syamsudin et al., 2013, extreme negative SSHD gave the positive effect to bigeye tuna because it make the thermocline layer is closer to the surface. In this chapter, extreme negative SSHD also give the positive effect to the number of bigeye tuna but it has high standard error. In this chapter, low positive SSHD give the lowest standard error of SSHD and gave the positive effect to the number of bigeye tuna in the study area.

Frequency distribution of each environment variable was used to evaluate the descriptive influence of each parameter to the bigeye tuna, which was classified into three

categories, “null catches”, “positive catches” and “high catches”, and then ECDF were applied to find the optimum range of environmental variables for bigeye tuna only for high catches.

This chapter showed that the highest number of bigeye tuna caught corresponds to the area of about 26.4°C of SST, 0.14 mg/m³ of SSC and -1.1 cm of SSHD (Figure 3.12). Hence, these areas were referred to as potential habitat for bigeye tuna (Figure 3.13). It is interesting to define that these biologically important areas can be plotted over a map to detect their spatial pattern. Moreover, bigeye tuna distributions were associated with the spatial pattern of productive habitat every year (Setiawati et al., 2015). Therefore, all environmental variables could be regarded as reasonable indices of environmental conditions used to find areas with the highest probability of bigeye tuna.

Overall, SST, SSC and SSHD ranges in the study area are relatively small compared with the subtropical area, and it makes difficult to understand the relationship of these data and bigeye tuna fisheries data by using statistical analysis. For that reason, some data treatment was used to minimize the large variance of the data. The advantage of this research is simple method can analyze the relationship of environmental remote sensing data and fisheries data which can be displayed both numerically and in graphics. However, all the predictor variables were analyzed separately and the functions need more smoothness. Then, we applied cubic spline smoother function in the Chapter 4.

3.6 Conclusions

The results showed that SST, SSC and SSHD had a high correlation with the bigeye tuna abundance. Therefore, all of environmental factor could be regarded as reasonable indices to study the bigeye tuna preferred habitat. The spatial patterns of bigeye tuna preference have a typical characteristic of low SST, low SSC and low positive SSHD and extreme SSHD values.

In the future research, more predictor variable are necessary to improve our understanding about the relationship between environmental variables and bigeye tuna fisheries and other statistical analysis should be used to analyze the interaction of environmental variables and bigeye tuna such as Generalized Additive Model (GAM) in which the data are not always necessary to be linear. Moreover, the combination of satellite remote sensing techniques and fisheries catches data could be used to identify habitat preference and migration movements of bigeye tuna.

CHAPTER 4

APPLICATION FOR OPEN OCEAN TUNA HABITAT 2

Characterization of Bigeye Tuna Habitat in the Southern Waters Off Java-Bali Using Remote Sensing Data

4.1 Introduction

The Southern Waters off Java and Bali, part of the Indian Ocean, are known as important spawning grounds for commercial tuna and tuna-like species (Nishikawa et al., 1985) and are identified as a potential fishing ground for large pelagic fish (Bailey et al., 1987; Osawa and Julimantoro, 2010). Biological and environmental data from the study area are needed to understand the preferred habitat for sustainable management of bigeye tuna resources. In this chapter, the same remote sensing environmental data (i.e., SST, SSH, SSC) and fisheries data as in Chapter 3 were used. In the previous chapter, all environmental variables have high correlation with the number of bigeye tuna. However, all the predictor variables were analyzed separately and the functions was conducted by averaging the predictor variable in each interval. In this chapter, we applied spline smoother function as an additive and all predictor variables were combined with the assumption interactions between predictor variables were excluded. This method is called Generalized Additive Model (GAM) which can deal with nonlinear data.

A GAM is a semi-parametric extension of a generalized linear model, which has the smooth components of the explanatory variables (Guisan et al., 2002) and has capacity to express highly nonlinear and non-monotonic relationships between the response and explanatory variables (Lizarazo, 2012). Moreover, GAM can handle large number of sample and it is not necessary to group continues variables (i.e., SST, SSH, SSC). GAMs can explain the fisheries data and environmental variables and enhance our understanding of ecological systems (Zagaglia et al., 2004; Song et al., 2008; Valavanis et al., 2008; Druon et

al., 2011). This method is basically similar with the previous study, but it rarely applied in the current study area. Moreover, only Syamsuddin et al., 2013 applied this method in the same study area, but they mainly concerned about the relationship between ELNINO and bigeye tuna catches in 1998-2000. More research in the same area is important to understand the influence of environmental variables to the existence of bigeye tuna. In addition, by comparing the previous result with the same method and same study area, generalization of habitat characteristics in the study area can be determined. Furthermore, statistical models and geographic information systems (GIS) have the ability to improve species habitat studies. Given this background, this work attempted to investigate the characteristics of bigeye tuna habitat in the Southern Waters off Java and Bali by utilizing satellite data and bigeye tuna catch data during 2006–2010. GAM and GIS data were combined to understand the characteristic of bigeye tuna habitat.

4.2 Materials and Methods

4.2.1 Study Area

The Southern Waters off Java and Bali, part of the Indian Ocean, is selected as a study area and is located between 10°S and 18°S latitude and 110°E and 118°E longitude as shown in Figure 4.1 which is made by combining Figure 1.2 and Figure 3.1. Five dominant waves and current systems pass study area; Indonesian Throughflow (ITF), Indian Ocean South Equatorial Current (SEC), South Java Current (SJC), Indian Ocean Kelvin Waves (IOKW), and Rossby Waves (RW). The ITF transfers high heat content from the Pacific Ocean to the Indian Ocean through a series of straits along the Indonesian archipelago, and initially accumulates the heat in the region between northwestern Australia and Indonesia (Qu and Meyers, 2005; Gordon et al., 2010). The SEC flows westward from the west side of Australia, and is a large-scale current in this region, where mass and property exchange

(Meyers, 1996). In the northern part of the study area, the SJC and the IOKW flow near the Sumatra–Java coast (Sprintall et al., 2010). The SJC changes direction twice each year when the IOKW associates with the SJC near this coast. The RW propagates westward at 12°S – 15°S (Gordon, 2005).

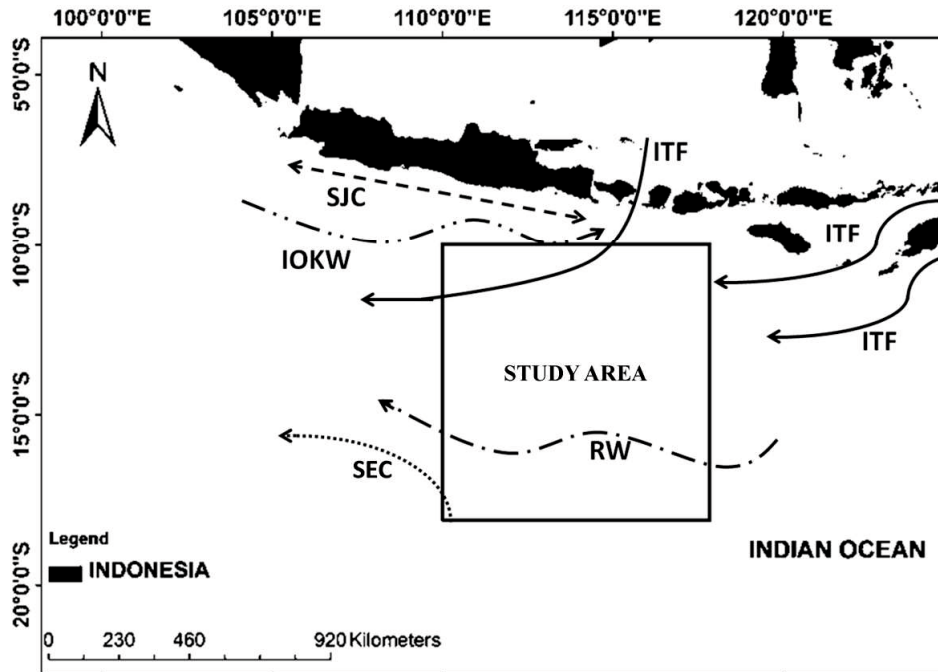


Figure 4.1 The study area in the Southern Waters off Java-Bali. This area has been passed by five dominant waves and current systems, namely, South Java Current (SJC), Indonesia Through Flow (ITF), Indian Ocean Kelvin Waves (IOKW), Rossby Waves (RW), and the Indian Ocean South Equatorial Current (SEC). (Modified from Syamsudin et al., 2013)

The study area is characterized by a tropical monsoon climate that results from the Asian-Australian monsoon wind systems that change direction seasonally. During July–September, the prevailing southeast monsoon favors upwelling along the coast of Java and Bali and Sumatra (Du et al., 2008; Ningsih et al., 2013). These conditions are reversed during the northwest monsoon from November to April and create warm SSTs (Susanto et al., 2006; Manessa and As-syakur, 2011). The Southern Waters off Java and Bali are not only forced by intense annually reversing monsoonal winds, but are also influenced by variability in throughflow currents (mainly the ITF) (Feng and Wijffels, 2002).

4.2.2 Fisheries data and classification

Data sets for bigeye tuna catch from January 2006 to December 2010 were used which provided by PT Perikanan Nusantara. The data sets consisted of geographic positions (latitude and longitude) of the fishing activities, the operational days, vessel numbers and the number of tuna caught per day during the period (see Table 3.1). We digitized and compiled all data into a monthly database. The unit of daily catch data referred to the number of bigeye tuna caught. We assume that fish catch was caught one boat in one location. So, it is proportional to fish density in one location. Classification of fisheries data was used in this chapter as in Chapter 3.

4.2.3 Remote sensing data

As an environmental database, monthly SST, SSC, and SSHD were used in this study, as in chapter 3. Monthly values of SST, SSC and SSHD data were extracted from each pixel corresponding to the location of fishing activities. The result was a full matrix of the number of bigeye tuna and the environmental variables. The full matrix was used in the GAM analysis.

4.2.4. Application of Generalized Additive Model (GAM)

GAM models were used in this chapter to assess the influence of environmental variables on potential bigeye tuna habitat. This statistical method has been commonly used to predict the habitat and fishing grounds of tuna in the Pacific and Atlantic oceans (Zagaglia et al., 2004; Zainudin et al., 2006, 2008; Mugo et al., 2010), but has rarely been applied in the current study area. The advantage of this statistical model is that it allows for analysis of non-parametric relationships and extends the use of additive models to data sets that have non-Gaussian distributions, such as binomial, Poisson and gamma distributions. The additive function of GAM is smoothing function in each predictor variables.

GAM model was created in *R version 3.0.2 software*, using the *gam* function of the *mgcv* package (Wood, 2006), with the number of bigeye tuna as a response variable and SST, SSC, and SSHD as predictor variables with the data structure in Table 4.1.

Table 4.1 Data structure of environmental variables and fish catch

N	X	Y	Z
N_1	X_1	Y_1	Z_1
N_2	X_2	Y_2	Z_2
N_m	X_m	Y_m	Z_m

Where N indicates number of bigeye tuna, X is SST, Y is SSC and Z is SSHD. By this data structure, the relationship of three predictor variables and bigeye tuna was conducted as explained in the following equation.

$$N = N_0 + \alpha X + \beta Y + \gamma Z \quad (4.1)$$

Where, N_0 is equal to constant value (i.e total average of N) and α , β , and γ represents the smoothing function as explained in the Eq.4.2

$$\hat{N} = N_0 + f_1 X + f_2 Y + f_3 Z + \varepsilon \quad (4.2)$$

Tibshirani and Hastie (1986) define partial residual in Eq. 4.3

$$R_j = \hat{N} - N_0 - \sum_{k \neq j} f_k(X_k) \quad (4.3)$$

where, R_j is partial residuals and f_k is smoothing function in each parameter. Then $(E(R_j|X_j) = f_j(X_j))$.

$$R_1 = \hat{N} - N_0 - (f_2 Y) - (f_3 Z) \quad (4.4)$$

where, $R_1 = f_1(X)$, $R_2 = f_2(Y)$, $R_3 = f_3(Z)$

$$R_1 = \hat{N} - N_0 - (R_2) - (R_3) \quad (4.5)$$

$$\hat{N} - N_0 = (R_1) + (R_2) + (R_3) \quad (4.6)$$

$$\hat{N} - N_0 = f_1(X) + f_2(Y) + f_3(Z) + \varepsilon \quad (4.7)$$

$$\hat{N} = N_0 + f_1(X) + f_2(Y) + f_3(Z) + \varepsilon \quad (4.8)$$

Where, f_1 , f_2 and f_3 are spline function, \hat{N} is equal to $g(\mu)$, g is link function (i.e Log10) and μ is number of bigeye tuna +1. So, the final GAM equation can be described in Eq.4.9

$$g(\mu) = N_0 + f_1(X) + f_2(Y) + f_3(Z) + \varepsilon \quad (4.9)$$

To calculate the smoother function, backfitting algorithm was conducted.

Initialization

$$N_0 = E(\hat{N}), f_1^1(\cdot) = f_2^1(\cdot) = f_3^1(\cdot) = 0 \quad (4.10)$$

Where:

$$f_j^m(X_j) = E[R_j|X_j]; \quad m= \text{iteration}; \quad j= 1,2,3; \quad X_1=X, \quad X_2=Y, \quad X_3=Z \quad (4.11)$$

$$R_j = \hat{N} - N_0 - \sum_{k=1}^{j-1} f_k^m(X_k) - \sum_{k=j+1}^3 f_k^{m-1}(X_k) + \varepsilon \quad (4.12)$$

$$\text{Until } \text{RSS} = (\hat{N} - N_0 - \sum_{j=1}^3 f_j^m(X_j))^2 \text{ fail to decrease} \quad (4.13)$$

Table 4.2 Iteration process

$m \setminus j$	1	2	3	RSS
1	$R_1 = \bar{N} - N_0$ $f_1^1 = 0$	$R_2 = \bar{N} - N_0$ $f_2^1 = 0$	$R_3 = \bar{N} - N_0$ $f_3^1 = 0$	$RSS = E(\bar{N} - N_0 - \sum_{j=1}^3 f_j^1(X_j))^2$ $= E(\bar{N} - N_0)^2 = \varepsilon^2$
2	$R_1 = \bar{N} - N_0$ $f_1^2(X) = E[\bar{N} - N_0 X]$	$R_2 = \bar{N} - N_0 - f_1^2(X)$ $f_2^2(Y) = E[\bar{N} - N_0 - f_1^2(X) Y]$ $= E[\bar{N} - N_0 Y] - E[f_1^2(X) Y]$	$R_3 = \bar{N} - N_0 - f_1^2(X) - f_2^2(Y)$ $f_3^2(Z) = E[\bar{N} - N_0 - f_1^2(X) - f_2^2(Y) Z]$ $= E[\bar{N} - N_0 Z] - E[f_1^2(X) Z] - E[f_2^2(Y) Z]$	$RSS = E(\bar{N} - N_0 - f_1^2(X) - f_2^2(Y) - f_3^2(Z))^2$ $= E[\bar{N} - N_0 - E[\bar{N} - N_0 X] - E[\bar{N} - N_0 Y] - E[f_1^2(X) Y] - E[\bar{N} - N_0 Z] + E[f_1^2(X) Z] + E[f_2^2(Y) Z]]^2 < \varepsilon^2$
3	$R_1 = \bar{N} - N_0 - f_2^2(Y) - f_3^2(Z)$ $f_1^3(X) = E[\bar{N} - N_0 - f_2^2(Y) - f_3^2(Z) X]$ $f_1^3(X) = E[\bar{N} - N_0 X] - E[f_2^2(Y) X] - E[f_3^2(Z) X]$	$R_2 = \bar{N} - N_0 - f_1^3(X) - f_3^2(Z)$ $f_2^3(Y) = E[\bar{N} - N_0 Y] - E[f_1^3(X) Y] - E[f_3^2(Z) Y]$	$R_3 = \bar{N} - N_0 - f_1^3(X) - f_2^3(Y)$ $f_3^3(Z) = E[\bar{N} - N_0 Z] - E[f_1^3(X) Z] - E[f_2^3(Y) Z]$	$RSS = E(\bar{N} - N_0 - f_1^3(X) - f_2^3(Y) - f_3^3(Z))^2$ $= E[\bar{N} - N_0 - E[\bar{N} - N_0 X] + E[f_2^2(Y) X] + E[f_3^2(Z) X] - E[\bar{N} - N_0 Y] + E[f_1^3(X) Y] + E[f_3^2(Z) Y] - E[\bar{N} - N_0 Z] + E[f_1^3(X) Z] + E[f_2^3(Y) Z]]^2 < \varepsilon^2$

The number of bigeye tuna caught data distribution was right skewness as shown in Figure 3.4. Hence, to reduce right skewness, logarithmic transformation was applied. Logarithmic transformation gives strong transformation effect on distribution shape and it's likely to be more symmetrically distributed. (Box and Cox, 1964). The number "1" was added to the number of bigeye tuna caught before log-transformation to avoid the singularity of zero values for bigeye tuna (Zagaglia et al., 2004). The number of bigeye tuna caught could be predicted using the *predict.gam* function in the *mgcv* package using similar covariates as were used to build the model. Zagaglia et al. (2004) and Mugo et al. (2010) employed this approach.

In this study, seven models were constructed from the simplest form by using only one independent variable (i.e., SST, SSC, SSHD) and combinations of variables (i.e., SST+SSC, SST+SSHD, SSC+SSHD and SST+SSC+SSHD) as listed in table 4.3. For example, x_{1i} correspond to SST in model 1; in model 7, x_{1i} corresponds SST, x_{2i} corresponds to SSC, and x_{3i} corresponds to SSHD. These models were evaluated based on the significance level of predictors (P-value), deviance explained (DE) and the Akaike information Criterion (AIC) value (Mugo et al., 2010). DE and AIC were used to determine

the best model. DE has the same meaning as coefficient determination (R^2) of classic regression as described in Eq. 4.14 and 4.15

$$DE = 1 - \frac{\text{Residual Sum Square}}{\text{The total sum of square}} \quad (4.14)$$

$$DE = 1 - \frac{\sum_{i=1}^m (N_i - \widehat{N}_i)^2}{\sum_{i=1}^m (N_i - \bar{N})^2} \quad (4.15)$$

While AIC describes the residual error which calculated by Eq. 4.16

$$AIC = D + 2df\phi \quad (4.16)$$

Where D is residual sum square, df is effective degree of freedom and ϕ is variance as describe in Eq. 4.17 and 4.18

$$D = \frac{1}{n} \sum_{i=1}^m (N_i - \widehat{N}_i)^2 \quad (4.17)$$

$$\phi = \frac{1}{n} \sum_{i=1}^m (N_i - \bar{N})^2 \quad (4.18)$$

The highest value of DE and the smallest value of AIC were selected as the best model. As a reference, the parameters of the respective degrees of freedom (DF) are also listed in Table 4.3. The predicted number of bigeye tuna was compared with the observed number using linear models. The optimal values of each predictor variable (SST, SSC and SSHD) determined by GAM were used as main parameters to predict bigeye tuna habitat.

Table 4.3 GAM models used in this study and obtained values for P-value, percent DE, AIC value, and DF, respectively (N=7751).

No	Model	Variable	P-value	DE	AIC	DF
1	SST	SST	$<2 \times 10^{-16}$	5.38%	2759.216	6.783
2	SSC	SSC	$<2 \times 10^{-16}$	2.90%	2962.338	8.055
3	SSHD	SSHD	$<2 \times 10^{-16}$	3.34%	2927.313	8.402
4	SST+SSC	SST	$<2 \times 10^{-16}$	5.94%	2724.76	6.168
		SSC	2.28×10^{-7}			6.517
5	SST+SSHD	SST	$<2 \times 10^{-16}$	8.03%	2551.88	5.345
		SSHD	$<2 \times 10^{-16}$			7.973
6	SSC+SSHD	SSC	$<2 \times 10^{-16}$	5.65%	2754.828	7.776
		SSHD	$<2 \times 10^{-16}$			8.036
		SST	$<2 \times 10^{-16}$			4.155
7	SST+SSC+SSHD	SSC	0.000117	8.39%	2531.947	6.468
		SSHD	$<2 \times 10^{-16}$			7.968

4.2.5 Habitat Suitability Index

Habitat suitability index (HSI) is a numerical index that represents the capacity of a given habitat to support a selected species (Oldham et al., 2000). An HSI is a numerical index, between 0 to 1 where 0 indicates unsuitable habitat and 1 represents an optimal habitat. We used raster calculator function in the spatial analysis tools in ArcGIS 10.1 to processed HSI. Combining the habitat factors based on GAMs and accomplished by an additive priority function P, as shown in equation (4.19). (Store and Jokimaki., 2003)

$$P = (0.5 * X) + (0.17 * Y) + (0.33 * Z) \quad (4.19)$$

Where P is habitat suitability index, X is SST, Y is SSC and Z is SSHD index (Eq. 4.20, 4.21, 4.22)

$$X = \begin{cases} 1, & \text{optimum range of SST} \\ 0, & \text{non optimum range of SST} \end{cases} \quad (4.20)$$

$$Y = \begin{cases} 1, & \text{optimum range of SSC} \\ 0, & \text{non optimum range of SSC} \end{cases} \quad (4.21)$$

$$Z = \begin{cases} 1, & \text{optimum range of SSHD} \\ 0, & \text{non optimum range of SSHD} \end{cases} \quad (4.22)$$

The optimum value of each variable was calculated according to GAM plot result which described in section 4.3.1. In addition, constant value of each variable is weight value which was calculated based on the proportion of important habitat predictor for bigeye tuna according to GAM result (Table 4.3). Where, SST is the most important variable followed by SSHD and SSC is the least important variable for bigeye tuna (i.e. according to the highest value of DE and the smallest value of AIC in each variable) as describe in Eq.4.23.

$$\text{weight} = \begin{cases} \text{SST}_{\text{weight}} = \frac{3}{(3+1+2)} \\ \text{SSC}_{\text{weight}} = \frac{1}{(3+1+2)} \\ \text{SSHD}_{\text{weight}} = \frac{2}{(3+1+2)} \end{cases} \quad (4.23)$$

4.3 Results

4.3.1 Analysis of habitat characteristics for bigeye tuna by using GAM

Prior to examining the relationship between the bigeye tuna catches and environmental variables, we examined the relationship between number of bigeye tuna caught and environmental variables. Table 4.1 lists the Model variable, P-value, DE, AIC and DF for some models. The predictor variables were highly significant ($P < 0.001$) for all of the models. High significance was indicated by the lowest AIC and the highest DE. DE has the same meaning as the determination value in the linear regression. SST showed the highest DE among the single-parameter models. Models developed from three parameters (i.e., model 7) had the highest DE and the lowest AIC values, which indicated that the combination of three parameters generated the best models.

Figure 4.2 shows GAM plots developed to interpret the individual effect of each predictor variable on the number of bigeye tuna. The effect of SST, SSC and SSHD on the number of bigeye tuna are shown in Figure 4.(2a), (b) and (c), respectively. There are

positive and negative effects of number of bigeye tuna in each variable. As seen in Eq.4.8, when the value of $f_1(X)$, $f_2(Y)$ and $f_3(Z)$ are positive, it means the prediction of bigeye tuna became high (i.e., $\hat{N} = N_0 + f_1(X) + f_2(Y) + f_3(Z) + \varepsilon$). However, when the value of $f_1(X)$, $f_2(Y)$ and $f_3(Z)$ are negative, it means the prediction of bigeye tuna became low because $\hat{N} = N_0 - f_1(X) - f_2(Y) - f_3(Z) + \varepsilon$.

A negative effect of SST on the number of bigeye tuna was observed at temperature is higher than 28.7°C. There was a positive effect of temperature on the number of bigeye tuna from 24.6 to 28.7 °C. Bigeye tuna appeared to prefer cooler water, but the number of sets performed at temperatures lower than 25°C was low. As a result, the confidence interval was wider for SST less than 25°C. There was an indication of greater number of bigeye tuna caught at lower SSTs, but the number of data points in the lower temperature range declined and the confidence level also declined. For SSC, a positive effect on the number of bigeye tuna occurred between 0.07 and 0.22 mg/m³ (Figure 4.2b). From 0.19 mg m⁻³ a decline occurred towards the highest SSC value. A GAM plot of SSHD showed a positive effect of this variable on the number of bigeye tuna caught between -3 and 7 cm in the region of high confidence level and in the extreme value of SSHD (Figure 4.2c).

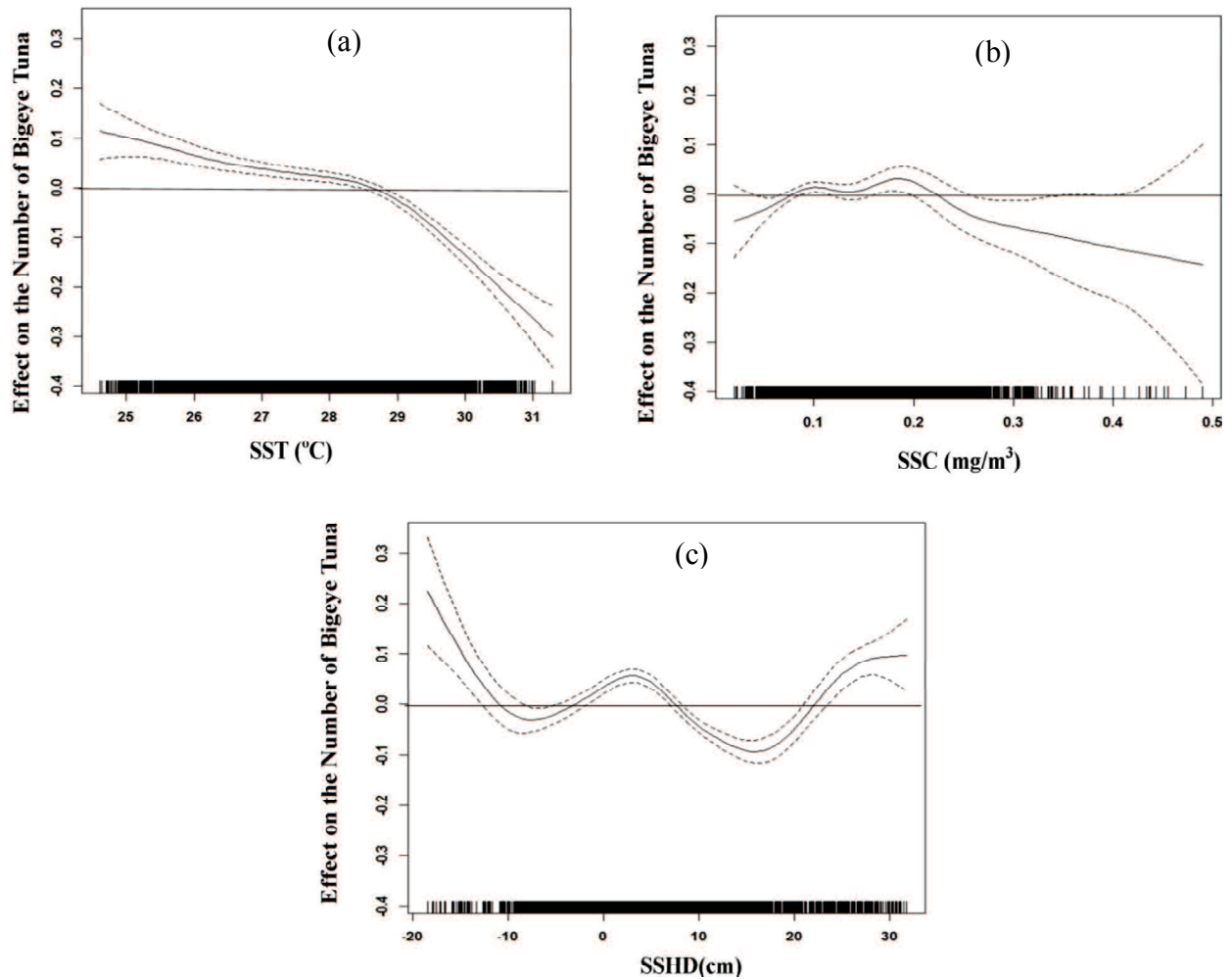


Figure 4.2 Effect of three oceanographic variables on the number of bigeye tuna (a) SST, (b) SSC and (c) SSHD. Tick marks at abscissa axis represent the observed data points. Full line is the GAMs function. Dashed dot lines indicate the 95% confidence level.

4.3.2 Model validation and bigeye tuna habitat prediction

A scatter plot of between the observed values and GAM model is presented in Figure 4.2. There are two kind of model validation method. First, Scatter plot was conducted by averaging bigeye tuna in each interval (chapter 3) then compared with predicted value and second, by taking sample in each number of bigeye tuna (i.e 30 sample in each class) then directly compared with prediction by GAM. The result stated that the adjusted simple linear regression line was significant ($P < 0.05$, $r^2 = 0.52$) by averaging bigeye tuna in each interval (Figure 4.3(a)). However, direct validation with high range of observed number of bigeye tuna stated that the result is not significant (Figure 4.3(b)) because smoother function of

GAM was conducted by averaging the number of bigeye tuna. Hence, GAM has difficulty to observe the high catches data.

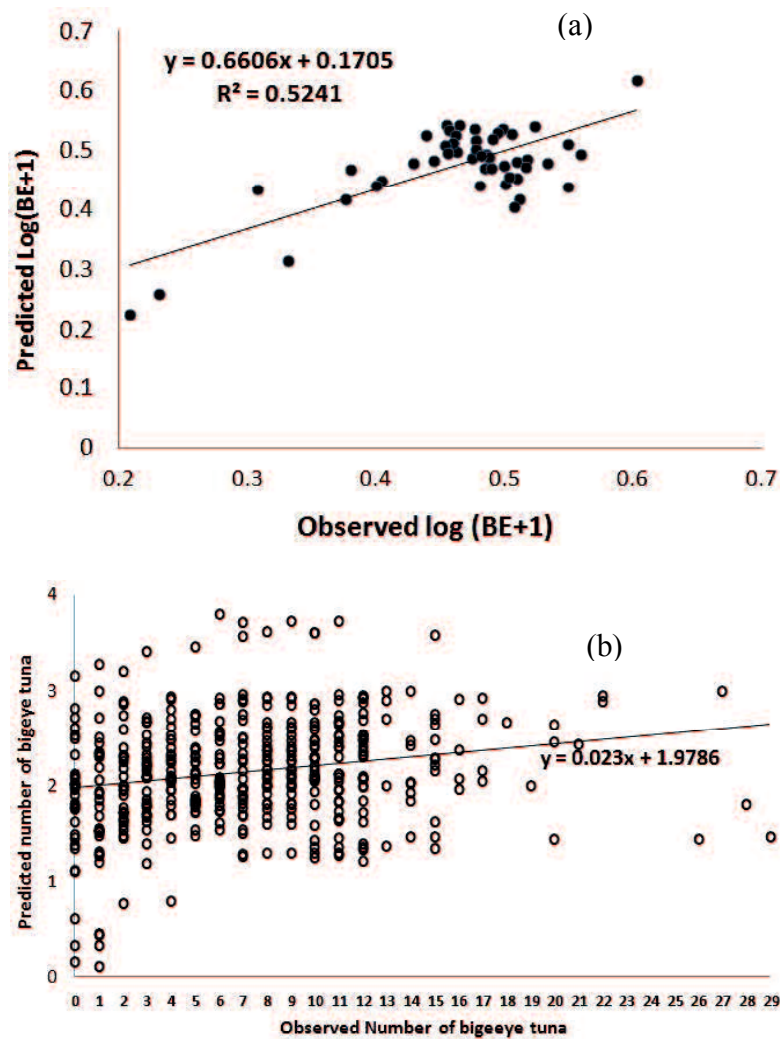


Figure 4.3 (a) A Scatter plot between the average observed values and GAM model predicted ones. (b) A Scatter plot between all ranges observed values and GAM model predicted ones.

Habitat suitability index (HSI) maps of bigeye tuna in 2009 are presented in Figure 4.4. The red color indicates the most suitable habitat for bigeye tuna, and blue color indicates unsuitable habitat for bigeye tuna. Most of the fishing activity was done in the yellow color (HSI = 0.6 - 0.7). According to HSI map bigeye tuna preference area changed depending on month as can be seen in Figure 4.4, but the fishing location seemed unchained. As shown in Figure 4.4, the high preferable bigeye tuna habitat tended to westward. This result was

supported by the previous research on the eastern coast of Australia, where fish move from east to the west (Gun et al., 2005).

4.4 Discussion

In general, fisheries data are abundant for developed countries, but the data are limited in terms of study area. That is why we used the number of bigeye tuna caught as an index of fish abundance. Because we used a different unit of fish abundance, classification of fisheries data was performed to define the type of fish catch data and was used as preliminary investigation to determine the best method of statistical analysis for our data. Here we examined our results and their inherent relevance as environmental indicator of bigeye tuna habitat.

Identification of bigeye tuna habitat in the Southern Waters off Java and Bali is a challenge because the distribution of habitat is variable over time. In addition, the bigeye tuna is classified as overexploited in most parts of Indonesia (Sunoko and Huang, 2014). For that reason identification of bigeye tuna habitat characteristic using remote sensing of biophysical environment parameters would be especially important to predict of stocks' responses to externalities such as climate change and fishing pressure.

The effect of environmental conditions, deduced from GAMs, indicated that environmental variables strongly influenced the numbers of bigeye tuna caught. SST was more important than SSC or SSHD in the study area. This was indicated by SST having the highest DE and lowest AIC in all models. In addition, the Pacific Ocean influences the transfer of heat energy to the Indian Ocean by ITF (Lee et al., 2001), which causes changes in SST. During southeast monsoon the reduction of heat transfer caused SST to be lower (approximately 26.7°C). Furthermore, SST is higher when the Intertropical Convergence Zone (ITCZ) occurs because of weak winds and high relative humidity that result in reduced evaporative cooling of SST (Farrar and Weller, 2003). Bigeye tuna catches increased in

areas with relatively low SST (24.5~28.7°C) and decreased in the areas with SST > 28.7°C. This was supported by previous research (e.g. Gun et al., 2005; Howell et al., 2010; Syamsudin et al., 2013). Furthermore, bigeye tuna preferred to remain in lower-temperature areas. Our finding seems to agree with the result of Brill et al. (1994), who explained that bigeye tuna move towards to the cooling habitat to prevent overheating.

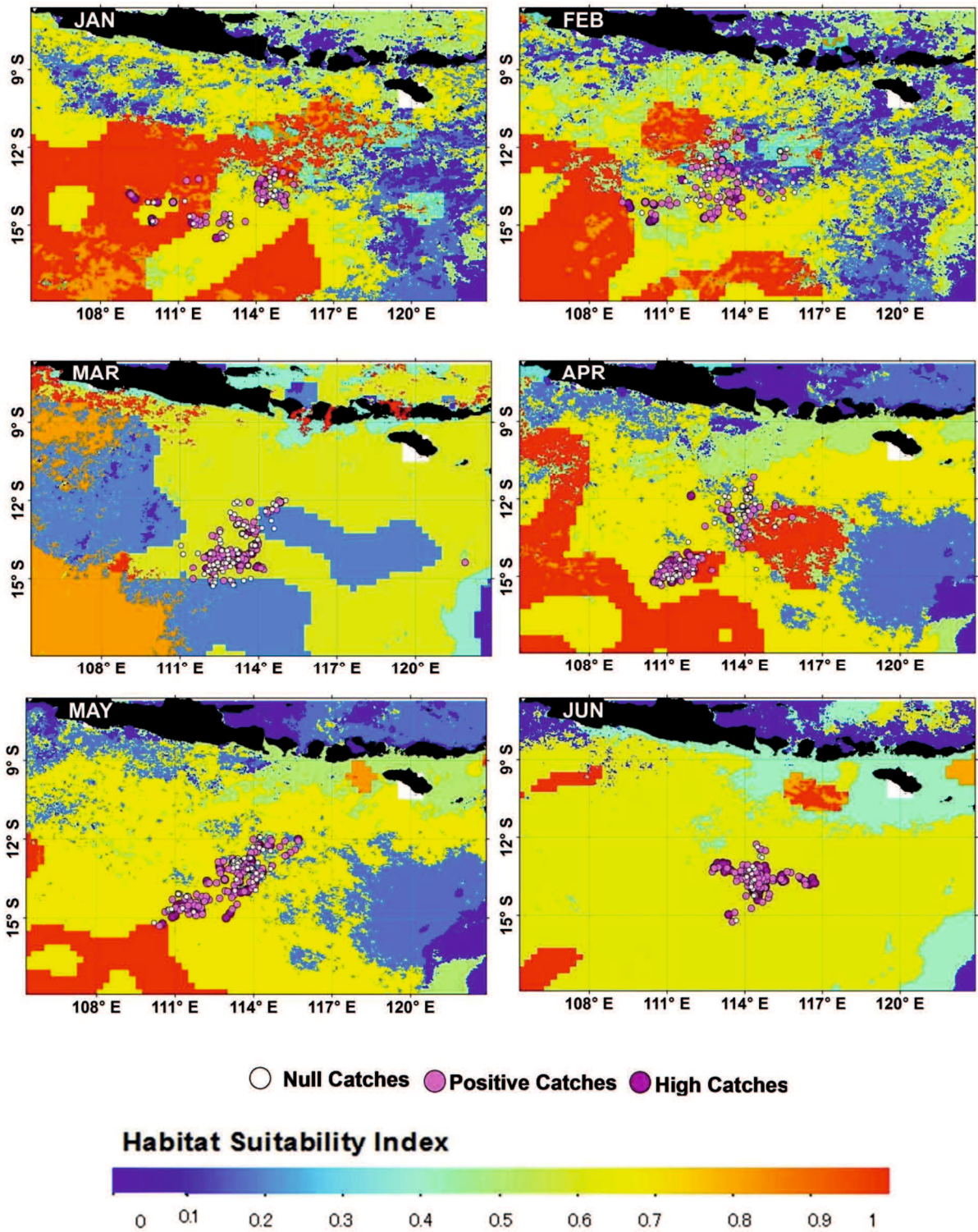


Figure 4.4 Habitat suitability index for bigeye tuna from January to December 2009 overlaid with bigeye tuna fishing location (continue to the next page).

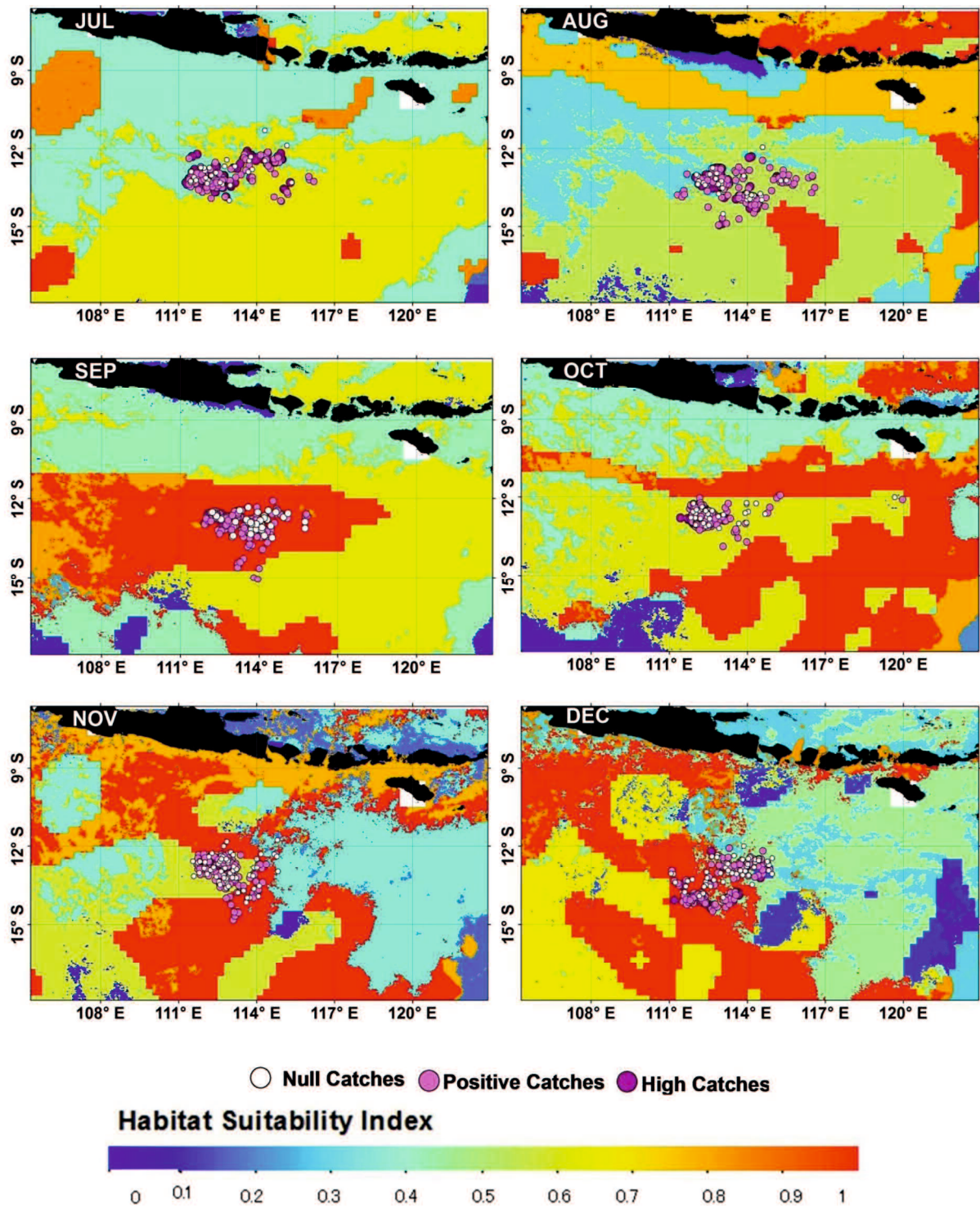


Figure 4.4 Habitat suitability index for bigeye tuna from January to December 2009 overlaid with bigeye tuna fishing location (from the previous page)

Temperature limit horizontal and vertical distribution of bigeye tuna and this varies by region and size (Miyabe Naozumi, 1993; Brill et al, 2005; Howell et al, 2010). Lehodey et al. (2010) reported that natural mortality of older stages of bigeye tuna in the Pacific Ocean increased due to too warm surface temperature and decreasing oxygen concentration in the sub-surface caused by global warming. Howell et al. (2010) reported that tagged bigeye tuna in the central North Pacific Ocean showed daily vertical movement, where they spent much of the time (61%) near the surface layer and above the thermocline layer during night time, but less time (39%) during daytime. Night time depth ranged from the surface to 100 m and where daytime dive beyond 500 m. Bigeye tuna regularly expose themselves to temperature change up to 20°C (from ~25°C surface layer temperature to 5°C at 500m depth during their daily vertical movement). Bigeye tuna occasionally makes an upward excursion into the mix layer water to warm their muscles (Brill et al., 2005). Such tagging experiments are important for understanding bigeye tuna vertical habitat utilization. Our result indicated that few fishing sets (8%) occurred at temperatures < 25°C (Figure 4.2a).

SSHD was the second most significant oceanographic predictor of bigeye tuna in the study area. We used SSHD to understand oceanic variability, such as current dynamics, eddies, convergences, and divergences, which can be used as proxies for the potential location of tuna catches (Polovina and Howell, 2005). Our study showed that bigeye tuna preferred areas with SSHD values of -3 to 7 cm and in the extreme area of SSHD (Figure 4.2c). Actually, the negative extreme values of SSHD had a positive effect on the number of bigeye tuna caught, but the number of observations was low and the confidence interval was wide.. Negative SSHD will push the thermocline upward near the surface layer and the elevation of thermocline will allow bigeye tuna from below to become accessible to longline gear. The upward movement of thermocline layer causes the temperature in the surface layer becomes cooler. According to Arrizabalaga et al. (2008) only for very negative SSHD,

bigeye in shallow waters are only attracted by the thermocline when this is closer to the surface. This phenomenon was reported by Syamsudin et al. (2013) that the El-Nino event in 1997, extreme minus SSHD with many observation points occurred and gave the positive effect to the abundance of bigeye tuna.

Among three environmental predictors used in the model, SSC was the least important, but was still statistically significant ($P < 0.001$). As a biological component available for satellite remote sensing, SSC is an index of phytoplankton biomass that provides valuable information about trophic interaction in marine ecosystem (Wilson et al., 2008). Chlorophyll-a data are a valuable proxy for water mass boundaries and upwelling events. High value of SSC was concentrated along the southern coast of Java (7-9°S) (Figure 4.5). Susanto et al. (2001) and Ningsih et al. (2013) reported that the seasonal appearance of chlorophyll front and the yearly upwelling phenomenon occurred in the Southern Waters off Java and Bali especially in the coastal area (Figure 4.5). Upwelling areas are potential convergence zone for plankton aggregation, attracting larger predator, such as tuna (Lehodey et al., 1997). Bigeye tuna is a visual predators where water clarity is important (Brill et al., 2005). The open ocean provides the optically clearest aquatic habitat (Jerlov, 1976). Hence, in the open ocean bigeye tuna can forage the prey optimally. Yearly upwelling occurred in the study area, especially in the coastal zone, so that SSC did not affect directly to the abundance of bigeye tuna. Overall, SST and SSHD mainly influenced bigeye tuna catches. In this study, the fishermen used the same fishing gear with similar fishing techniques. Therefore, we assumed that differences in fishing gear did not affect the catchability of bigeye tuna.

Spatial mapping of bigeye tuna habitat was conducted by HSI approach. The HSI map from January to December was shown in Figure 4.4. It explained that most of fishing activity were located when HSI was 0.6 to 0.7, but in September fishing activities were

located in the most suitable habitat (HSI =1). HSI showed concurrence with actual fishing location for the month from September to December. This is also the period that showed low null catches frequencies (Figure 3.5d). However the model appears to have difficulties in predicting high catches data (Figure 4.3) because the smoothing function of GAM estimates the dependence of the mean of number of bigeye tuna on the predictors. The prediction of bigeye tuna by GAM showed a significant relationship with the average observed value with a confidence level of 95% ($r^2=0.52$) (Figure 4.3). Zagaglia et al. (2004) also reported the significant relationship between observed catch per unit effort (CPUE) and predicted CPUE from GAM ($r^2=0.51$) for yellowfin tuna in the equatorial Atlantic Ocean. Mugo (2010) also applied GAM to skipjack tuna in the western part of the North Pacific Ocean and found a significant relationship between observed CPUE and predicted CPUE from GAM ($r^2=0.64$). Our results cannot correctly predict the number of bigeye tuna caught as in Mugo et al. (2010). This is because we used daily catch data as numbers of bigeye tuna caught and this was difficult when we predict null catches. Nevertheless, our model explained 8.39 % (Table 4.1, No.7) of variability in bigeye tuna abundance based on environmental variables only; the model generated by Mugo et al. (2010) explained 13.3% of variability. This indicates that our method is useful. Environmental variables are important to predicting the bigeye tuna habitat, but are probably not only the factors that influence fishing locations for this species. In addition, data which have a high temporal resolution and more years are likely to generate a better model to predict bigeye tuna habitat in the study area.

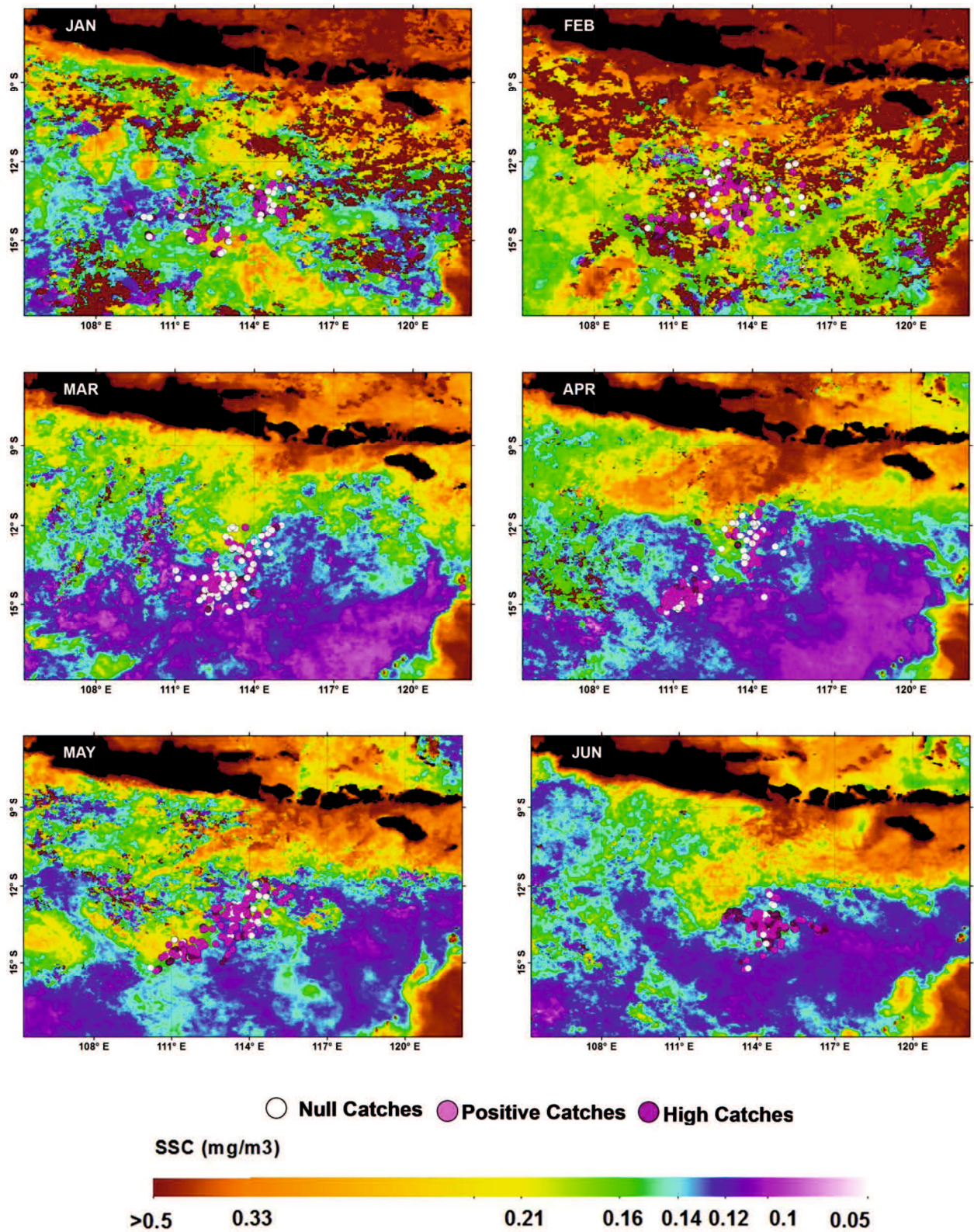


Figure 4.5 The spatial distribution of SSC and bigeye tuna catches in Southern Waters off Java-Bali in 2009 (continue to the next page).

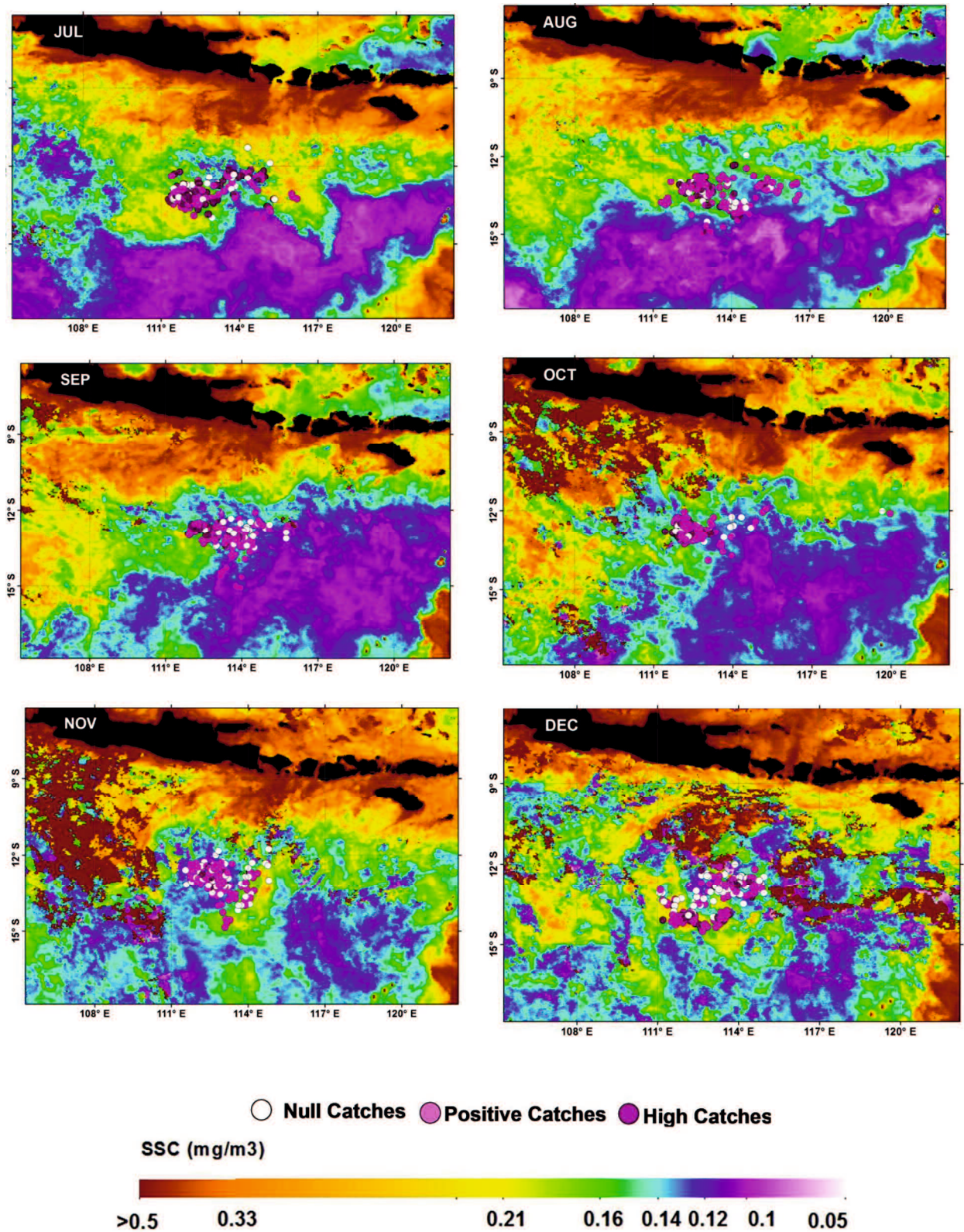


Figure 4.5 The spatial distribution of SSC and bigeye tuna catches in Southern Waters off Java-Bali in 2009 (from the previous page)

4.5 Conclusions

Characterization of bigeye tuna habitat in the Southern Waters off Java and Bali using a remote sensing approach has been performed. Daily in-situ fish catch data from PT Perikanan Nusantara and monthly remotely sensed environmental data of SST, SSC, and SSHD for period of 2006-2010 were used here. The GAM statistical method and GIS were combined. Seven GAM models were generated with the number of bigeye tuna caught as a response variable, and SST, SSC, SSHD as predictor variables. The results showed that SST was the most important habitat predictor for bigeye tuna migration in the Southern Waters off Java and Bali, followed by SSHD and SSC. The spatial pattern of bigeye tuna habitat characteristic gave typical low SST, low positive and negative SSHD and extreme SSHD and low to moderate SSC. Thermocline layer or depth is the important feature to predict the vertical migration of bigeye tuna and SSHD seems to be a good parameter to forecast the thermocline depth.

The results revealed that fishermen still obtained null catches with a frequency of 19% over the 5-year period, which indicated suboptimal success in identifying favorable bigeye tuna habitat. Meanwhile, the El Niño–Southern Oscillation (ENSO) also might affect the number of null catches, as indicated by an increase during the La Niña event.

GAM only measured the effect of environmental variables without considering the interaction of each variable to the number of bigeye tuna. For future work, developing a method which measures the interaction of predictor variables to the fish catch data is necessary to develop.

CHAPTER 5

APPLICATION FOR PRECIPITATION STUDIES

Evaluation and Bias Correction of GSMaP Daily Rainfall Satellite Data for Flood Monitoring In Kyushu Island, Japan by Generalized Additive Model Approach

5.1 Introduction

Reliable global precipitation information and accurate temporal precipitation estimates are essential to manage freshwater resources and to predict high impact weather events such as hurricanes, typhoon, heavy rains which cause flood and landslide (Kamarianakis, Y et al., 2006 and Hou et al., 2008). However, measuring the precipitation is one of the most difficult observational challenges of meteorology because precipitation occurs intermittently and with pronounced geographic and temporal variability (NOAA, 2006).

Conventional rain gauge networks provide relatively accurate point measurements of precipitation (Feidas et al., 2008 and Feidas, 2010). However, the uneven distribution of gauges and their limited sampling area burden an important problem regarding to the effectiveness of spatial coverage (Xie and Arkin 1996a). Moreover, uninhabited and remote areas are not covered by rain gauge networks (Feidas et al., 2008 and Feidas, 2010). Furthermore, continues spatial and temporal distribution of rainfall are provided by radar, but the quantitative range of their measurements is generally limited to 150 km or less and produce incomplete coverage (Feidas et al., 2008 and Feidas, 2010). On the other hand, satellite remote sensing technique became an interesting option for monitoring rainfall over a large area and high temporal resolution in near real time. In addition, satellite precipitation provides integrated spatial coverage of rainfall measurements even in remote land and ocean areas (Chokngamwong and Chiu., 2004; Feidas et al., 2008; Feidas, 2010). A combination of gauge data, radar data and satellite data are substantially needed to enhance space and time rainfall estimation (Chiu et al., 2006a).

As satellite data, Infrared and microwave satellite products, such as the Global Satellite Mapping of Precipitation (GSMaP) as a combination of multiple precipitation satellite data, could be used to derive estimates of large scale precipitation over a global area (Okamoto et al., 2005). The GSMaP rain product is based on using four satellite microwave radiometer combine with Geo Infrared radiometer data to produce 0.1 degree spatial resolution (Aonashi et al, 2009). There are several types of GSMaP rain product as explained later in section 5.2. In this paper, GSMaP_MVK Version 5 was used. It was used because heavy rainfall data which caused flooding in Kyushu Island could be obtained.

Comprehensive details about the GSMaP_MVK ground validation program, algorithms and data processing was provided by Kubota et al. (2007). In addition, GSMaP_MVK was verified from January through December 2004 in Japan to determine whether monthly data, daily data and 3 hourly data matched rain gauge data (Kubota et al., 2009). The result showed that GSMaP_MVK of monthly, daily and 3 hourly data from May to October had high correlation and had the same trend as rain gauge data, but in some cases, GSMaP_MVK data still underestimate with the rain gauge data. For several years, other groups studied different locations to validate GSMaP_MVK data. According to their researches, the GSMaP_MVK data could detect a precipitation occurrence with the same trend as rain gauge data, but the precipitation amount generally underestimated in some cases (Seto et al., 2009; Fukami, 2010; Ushio and Kachi, 2010; Tian et al., 2010; Yamamoto et al., 2011; Shrestha et al., 2011; Taniguchi et al., 2013; Setiawati et al., 2013; Veerakachen et al., 2014) and according to Dinku et al. (2009) GSMaP_MVK had serious underestimation of rainfall amount compared with other precipitation satellite. For these reasons, improving the GSMaP_MVK data verification result is important, especially when heavy rainfall occurs. In this study, first, we evaluated GSMaP_MVK data during rainy

season in Japan, then we evaluated separately based on elevation, location, during the rainy days and finally we evaluated only in the heavy rains category.

The objectives of this study are to advance the quantitative and qualitative understanding of GSMaP_MVK product and to correct GSMaP_MVK product to achieve better agreement with rain gauge data for flood monitoring. In addition, Generalized Additive Model (GAM) was used for improving the GSMaP_MVK ability. GAM is the statistical analysis which allows non-parametric distribution and extends the use of additive models to data sets as explained in the previous chapter. GAMs are rarely used to improve the accuracy of satellite precipitation data, but it was used to forecast daily precipitation data over the basin (Chi et al., 2012) and to forecast the frequency of extreme daily precipitation (Jones et al., 2013). We used this method due to non parametric rain gauge data distribution and promising models for daily precipitation data (Yang et al., 2012). By this method, we expected to improve the estimated rainfall amount by GSMaP_MVK data during heavy rainfall in Kyushu Island, Japan.

5.2 Materials and Methods

5.2.1 Study Area

Japan is particularly vulnerable to flooding because of its steep geography and humid climate characterized by heavy rains and typhoons (Kazama et al., 2009). The number of floods, and, hence, the damage due to flooding, have increased since 2004 (Kazama et al., 2009). Several local heavy rainfalls have been recorded in Kyushu, Japan, in recent years (Miyazaki: 4-7 September 2005; Kumamoto: 3 July 2006; Kumamomoto, Kagoshima, Miyazaki: 20-23 July 2006; Kagoshima, Miyazaki, Kumamoto: 11-17 July 2007). All of these heavy rainfalls created local floods and damage, leading to significant economic losses (Tezuka et al., 2014).

Kyushu Island, the study area, is shown in Figure 5.1. It locates in the south part of Japan and has an area of 35,640km² from latitude 31°N to 34°N and longitude 129°30'E to 132°E. It has a humid subtropical climate and has an elevation ranging from 0 m to 1791 m above the sea level. Kyushu Island is mountainous, with hills that run from north to south in the center of the island. Generally, the land use in this island is dominated by agriculture. Precipitation occurs throughout the year with the heaviest in the summer season, especially in rainy season (i.e., May, June, July). During the summer season the variability of temperature range is from 16°C to 31°C and the annual precipitation is about 1760mm/year (Komatsu et al., 2007).

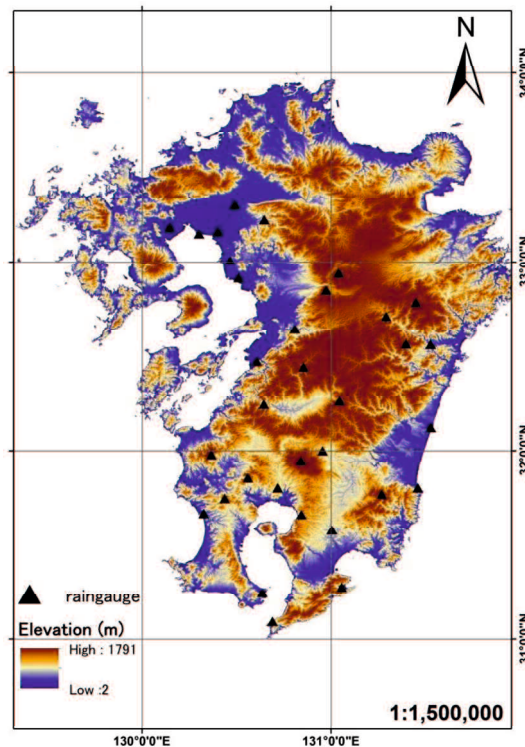


Figure 5.1 The study area, Kyushu Island, and its topography. Black triangle indicates the rain gauge locations

5.2.2 Rain Gauge Data

Daily observed rainfall data from 34 rain gauges over Kyushu island were used as reference data to validate the GSMaP_MVK estimation. The rain gauge data were obtained from AMEDAS (Automated Meteorological Data Acquisition System) developed by the

Japan Meteorological Agency (JMA) during 2005 to 2007 through the rainy season, from May to July. The distribution of the rainfall stations are used in this study is shown in Figure 5.1. The total observation data were obtained by multiplying the total day (92 days x 3 years) and the number of rain gauge data (34 points). Due to some lack of in-situ data, the total of observational data was 9276. The data are available online at the JMA website (<http://www.data.jma.go.jp>).

5.2.3 GSMaP Data

GSMaP was initiated by the Japan Science and Technology Agency (JST) in 2002 and has been promoted by the Japan Aerospace Exploration Agency (JAXA) Precipitation Measuring Mission (PMM) science team since 2007 to produce a global precipitation product with high temporal and spatial resolution (Ushio et al., 2009). GSMaP is a project aiming (1) to produce high-precision and high-resolution global precipitation maps using satellite-borne microwave radiometer data, (2) to develop reliable microwave radiometer algorithms, and (3) to establish precipitation map techniques using multi-satellite data for the coming GPM (Global Precipitation Measurement) era (Ushio and Kachi, 2010). Currently, the data set produced by GSMaP product can be downloaded from their website: http://sharaku.eorc.jaxa.jp/GSMaP_crest/html/data.html. The standard version of the GSMaP data sets includes GSMaP_TMI (retrieved from TRMM/TMI algorithm), GSMaP_MWR (retrieved from six spaceborne microwave radiometers), GSMaP_MWR+ (retrieved from six spaceborne microwave radiometers with AMSU-B product), GSMaP_MVK (retrieved from MWR GEO IR combined algorithm), GSMaP_MVK+ (retrieved from MWR GEO IR combined algorithm with AMSU-B product) and other rainfall estimates from passive microwave radiometer (Liang et al., 2012).

The GSMaP rainfall product used here for comparison with reference gauge data set is GSMaP_MVK product version 5. This product is the combination of low earth orbit multi

satellite microwave radiometer data and infrared radiometer (IR) on geostationary (Geo) orbit as explained in Chapter 2. The available microwave sensors are SSM/I (Special Sensor Microwave/Imager), TMI (TRMM Microwave Imager), and AMSR-E (Advanced Microwave Scanning Radiometer for EOS). Whereas, the IR data sets used in the current version of the system are from the CPC (Climate Prediction Center) (Ushio and Kachi, 2010). The algorithm to regain surface precipitation rate based on the Aonashi et al. (1996) was conducted in this product. The brightness temperature at microwave frequencies as the main input of GSMaP_MVK system was converted into precipitation data (Ushio and Kachi, 2010). The combination technique to produce 0.1° in latitude and longitude and 1 hour resolution with the domain covering 60°N to 60°S was obtained using a morphing technique based on an infrared cloud moving vector and Kalman Filter technique (Ushio et al., 2009). GSMaP_MVK version 5 is available from March 2000 until December 2010. Thus the history of rainfall data which caused flood in Kyushu Island can be obtained. The rain rate daily data of GSMaP_MVK from May to July in 2005 to 2007 were downloaded and then converted into accumulated daily rainfall of GSMaP_MVK. GSMaP_MVK was processed by using OpenGRADS software and one pixel average of precipitation data was calculated based on the rain gauge data position.

5.2.4 Validation and Intercomparison

The data coverage of this study was three years (2005 to 2007) in the rainy seasons. It was selected based on the annual flood occurrence in the study area. The main validation was for daily satellite rainfall product. As shown in Figure 5.1, the validation region has very complex terrain. Thus validation data from the whole island may not give the whole picture. Therefore, validation of the daily satellite products was conducted separately for the elevation (highland and lowland part of Kyushu), location (west and east of Kyushu), during rainy days and only in heavy rainfall to investigate the performance of the product over

different climatic regimes. Lowland was defined where the elevation was under 500 m and highland was defined where the elevation was above 500 m (Dinku et al., 2009). The west and east Kyushu were defined by dividing the prefectures according to the wind direction. Rainy days were defined when the AMEDAS data value were equal or more than one mm/day. In addition, heavy rain was defined as daily rainfall exceeding the 95th percentile (rain_P95) for all stations and all categories (Iwasaki, 2014). Point by point analysis and spatial average analysis were conducted to compare gauge data and satellite data. As-syakur et al. (2011) and Prasetia et al. (2013) also applied this method.

Standard validation statistics are used to evaluate the GSMaP_MVK product to the rain gauge data. Qualitative and quantitative validations were conducted as follows. Qualitative method is to measure the correspondence between the value of the estimates and the observations. To quantify the correspondence value, the following five statistical indices were used (Jiang et al., 2010), the relative bias (B), the mean error (E), the Nash-Sutcliffe (C_{NS}), the Root Mean Square Error (RMSE) and the correlation coefficient (r). These indices are given by following equations.

$$B = \frac{\sum_{i=1}^n (S_i - G_i)}{\sum_{i=1}^n G_i} \times 100\% \quad (5.1)$$

$$E = \frac{1}{n} \sum_{i=1}^n (S_i - G_i) \quad (5.2)$$

$$C_{NS} = 1 - \frac{\sum_{i=1}^n (S_i - G_i)^2}{\sum_{i=1}^n (G_i - \bar{G})^2} \quad (5.3)$$

$$RMSE = \sqrt{\frac{1}{n} \sum_{i=1}^n (S_i - G_i)^2} \quad (5.4)$$

$$r = \frac{\sum_{i=1}^n (G_i - \bar{G})(S_i - \bar{S})}{\sqrt{\sum_{i=1}^n (G_i - \bar{G})^2} \sqrt{\sum_{i=1}^n (S_i - \bar{S})^2}} \quad (5.5)$$

Where, n is the total number of the rain gauge data or GSMaP data; S_i is the satellite estimates and G_i is the rain gauge observation values.

The other validation statistics is the quantitative method which based on the contingency tables shown in Table 5.1. The rainfall threshold used for rain/non rain discrimination is 0 mm/day.

Table 5.1. Contingency table of yes or no events/ with rain or no rain.

		Estimated rainfall (GSMaP_MVK)	
		Yes	No
Observed Rainfall (AMEDAS)	Yes	A	C
	No	B	D

In Table 5.1, A, B, C, and D represent “hit”, “false alarm”, “miss” and “correct negative”. “Hit” represents correctly estimated rain events, “miss” describes when rain is not estimated but actual rain occurs, “false alarm” represents when rain is estimated but actually rain doesn’t occur, and “correct negative” represents correctly estimated no-rain events. Using the results shown in Table 1, Probability of Detection (POD), False Alarm Ratio (FAR), and Heidke skill score (HSS) statistics parameters are calculated by following equations.

$$POD = \frac{A}{A+C} \quad (5.6)$$

$$FAR = \frac{B}{A+B} \quad (5.7)$$

$$HSS = \frac{2(AD-BC)}{(A+C)(C+D)+(A+B)(B+D)} \quad (5.8)$$

Where, POD explains how good the GSMaP estimates are in detecting the occurrence of rainfall. FAR shows how often the GSMaP detects rainfall when rain gauge measurement is zero. Furthermore, HSS measures the rainfall detection accuracy of the satellite estimates relative to matches resulting from random chance.

5.2.5 Determining a bias correction by power function

Comparison between GSMaP_MVK data with ground station measurement showed large differences during heavy rainfall as shown in the following sections. Therefore, the previous researchers obtained bias correction equations to achieve the best result. To accommodate for finding the relative bias varied with daily rainfall, a power function was applied to derive bias corrected rainfall (P^*) (Vermenten et al., 2012) as follows:

$$P^* = a * \left(\frac{P}{P_0}\right)^b \quad (5.9)$$

Where P is GSMaP_MVK, P_0 is the reference daily rainfall (1mm/day), a (mm) is the constant and b is the power function. The linear regression analysis was previously applied to obtain the values of a (1.41 mm/day) and b (0.15) where all the data were transformed into logarithmic. This analysis is as a reference test for correction only for heavy rainfall section because this correction method has not been applied to the heavy rainfall case.

5.2.6 Determining a bias correction by Generalized Additive Models (GAM)

According to the previous research, GSMaP_MVK had underestimated the rain gauge data. Therefore, a bias correction equation was applied to achieve a closer fit between daily GSMaP_MVK and rain gauge data. GAM was applied because it has been widely adopted as an effective model and it has smoothing functions to analyze many complex time series data (Wood, 2006). GAM have been widely employed in other disciplines to model the health impacts of air pollution or long term variability in biota spatial density, but rarely applied in hydrology (Morton and Henderson, 2008; Underwood, 2009).

GAM was created by *R version 3.0.2 software*, using the *gam* function of the *mgcv* package (Wood, 2006), with the rain gauge data as response variables and GSMaP data as predictor variables. GAM model in the form of an Eq. (5.10) was applied:

$$g(\mu) = \alpha_0 + f_1(X) \quad (5.10)$$

Where g is the link function (identity link), μ is the expected value of the rain gauge data, α_0 is the model constant and f_1 is a smoothing function of the X (which corresponds to the daily GSMaP_MVK data) (Wood, 2006). The α_0 was calculated according to the total average of AMEDAS data (i.e 12.4 mm/day). In addition, when the GSMaP_MVK *value* is zero, the expected value of rain gauge data is equal to 2.16 mm/day.

The Gaussian distribution is generally used in GAM, but we did not use the Gaussian distribution because the distribution of the rain gauge data was asymmetric. The rain gauge data could be predicted using the *predict.gam* function in the *mgcv* package using similar covariates as were used to build the model.

5.3 Results and Discussion

5.3.1 General comparison of daily rain gauges with GSMaP_MVK data

This study first compared daily rain gauge data (AMEDAS) with GSMaP_MVK data. Figure 5.2 shows the scatter plot of AMEDAS data versus daily GSMaP_MVK data, the total data number and the mean values are also indicated in the plot. The validation statistics of GSMaP_MVK are listed in Table 5.2. In general, rainfall from GSMaP_MVK was lower than rainfall from rain gauge data: the average rainfall from rain gauge data was 12.39 mm/day, whereas the average rainfall from GSMaP_MVK was 6.59 mm/day. GSMaP_MVK data in the study area have a strong correspondence with rain gauge data ($r=0.74$), with the bias value was -46.78%. Moreover, the values of E and RMSE were -5.8 mm/day and 22.82 mm/day, respectively. Furthermore, the consistency of GSMaP_MVK to measure the rainfall amount can be described through C_{NS} index. The C_{NS} index of the study area was 0.46 (46%), it means that GSMaP_MVK has the consistency to measure the rainfall amount about 46%. POD of GSMaP_MVK are close to 81% and FAR is generally

small (18%). The HSS statistic shows that the GSMaP_MVK estimates have reasonably good skills in detecting the occurrence of rainfall (67%).

A comparison of long term means of daily rainfall measured by GSMaP_MVK and rain gauge data for a three-year period was shown in Figure 5.3. Figure 5.3 indicates that the pattern of daily means is similar and has a very strong correspondence to rain gauge data ($r=0.9$), but GSMaP_MVK data were underestimated, with the bias, mean error and RMSE are -46.75%, -5.78 mm/day and 9.02 mm/day, respectively. In addition, GSMaP_MVK has high consistency with the C_{Ns} value of 0.53. In general, GSMaP_MVK product has underestimated. This will be partly because the current algorithm of microwave radiometer does not include the topographical effect and the brightness temperature from microwave radiometer has directly underestimate relation with precipitation (Ushio et al., 2009). Consequently, GSMaP_MVK data correction is needed to reduce bias, error and RMSE and to increase C_{Ns} and correlation coefficient. In this study, GAM approach was applied for bias correction.

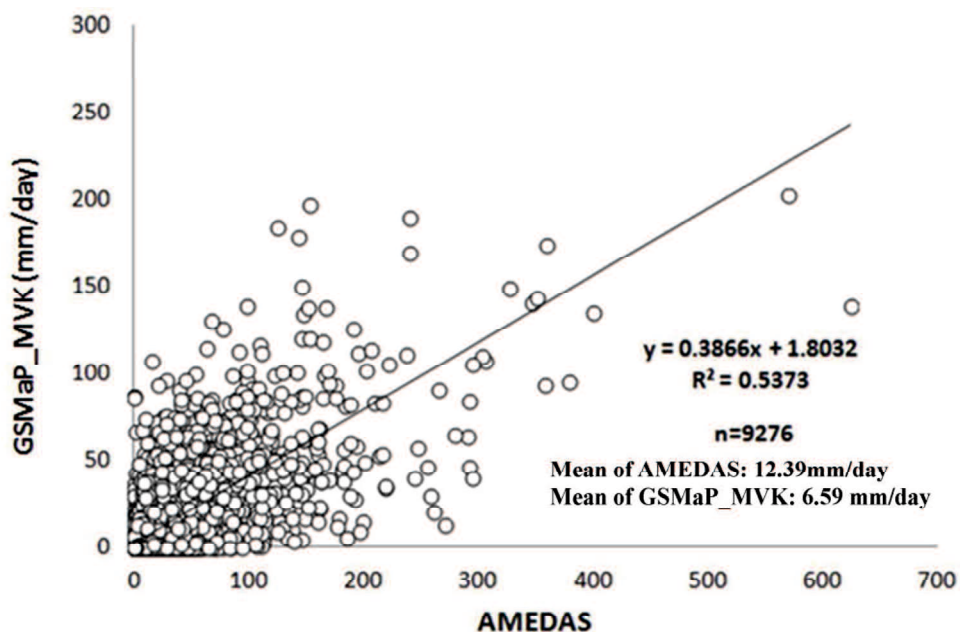


Figure 5.2 Scatter plot of daily rain gauge data versus GSMaP_MVK product during rainy season from 2005 to 2007

Table 5.2. Validation statistics of daily GSMaP_MVK product during rainy season from 2005 to 2007.

Statistical indices	Value
Bias	-46.78%
Error	-5.8 mm/day
RMSE	22.82 mm/day
C _{NS}	0.46
r	0.74
POD	81%
FAR	18%
HSS	67%

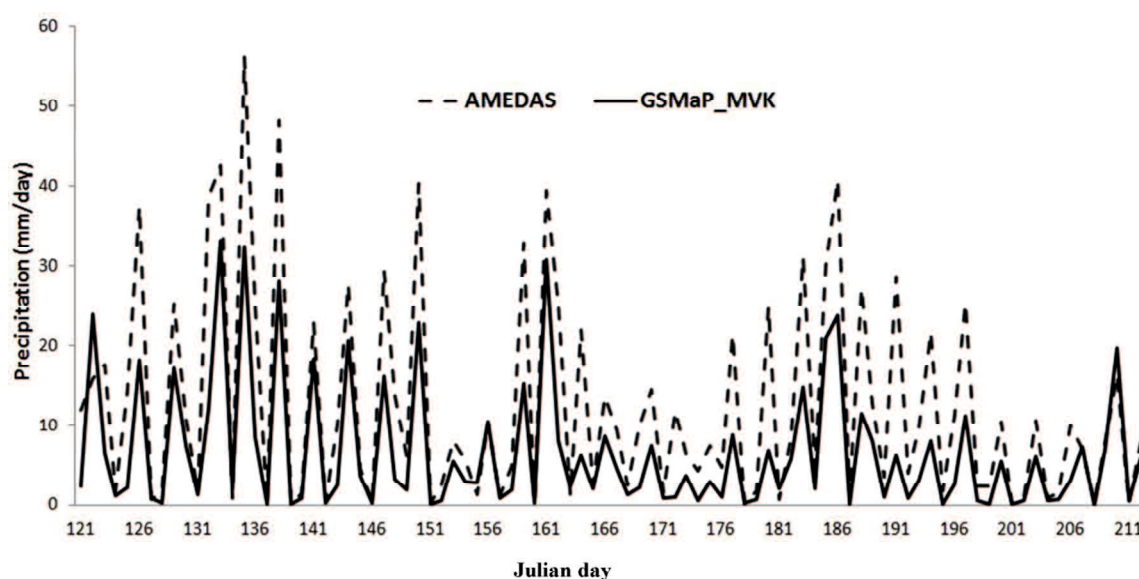


Figure 5.3 Long term mean of daily rainfall measured by AMEDAS and GSMaP_MVK for three years during rainy season. Daily rainfall is spatially averaged over 34 rain gauges.

5.3.2 Validation and correction of GSMaP_MVK in the highland and lowland

The main topographic feature of Kyushu island is the large mountain ranges which located in the center of the island and the plain regions that cover the eastern and western part of the island. The elevation of mountainous region can exceed 1700 m while the eastern and western parts are below 500m. In this study, we first divided the validation and correction based on the elevation because it has significant influence on the rainfall climatological pattern (Dinku et al., 2005). The eastern and western plain region receives about 2071 mm of annual rainfall while in the mountainous region receives about 3321mm

of annual rainfall. It is said that in the highland region rainfall amount is higher than in the lowland region. In addition, heavy rain is strongly influenced by topography (Iwasaki, 2014). In other words heavy rainfall often occurs in the mountainous site.

To assess the *orographic* effects, the validation of GSMaP_MVK in the highland and lowland region was conducted in this section. Table 5.3 compares the validation and correction result of GSMaP_MVK in the highland and lowland regions. In the highland the bias, error, RMSE, and C_{NS} are -56.18%, -8.69 mm/day, 29.5 mm/day and 0.4, while in the lowland they are -41.27%, -4.58 mm/day, 26.3 mm/day and 0.5, respectively. These results show that the performance of satellite product is superior over the lowland, with lower bias, error and RMSE and better consistency measurement for rainfall estimates. In contrast, the performance of satellite product is seriously underestimated and has lower consistency measurement for rainfall estimates over the highland. This will be partly because the current algorithm of microwave radiometer does not include the topographical effect. This result should be noted that topography obviously influences the accuracy of the satellite product. Moreover, detection probability and HSS also gave the same result that is POD and HSS were higher in the lowland (82 % and 68 %), than in the highland (78% and 65%) while FAR was lower in the lowland (15%) than in the highland (19%) as shown in Table 5.3.

GSMaP_MVK data have underestimated both in the lowland and highland therefore, the correction was conducted. In this study, GAM was conducted for bias correction. The results showed that the bias, error and RMSE in the highland region decreased significantly and the C_{NS} value increased. However, GAM did not give the significant impact for the lowland area. It should be noted that GAM only worked in the highland region. It is said that GAM tends to overestimate for forecasting (He et al., 2006). In addition, GAM can solve the underestimate problems when the bias percentage is large. In contrast, the correlation coefficient was not significantly different among high land and

lowland, before correction and after correction (Figure 5.4). However, after correction the scatterplot pattern were concentrated under 100mm/day. This condition was caused by GSMaP data observation point were dominant from 0 mm/day to 70 mm/day where the expected value of those range were 2.16 mm/day to 92.4 mm/day as explained in the Figure 5.5. The same explanation for the section 5.3.3 and 5.3.4

Table 5.3. Validation statistics over the highland and lowland before and after corrected by GAM

	Highland		Lowland	
	GSMaP_MVK	Corrected by GAM	GSMaP_MVK	Corrected by GAM
Bias	-56.18%	2.53%	-41.27%	44.83%
Error	-8.69 mm/day	0.39 mm/day	-4.58 mm/day	5.08 mm/day
RMSE	29.5 mm/day	25.65 mm/day	26.3 mm/day	22.42 mm/day
C _{NS}	0.4	0.6	0.5	0.33
r	0.74	0.75	0.74	0.73
POD	82%	82%	78%	78%
FAR	19%	19%	15%	15%
HSS	68%	68%	65%	65%

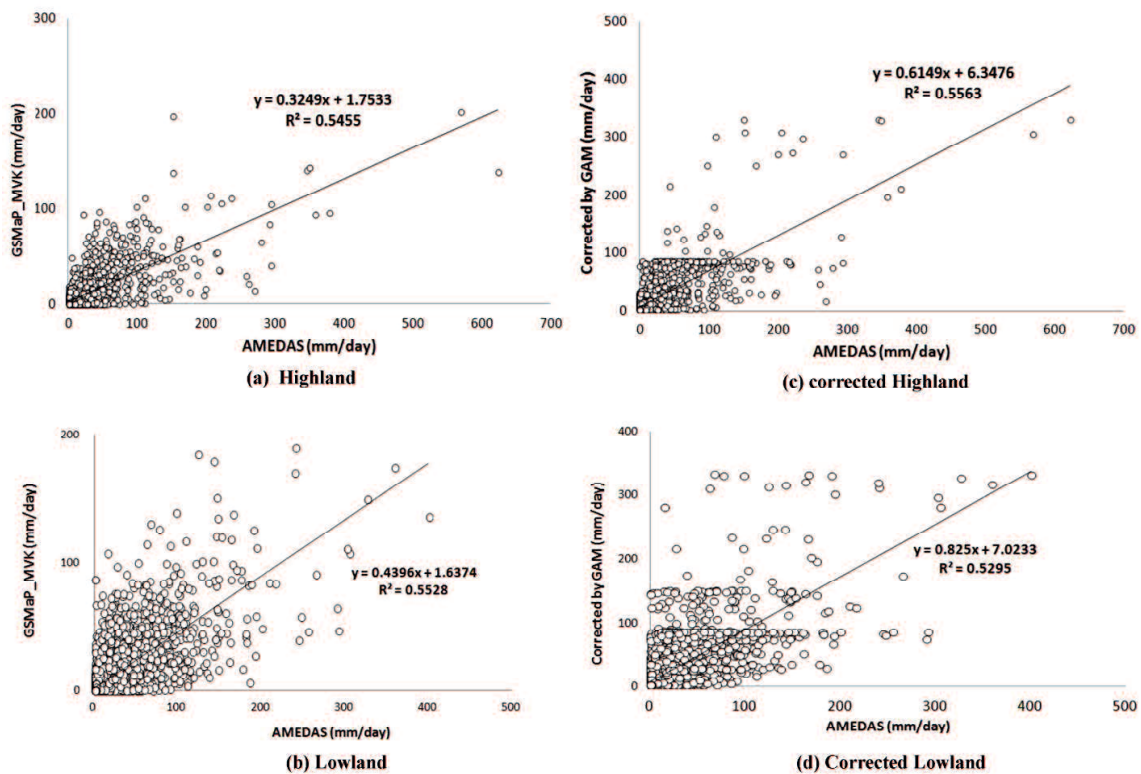


Figure 5.4 Comparison of the performance GSMaP_MVK in the highland (a), lowland (b), corrected highland (c), corrected lowland (d)

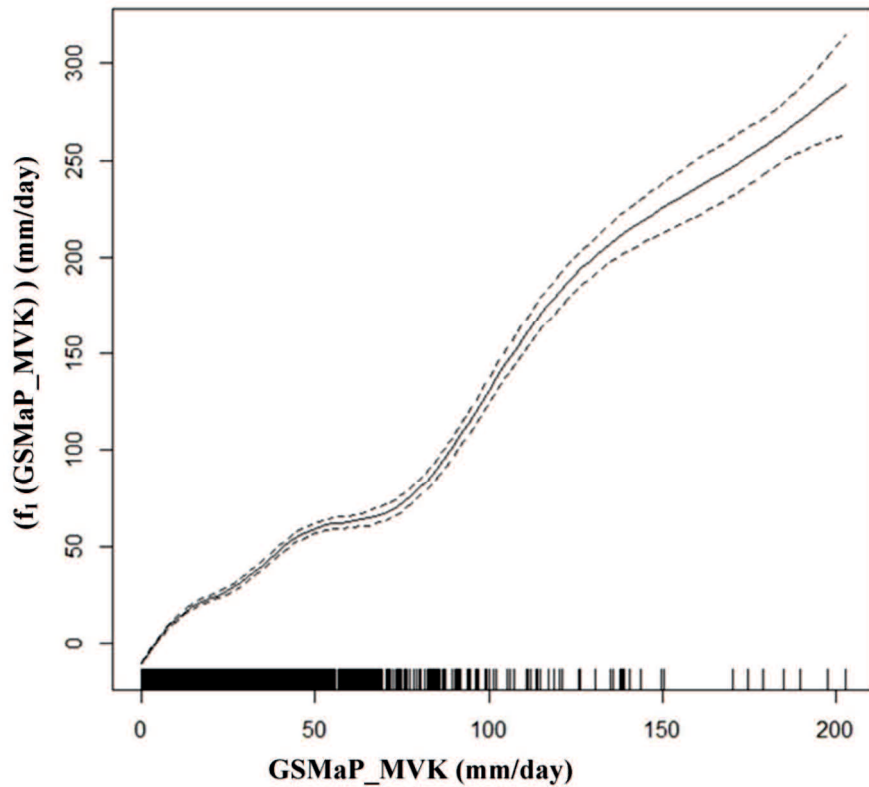


Figure 5.5 Smoothing function of GSMaP_MVK

5.3.3 Validation and correction of GSMaP_MVK in the eastern part and western part of Kyushu

As explained before, the mountain region of Kyushu island is located in the central of the island from north to south and it will affect the rainfall pattern over the region. Therefore, to assess the region effect, validation of GSMaP_MVK in the eastern part and the western part was conducted. The western part locates in the Kumamoto, Saga and Fukuoka Prefectures while the eastern part locates in Kagoshima and Miyazaki. Moreover, Kumamomoto, Kagosima and Miyazaki were hit by flash flood in July 2006 and 2007. Table 5.4 shows the validation and correction result of GSMaP_MVK in the eastern part and the western part of the region. In the eastern part the bias, error, RMSE, and C_{NS} are -40.1%, -4.95 mm/day 21.37 mm/day and 0.52 while in the western part they are -55.07%, -7 mm/day, 24.73 mm/day and 0.4. These results indicate that the performance of satellite

product is better over the eastern part, with lower bias, error and RMSE and better consistency measurement for rainfall estimates. It was strongly influenced by the location of the mountain area which affected local wind directions, then influenced the rainfall pattern. According to Figure 5.6, the wind direction in the study area moves from west to east. The water vapor as a main source of precipitation was not distributed perfectly in the region because the mountain is located in the central area as a barrier for cloud distribution. As a result, the rainfall pattern will be different.

However, the result showed that both in the western part and the eastern part of Kyushu, GSMaP_MVK data has underestimated. Thus, a correction was needed. The results showed that the bias, error and RMSE in the western part of the region decreased significantly and the C_{NS} value increased. However, GAM did not give the significant impact for the eastern part of the region. It should be noted that GAM only worked in the western part of the region. The same statement can be concluded that, GAM can greatly correct the GSMaP_MVK data if the bias percentage is large (i.e., more than 55%). In contrast, the correlation coefficient did not change significantly among eastern part, western part, before and after correction. Additionally, detection probability, FAR and HSS also did not give the different result between the eastern part (81%, 18% and 68%) and western part (81%, 18% and 67%).

Table 5.4. Validation statistics over the eastern part and western part part before and after corrected by GAM

	Eastern part		Western part	
	GSMaP_MVK	Corrected by GAM	GSMaP_MVK	Corrected by GAM
Bias	-40.10%	45.23%	-55.07%	9.80%
Error	-4.95 mm/day	5.58 mm/day	-7 mm/day	1.24 mm/day
RMSE	21.37 mm/day	25.39 mm/day	24.73 mm/day	20.72 mm/day
C_{NS}	0.52	0.31	0.4	0.58
r	0.75	0.72	0.75	0.76
POD	81%	81%	81%	81%
FAR	18%	18%	18%	18%
HSS	68%	68%	67%	67%

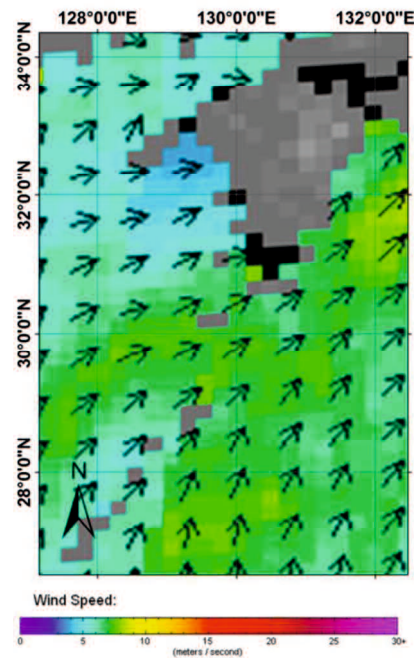


Figure 5.6 The wind direction of southern part of Japan in June 2006 (source: ASCAT, 2014)

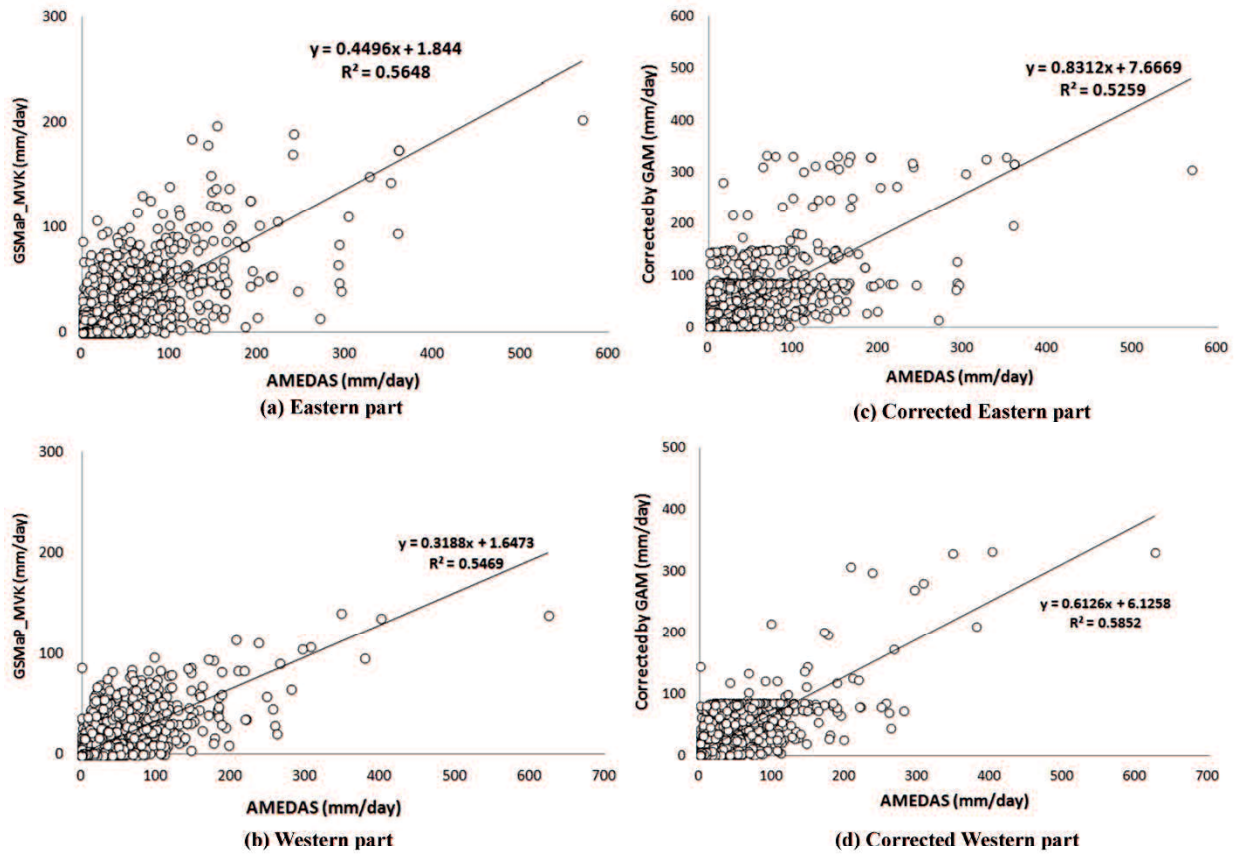


Figure 5.7 Comparison of the performance GSMaP_MVK in the Eastern part (a), western part (b), corrected Eastern part (c), corrected western part (d)

5.3.4 Validation and Correction of GSMaP MVK during rainy days

In this section we focused on the performance of GSMaP_MVK to detect rainfall amount during rainy days. So, non rainy days were excluded in this analysis, which reduced the total sample data from 9276 to 4779. This analysis is necessary because flood only occurs during rainy days. Figure 5.8 shows the scatter plot of AMEDAS data versus daily GSMaP_MVK and corrected GSMaP_MVK. Table 5.5 shows the validation statistic and bias correction of GSMaP_MVK. During rainy days, the bias, error, RMSE and C_{NS} of uncorrected GSMaP_MVK are -46.78% , -11.25 mm/day, 31.79 mm/day and 0.37 while the bias, error, RMSE and C_{NS} of corrected of GSMaP_MVK are 20.80% , 5 mm/day, 32.54 mm/day and 0.34 . These results indicate that validation of GSMaP_MVK tend to underestimate while the corrected ones indicate that GSMaP_MVK tend to overestimate. In

addition, RMSE of corrected GSMaP_MVK increased and correlation coefficient and C_{NS} value decreased. It indicates that GAM did not give a significant result for correction. It was probably because the underestimate bias value was less than 55%.

Table 5.5 Validation statistics during rainy days

	GSMaP_MVK	Corrected by GAM
Bias	-46.78%	20.80%
Error	-11.25mm/day	5 mm/day
RMSE	31.79 mm/day	32.54 mm/day
C_{NS}	0.37	0.34
r	0.69	0.67

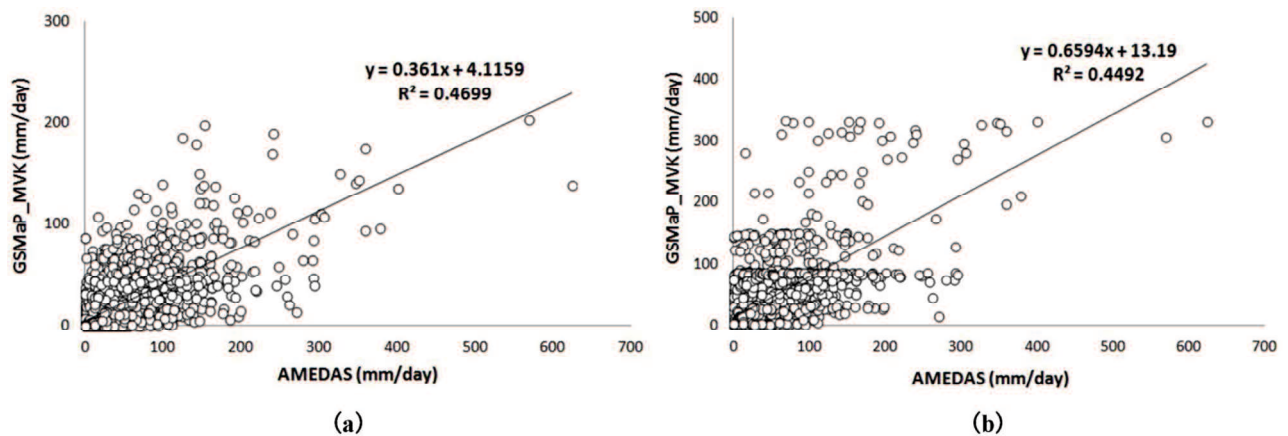


Figure 5.8 The performance of GSMaP_MVK during rainy days (a), corrected by GAM (b)

5.3.5 Validation and Correction of GSMaP MVK during heavy rainfall

Heavy rainfall is one of the important factors which trigger the occurrence of flash floods. Thus, predicting the amount of heavy rainfall by satellite precipitation, which close to rain gauge data is necessary. Here, heavy rain is defined as daily rainfall exceeding the 95th percentile (rain_P95) for all stations and all categories (Iwasaki, 2014). In addition, extreme rain is described as daily rainfall exceeding the 99th percentile (rain_P99) for all stations and all categories (Iwasaki, 2014). According to the definition, the heavy rains ranged equal and more than 66 mm/day ($n= 465$) and the extreme rainfalls ranged equal and more than 146 mm/day ($n= 95$). According to Dinku et al. (2009) and Kubota et al. (2009)

stated that GSMaP_MVK had serious underestimation when heavy rainfall occurred. Thus, validation and correction of GSMaP_MVK during heavy rainfall is a challenge.

Table 5.6 describes the validation and correction result of GSMaP_MVK during heavy rainfall. During heavy rainfall, the bias, error, RMSE and C_{NS} of uncorrected GSMaP_MVK are -59.5%, -70.3 mm/day, 90.6 mm/day and -0.98. Validation of uncorrected GSMaP_MVK results showed that the performance of satellite products was a serious underestimate because the bias was the highest compare from other categories. This is probably because sudden increase in rain rate did not reflect the IR brightness temperature in this time scale (Ushio et al., 2009). In this section, GAM and power function (Vernimmen et al., 2012) for bias correction were applied. We did both correction method and then compared. After GSMaP_MVK was corrected by power function, the bias, error, RMSE and C_{NS} are -63.2%, -63.1 mm/day, 85.6 mm/day and -0.77 while by GAM they are -8.8%, -10.44mm/day, 55.44 mm/day and 0.26, respectively. After correction, the bias, error and RMSE values decreased dramatically and the C_{NS} values increased of both correction methods. However, the GAM correction method gave the most significant result to reduce the error index. Moreover, when the values of C_{NS} is positive, the correcting of GSMaP_MVK indicates that almost accurate (i.e. $C_{NS} = 0$ means the models are accurate while C_{NS} one means the models are perfectly accurate) (Krause et al., 2005).

Because GAM approach gave the best result, Figures 5.9 and 5.10 only compare AMEDAS, GSMaP_MVK and corrected GSMaP_MVK by GAM. Figure 5.9 shows the heavy rainfall graphic of AMEDAS, GSMaP_MVK and corrected GSMaP_MVK by GAM. It described that the underestimate of GSMaP_MVK could be reduced almost in all points. Figure 5.10 shows the extreme rainfalls, which caused flooding in the Miyazaki, Kagoshima and Kumamoto in 2006 and in Kumamoto in 2007. In the extreme rainfalls the bias of

GSMaP_MVK is very large. On the other hand, the GAM can reduce the bias of GSMaP_MVK data.

Table 5.6 Validation statistics during heavy rainfall

	GSMaP_MVK	Corrected by power function	Corrected by GAM
Bias	-59.50%	-63.2%	-8.8%
Error	-70.3 mm/day	-63.1 mm/day	-10.44 mm/day
RMSE	90.6 mm/day	85.6 mm/day	55.44mm/day
C_{NS}	-0.98	-0.77	0.26
r	0.47	0.47	0.55

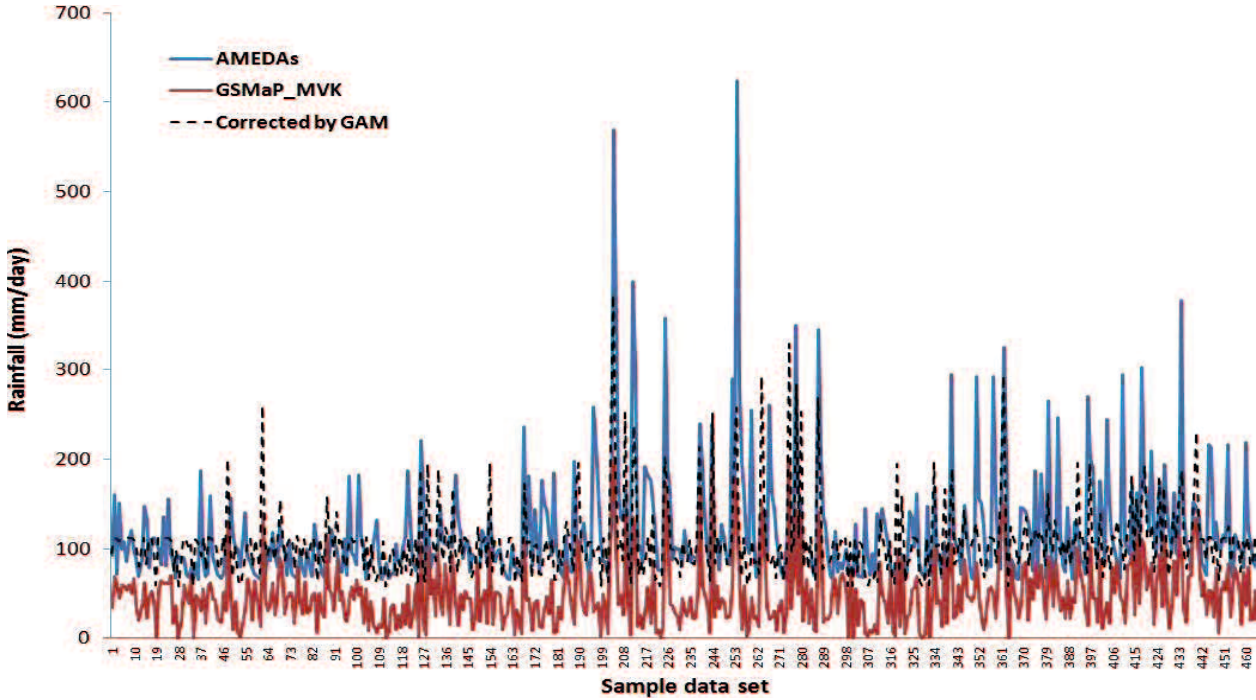


Figure 5.9 Heavy rainfall measurement by AMEDAS, GSMaP and corrected by GAM for three years.

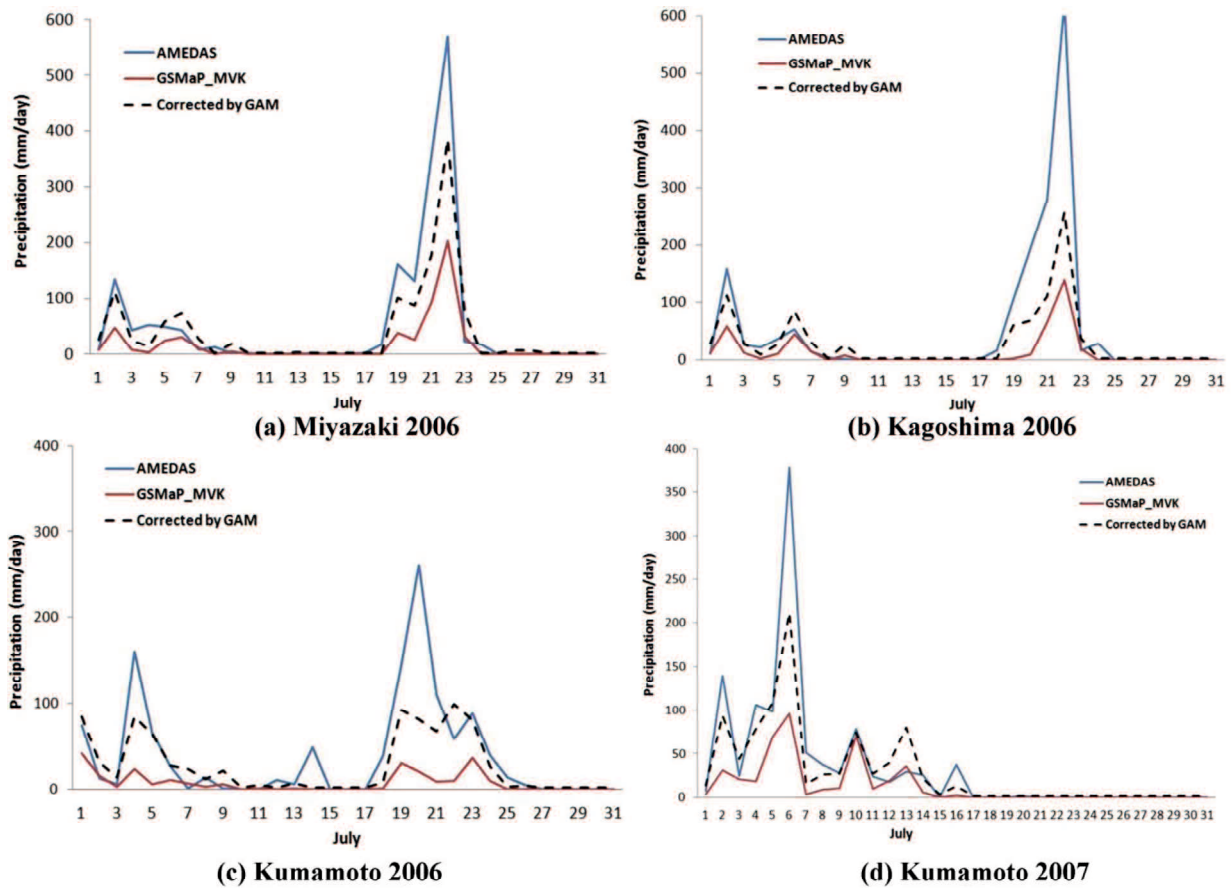


Figure 5.10 Extreme rainfall, which caused flood in Miyazaki 2006 (a), Kagoshima 2006 (b), Kumamoto 2006 (c), Kumamoto 2007 (d)

5.4 Conclusions

In this study, daily GSMaP_MKV rainfall estimates were compared with daily rain gauge measurements from AMEDAS. Data from 34 rain gauges in Kyushu Island, covering 3-year period (2005–2007), were used to evaluate daily rainfall pattern of GSMaP_MVK data. Point-by-point and spatial average analysis compared the closeness of GSMaP_MVK and rain gauge data using bias, error, RMSE, C_{NS} and correlation coefficients (r). In addition, GAM model have been applied to correcting the GSMaP_MVK data.

Intercomparison and correction were conducted between highland and lowland, between eastern part and western part, during rainy days and during heavy rainfall. From the analysis following are obtained as results;

- 1) Daily rainfall data from GSMaP_MVK has a great performance in lowland, eastern part of the study area and during the rainy days.
- 2) Daily rainfall data from GSMaP_MVK has serious underestimate in the highland, western part of the study area and during heavy rainfall.
- 3) GAM correction only can be applied when the bias percentage was more than 55 % of underestimate value. Therefore, it was well applied in the highland area, in the western part of Kyushu, and during heavy rainfall.

In addition, high bias was produced mostly due to heavy rainfall. This is probably due to topography effect. Consequently, to obtain better results, the quality of remote-sensing satellite data needs to be improved for better result in complex topography.

The quality of the satellite rainfall measurements needs to be evaluated continuously and averaged over several years to accurately reveal climatological features. In general, the data from GSMaP_MVK are potentially usable to replace rain gauge data, especially with the data over lowland area, if the inconsistencies and errors are taken into account. Thus GAM is promising way to predict the rainfall amount for flood and landslide monitoring, especially in the area where rain gauge data are limited.

CHAPTER 6

CONCLUSIONS

In this study, application of multi-sensor satellite data for open ocean tuna habitat and precipitation studies were demonstrated. The objectives of this study are to introduce the simple method to analyze the relationship between bigeye tuna and environmental variable by using scatterplot smoothers and empirical cumulative distribution function (ECDF), to introduce Generalized Additive Model (GAM) for dealing with nonlinear data, to determine the best model for bigeye tuna habitat in the study area, to evaluate the ability of GSMaP data as satellite precipitation during rainy season and to reduce the bias of GSMaP product during heavy rainfall. To assess all the research objective, integration of time series data, multi sensor analysis and statistical models were conducted.

In chapter 3, scatterplot smoother and empirical cumulative distribution function (ECDF) as statistical models were applied to determine the relationship between environmental variables and bigeye tuna abundance in the Southern waters off Java and Bali. By using scatter plot smoother, the trend of bigeye tuna related to each predictor variables can be distinguished and the almost variance of bigeye tuna in each predictor variables can be obtained. The result state that SST, SSC, and SSHD have strong correlation with the number of bigeye tuna. In addition, bigeye tuna has typical habitat of low SST, low SSC and low positive SSHD and extreme value of SSHD. By using ECDF, the optimum range of each variable can be determined, but how strong the relationship between the environmental variables and bigeye tuna can't be distinguished. By using ECDF method, simple predicted map of bigeye tuna habitat can be generated.

In the chapter 4, GAM as modern statistical methods were introduced to determine the habitat characteristic of bigeye tuna in the Southern waters off Java and Bali. This method is the next step of scatter smoothers method in the chapter 3. In addition, the same

data were used as in chapter 3. By using GAM, the relationship between environmental variables and bigeye tuna, the optimum range of each variable, the degree of influence of each variable can be determined without eliminating of the raw data. In addition, the typical habitat characteristic can be distinguished that are the spatial pattern of bigeye tuna habitat characteristic gave typical low SST, negative to low SSHD and extreme SSHD value and low SSC. In addition, SST was the most important habitat predictor for bigeye tuna migration in the study area, followed by SSHD and SSC

In the chapter 5, validation and correction of GSMaP_MVK product was conducted. For validation, the result stated that daily rainfall data from GSMaP_MVK has a great performance in lowland, eastern part of the study area and during the rainy days. To reduce the bias, GAM also applied in this chapter and by using this statistical method, it can reduce the bias of GSMaP_MVK in the highland, western part of the study area and during heavy rainfall. In addition, during heavy rainfall GAM can reduce GSMaP_MVK bias almost 80%. This research chapter is very important for the areas which do not have enough rain gauge data and for flood monitoring.

In this study, we have demonstrated that satellite remote sensing and GAM have made crucial contributions to our understanding for open ocean tuna habitat and precipitation studies. The advantage of this research is all the satellite remote sensing data which we used are open access and it can be applied in the developing countries. For the future research for tuna habitat, developing a method which measures the interaction of predictor variables to the fish catch data is necessary to develop. In precipitation studies, correction of GSMaP_MVK data product is the first step to make a model for flood prediction map more accurate.

ACKNOWLEDGEMENT

I would like to express my sincere gratitude to my supervisor Prof. Fusanori Miura for the continuous support of my doctoral study, for his patience, motivation, and immense knowledge.

I would like to thank the rest of my dissertation committee: Prof. Hideaki Nakamura, Prof. Masahiko Sekine, Prof. Tasuku Tanaka, Prof. Koji Asai and Assoc.Prof. Koichi Yamamoto, for their encouragement and insightful comments.

My sincere thanks also goes to Abd.Rahman Ass-syakur, M.Si, Dr. Eng Abu Bakar Sambah and Shota Makino, M. Eng for their expertise, comments and suggestions.

I would like to thank to Indonesia Endowment Fund of Ministry of Finance (LPDP) for financial support of my doctoral program in Yamaguchi University.

I also thank PT. Perikanan Nusantara, Bena, Bali, Indonesia for providing fisheries data and Japan Meteorological Agency (JMA) for providing rain gauge data. I also gratefully acknowledge NASA for the ocean color AQUA-MODIS SST and chlorophyll-a data that were downloaded from ocean-color homepage, Aviso for the use of altimetry data (SSH data sets) and Japan Aerospace and Exploration Agency (JAXA) for daily GSMaP_MVK data.

REFERENCES

- Abbott, M.R., Letelier, R.M., 1999. Chlorophyll fluorescence (MODIS product number 20). NASA Algorithm Theoretical Basis Document.
http://modis.gsfc.nasa.gov/data/atbd/atbd_mod22.pdf.
- Andrade, H.A., Garcia, C.A., 1999. Skipjack tuna fishery in relation to sea surface temperature off the southern Brazilian coast. *Fish Oceanogr.* 8, 245–254.
- Aonashi K., Shibata A., Liu G., 1996. An over ocean precipitation retrieval using SSM/I multichannel brightness temperature. *J. Appl. Meteor.* 74, 617-637.
- Aonashi, K., Awaka, J., Hirose, M., Kozu, T., Kubota, T., Liu, G., Shige, S., Siga, S., Seto, S., Takahashi, N., Takayabu, Y. N., 2009. GSMaP passive microwave precipitation retrieval algorithm: Algorithm description and validation. *J. Appl. Meteor.* 87A, 119-136.
- Arrizabalaga, H., Pereira J.G., Royer, F., Galuardi B., Goni N., Artetxe I., Arregi I., Lutcavage. *Fish Oceanogr.* 17, 74-83.
- As-syakur, A.R., Tanaka,T., Prasetia, R., Swardika, I.K., Kasa, I.W., 2011. Comparison of TRMM multisatellite precipitation analysis (TMPA) products and daily-monthly gauge data over Bali. *Int. J. Remote Sens.* 32 (24), 8969-8982.
- Austin, M.P., 1987. Models for the analysis of species response to environmental gradients. *Vegetatio.* 69, 35-45.
- Aviso., 1996. aviso user handbook merged topex/poseidon products (gdr-ms).
http://www.aviso.altimetry.fr/fileadmin/documents/data/tools/hdbk_tp_gdrm.pdf
- Bailey, C., Dwiponggo, A., Marahudin, F., 1987. Indonesia Marine Capture Fisheries. Manila: International Center for Living Aquatic Resources.

- Bertrand, A., Josse, E., Bach, P., Gros, P., and Dagorn, L., 2002. Hydrological and trophic characteristics of tuna habitat: consequences on tuna distribution and longline catchability. *Can. J. Fish. Aquat. Sci.* 59, 1002–1013.
- Blackburn, M., 1968. Micronekton of the eastern tropical Pacific Ocean: family composition, distribution, abundance and relation to tuna. *Fish. Bull. US.* 67,71–115.
- Brill, R.W., Dewar, H., Graham, J.B., 1994. Basic concepts relevant to heat transfers in fishes, and their use in measuring the psychological thermoregulatory abilities of tuna. *Environ. Biol. Fishes.* 40, 109-124.
- Brill, R.W., Bigelow, K.A., Musyl, M.K., Fritches, K.A., Warrant, E.J., 2005. Bigeye tuna (*Thunnus obesus*) behaviour and physiology and their relevance to stock assessments and fishery biology. *Collective Volume of Scientific Papers-ICCAT.* 57, 142–161.
- Brown, O.B., Minnet, P.J., 1999. MODIS infrared sea surface temperature algorithm algorithm theoretical basis document version 2.0.
http://modis.gsfc.nasa.gov/data/atbd/atbd_mod25.pdf
- Chai, F., Jiang, M., Barber, R.T., Dugdale, R.C., Chao, Y., 2003. Interdecadal variation of the transition zone chlorophyll front: A physical-biological model simulation between 1960 and 1990. *J. Oceanogr.* 59, 461–475.
- Chassot, E., Bonhommeau, S., Reygondeau, G., Nieto, K., Polovina, J., Huret, M., Dulvy, N.K., Demarcq, H., 2011. Satellite remote sensing for an ecosystem approach to fisheries management. *ICES J. Mar. Sci.* 68, 651–666.
- Chiu, L.S., Liu, Z., Vongsaard, J., Morain, S., Budge, A., Neville, P., Bales, C., 2006a. Comparison of TRMM and water district rain rate over New Mexico. *Adv. Atmos. Sci.* 23, 1–13.

- Chokngamwong, R., Chiu, L.S., 2006. TRMM and Thailand daily gauge rainfall comparison. In American Meteorology Society, Conference Proceedings in 86th AMS Annual Meeting, 29 January–2 February 2006, Atlanta, GA (Atlanta: American Meteorological Society), 11 pp.
- Dinku, T., Ruiz, F., Connor, S.J., Ceccato, P., 2009. Validation and intercomparison of satellite rainfall estimates over Colombia. *J. Appl. Meteorol Clim.* 49, 1004-1014.
- Druon, J.N., 2010. Habitat mapping of the Atlantic bluefin tuna derived from satellite data: Its potential as a tool for the sustainable management of pelagic fisheries. *Mar. Policy.* 34, 293–297.
- Druon, J.N., Fromentin, J.M., Aulanier, F., and Heikkonen, J., 2011. Potential feeding and spawning habitats of Atlantic bluefin tuna in the Mediterranean Sea. *Mar. Ecol. Prog.* 439, 223–240.
- Du, Y., Qu, T., and Meyers, G., 2008. Interannual Variability of Sea Surface Temperature off Java and Sumatra in a Global GCM. *J. Climate.* 21, 2451–2465.
- Esaias, W.E., Abbott, M.R., Barton, I., Brown, O.B., Campbell, J.W., Carder, K.L., Clark, D.K., Evans, R.H., Hoge, F.E., Gordon, H.R., Balch, W.R., Letelier, R., Minnett, P.J., 1998. An overview of MODIS capabilities for ocean science observations. *IEEE T. Geosci. Remote.* 36, 1250–1265.
- Farrar, T., Weller, R., 2003. Where the trade winds meet: air-sea coupling in the inter-tropical convergence zone. Maryland-USA: NOAA Research Archive of Spotlight Feature Articles, Office of Oceanic and Atmospheric Research "In the spotlight" internet article http://www.oar.noaa.gov/spotlite/archive/spot_pacs.html
- Feng, M., Wijffels, S., 2002. Intraseasonal variability in the South Equatorial Current of the east Indian Ocean. *J. Phys. Oceanogr.* 32, 265–277.

- Feng, M., McPhaden, M.J., Xie, S.P., Hafner, J., 2013. La Niña forces unprecedented Leeuwin Current warming in 2011. *Scientific reports*. 3, 1–9.
- Fonteneau, A, and P Pallarés., 2004. Tuna natural mortality as a function of their age: the bigeye tuna case. IOTC-2004- WPTT-INF02.
<http://www.iotc.org/English/meetings/wp/wpttcurrent.php>
- Froese, R., Pauly, D (Eds) ., 2007. FishBase. World Wide Web electronic publication.
Available at www.fishbase.org, version (02/2007). Viewed 29 March 2007.
- Feidas.H., Kokolatos2.G., Negri.A., Manyin.M., Chrysoulakis.N., Kamarianakis.Y., 2008. Validation of an infrared-based satellite algorithm to estimate accumulated rainfall over the Mediterranean basin. *Theor. Appl. Climatol*.
DOI 10.1007/s00704-007-0360-y
- Feidas. H., 2010. Validation of satellite rainfall products over Greece. *Theor Appl Climatol*. 99, 193–216.
- Fukami K., Shirashi Y., Inomata H., Ozawa G., 2010. Development of integrated flood analysis system (IFAS) using satellite-based rainfall products with a self-correction method, International centre for water hazard and risk management under auspices of UNESCO (ICHARM), Public Works Research Institute, Tsukuba, Japan.
- Ghent, D., Kaduk, J., Remedios, J., Balzter, H., 2011. Data assimilation into land surface models: The implications for climate feedbacks. *Int. J. Remote Sens*. 32, 617–632 .
- Gillet, R., 2013. Tuna for Tomorrow: Information on an Important Indian Ocean Fishery Resource. *Smart Fish Working Paper*. 11, 1–55.
- Guisan, A., Edwards Jr, C.T., Hastie, T., 2002. Generalized linear and generalized additive models in studies of species distributions: setting the scene. *Ecol. Model*. 157, 89–100.
- Gunn, J., Hampton, J., Evans, K., Clear, N., Patterson, T., Bigelow, K., Langley, A., Leroy, B., Williams, P., Miyabe, N., Sibert, J., Bestley, F., Hartmann, K., 2005. Migration and

- habitat preferences of bigeye tuna, *Thunnus obesus*, on the east coast of Australia – a project using archival and conventional tags to determine key uncertainties in the species stock structure, movement dynamics and CPUE trends. Canberra-Australia: Project no. 1999/109, CSIRO Marine Research.
- Hastie, T.J., Tibshirani, R.J., 1986. Generalized additive models. *Stat. Sci.* 1, 297-318.
- Hanamoto, E., 1987. Effect of Oceanographic Environment on Bigeye Tuna Distribution. *Bull. Jpn. Soc. Fish. Oceanogr.* 51, 203–216.
- Hendiarti, N., Siegel, H., Ohde, T., 2004. Investigation of different coastal processes in Indonesian waters using SeaWiFS data. *Deep Sea Res. Part. 2 Top Stud. Oceanogr.* 51, 85–97.
- Hendiarti, N., Suwarso, Aldrian, E., Amri, K., Andiaستی, R., Sachoemar, S.I., Wahyono, I.B., 2005. Seasonal Variation of Pelagic Fish Catch Around Java. *Oceanogr.* 18, 112–123.
- He, S., Mazumdar, S., Arena, V.C., 2006. A comparative study of the use of GAM and GLM in air pollution research. *Environmetrics.* 17, 81-93.
- Howell, E.A., Hawn, D.R., and Polovina, J.J., 2010. Spatiotemporal variability in Bigeye tuna (*Thunnus obesus*) dive behaviour in the Central North Pacific Ocean. *Prog. Oceanogr.* 86, 81–93.
- Hou, A.Y., Skofronick-jackson, G., Kummerow, C., Shepherd, M., 2008. Global precipitation measurement. In *Precipitation. Advances in Measurement, Estimation and Prediction*, S.C. Michaelides (Ed.), pp. 131–170 (Berlin: Springer-Verlag).
- Hosokawa, K., 1969. Distribution of Heavy Rainfall Frequency and its Seasonal Patterns in Tohoku District. *Annals of The Tohoku Geographical Association.* 7 (4), 204-207.
- ICCAT ., 2006a. Report of the Standing Committee on Research and Statistics (SCRS), Madrid, Spain, October 2 to 6, 2006.

- Available at <http://www.iccat.es/Documents/Meetings/Docs/PLE-014%20EN.pdf>
- IOCCG., 2014. MODIS – Aqua. <http://www.ioccg.org/sensors/aqua.html>. view acces 11 February 2015
- IOTC., 2006a. Report of the Ninth Session of the Scientific Committee, Victoria, Seychelles, 6-10 November 2006.
- Iwasaki, H., 2014. Increasing trends in heavy rain during the warm season in eastern Japan and its relation to moisture variation and topographic convergence. International journal of climatology.
- DOI: 10.1002/joc.4115
- Jerlov, N.G., 1976. Marine Optics. Amsterdam: Elsevier.
- Jiang S., Ren L., Yong B., Yang X., Shi L., 2010. Evaluation of high-resolution satellite precipitation products with surface rain gauge observations from Laohahe Basin in northern China. Water Sci. Eng. 3 (4), 405-417.
- Jones, M.R., Blenkinsop, S., Fowler, H.J., Sephenson, D.B., Kilsby, C.G., 2013. Generalized additive modelling of daily precipitation extremes and their climatic drivers. National Center for Atmospheric Research (NCAR) Technical Notes.
- <http://nldr.library.ucar.edu/collections/technotes/TECH-NOTE-000-000-000-868.pdf>
- Joseph, G., 2005. Fundamentals of remote sensing second edition. Himayatnagar: Universities Press (India).
- Joyce, R., Janowiak, J.E., Huffman, G.J., 2011. Latitudinally and seasonally dependent zenith angle correction for geostationary satellite IR brightness temperature. J. App.Meteo. 40, 689-703.
- Kobold, M. and M. Suselj. 2005. Precipitation forecast and their uncertainty as input into hydrological models. Hydrol. Earth Syst. Sci. 9(4): 322-332.

- Kachi, M., Kubota, T., Ushio, T., Shige, S., Kida, S., Aonashi, K., Oki, R., 2011. Development and Utilization of "JAXA Global Rainfall Watch" System based on Combined Microwave and Infrared Radiometers Aboard Satellites. *IEEJ Transactions on Fundamentals and Materials*. 131, 729-737.
- Karl, T. R. et al., 2010. Observation needs for climate information, prediction and application: Capabilities of existing and future observing systems. *Procedia Environ. Sci.* 1, 192–205.
- Kazama, S., Sato, A., Kawagoe, S., 2009. Evaluating the cost of flood damage based on changes in extreme rainfall in Japan. *Sustain Sci.* 4, 61–69.
- Kamei, G., Felix, J.F., Shenoy, L., Shukla, S.P., Devi, H.M., 2014. Application of Remote Sensing in Fisheries: Role of Potential Fishing Zone Advisories. In J. Sundaresan, K.M. Santosh, A. Déri, R. Roggema, and R. Singh (Eds.), *Geospatial Technologies and Climate Change*. 175–186. Amsterdam-Netherlands: Springer International Publishing.
- Kikawa, S and Ferraro, M.G., 1966, Maturation and spawning of tunas of Indian Ocean. *Proc. Indo-Pacific Fishery Council*. 12, 65-78.
- Kim, W. M., Yeh, S. W., Kim, J.H., Kug, J.S., Kwon, M.H., 2011, The unique 2009–2010 El Niño event: A fast phase transition of warm pool El Niño to La Niña. *Geophys Res. Lett.* 38, 1-5.
- Kitchell, J.F., Boggs, C.H., He, X., Walters, C., 1999. Keystone predators in the central Pacific. P. 665-683. In: *Ecosystem Approaches for Fisheries Management*. Alaska Sea Grant College Program. AK-SG- 99-01, 1999. 756 pp.
- Kirby, D.S., Fiksen, Ø., Hart, P.J.B., 2000. A dynamic optimization model for the behavior of tunas at ocean front. *Fish. Oceanogr.* 9, 317–325.

- Klemas, V., 2013. Fisheries applications of remote sensing: an overview. *Fish. Res.* 148, 124–136.
- Krause, P., Boyle, D.P., Base, F., 2005. Comparison of different efficiency criteria for hydrological model assessment. *Adv. Geosci.* 5, 89–97.
- Kubota, T., Shige, S., Hashizume, H., Aonashi, K., Takahashi, N., Seto, S., Takayabu, Y.N., Ushio, T., Nakagawa, K., Iwanami, K., Kachi, M., Okamoto, K., 2007. Global Precipitation Map Using Satellite-Borne Microwave Radiometers by the GSMaP Project: Production and Validation. *IEEE Trans. Geosci. Remote Sens.* 45(7), 2259–2275.
- Kubota T., Ushio T., Shige S., Kida S., Kachi M., Okamoto K., 2009, Verification of high resolution satellite-based rainfall estimates around Japan using a gauge calibrated ground radar data set. *J. Meteor. Soc. Japan.* (87A), 203-222.
- Lan, K.W., Lee, M.A., Lu, H.J., Shieh, W.J., Lin, W.K., Kao, S.C., 2011. Ocean variations associated with fishing conditions for yellowfin tuna (*Thunnus albacares*) in the equatorial Atlantic Ocean. *ICES J. Mar. Sci.* 68, 1063–1071.
- Laurs, R.M., 1986. Applications of satellite remote sensing to fisheries. *Society of Airborne and Satellite. J. Phys. Oceanogr.* 8, 139–150.
- Laurs, R.M., Fiedler, P.C., Montgomery, D.R., 1984. Albacore tuna catch distributions relative to environmental features observed from satellites. *Deep-Sea res.* 31, 1085–1099.
- Lee, T., Fukumori, I., Minemenlis, D., Xing, Z., Fu, L.L., 2001. Effects of the Indonesian Throughflow on the Pacific and Indian Oceans. *J. Phys. Oceanogr.* 32, 1404–1429.
- Lehodey, P., Bertignac, M., Hampton, J., Lewis, A., Picaut, J., 1997. El Nino Southern Oscillation and tuna in the western Pacific. *Nature.* 389, 715–718.

- Lehodey, P., Senina, I., Sibert, J., Bopp, L., Calmettes, B., Hampton, J., Murtugudd, R., 2010. Prog. Oceanogr. doi:10.1016/j.pocean.2010.04.021
- Lennert-Cody, C.E., Roberts, J.J., and Stephenson, R.J., 2008. Effects of gear characteristics on the presence of Bigeye tuna (*Thunnus obesus*) in the catches of the purse-seine fishery of the eastern Pacific Ocean. ICES J. Mar. Sci. 65, 970–978.
- Liepert, B. G., Previdi, M., 2009. Do models and observations disagree on the rainfall response to global warming? J. Clim. 22, 3156–3166.
- Liang, S., Li, X., Wang, J., 2012. Advanced Remote Sensing: Terrestrial Information Extraction and Applications. Academic Press first Edition.
- Liu, C.T., Nan, C.H., Ho, C.R., Kuo, N.K., Tsu, M.K., Tseng, R.S., 2004, Application of Satellite Remote Sensing on the Tuna Fishery of Eastern Tropical Pacific. Satellite Altimetry for Geodesy, Geophysics and Oceanography. International Association of Geodesy Symposia. 126, 175-182.
- Liu, C., Allan, R. P., 2012. Multisatellite observed responses of precipitation and its extremes to interannual climate variability. J. Geophys. Res. 117, D03101.
- Lizarazo, I., 2012. Quantitative land cover change analysis using fuzzy segmentation. Int. J. Appl. Earth Obs. Geoinf. 15, 16–27
- Lu, H-J., Lee, K-T., Lin, H-L., and Liao, C-H., 2001. Spatio-temporal distribution of yellowfin tuna *Thunnus albacares* and bigeye tuna *Thunnus obesus* in the Tropical Pacific Ocean in relation to large-scale temperature fluctuation during ENSO episodes. Fisheries Sci. 67, 1046–1052.
- Manessa, M.D.M., As-syakur, A.R., 2011. Observation of SST variability and their relationship with ENSO over Coral Triangle region using satellite data. Proceeding of the International Seminar on Marine: Implication of Climate Change in Coral Triangle

- Initiative (CTI) Region (pp. 199–212). Denpasar-Indonesia: Institute for Marine Research and Observation, Indonesian Ministry of Marine Affairs and Fisheries.
- Maritorena, S., d'Andon, O.H.F., Mangin, A., and Siegel, D.A., 2010. Merged satellite ocean color data products using a bio-optical model: Characteristics, benefits and issues. *Remote Sens. Environ.* 114, 1791–1804.
- Miyabe, Naozumi., 1993. A review of the biology and fisheries for bigeye tuna, *Thunnus obesus*, in the Pacific Ocean. *FAO Fisheries Technical Papers* 336. 2, 207-244.
- Mohri, M., 1999. Seasonal change in Bigeye tuna fishing areas in relation to the oceanographic parameters in the Indian Ocean. *Journal of National Fisheries University.* 47, 43–54.
- Mohri, M., and Nishida, T., 1999. Distribution of Bigeye tuna and its relationship to the environmental conditions in the Indian Ocean based on the Japanese longline fisheries information. *IOTC Proceedings.* 2, 207–220.
- Mugo, R., Saitoh, S-I., Nihira, A., Kuroyama, T., 2010. Habitat characteristics of skipjack tuna (*Katsuwonus pelamis*) in the Western North Pacific. *Fish. Oceanogr.* 19, 382–396.
- Morton, R., and Henderson, B.L., 2008, Estimation of nonlinear trends in water quality: An improved approach using generalized additive models. *Water Resour Res.* 44, W07420. doi:10.1029/2007wr006191.
- Mugo, R., Saitoh, S.-I., Nihira, A., Kuroyama, T., 2010. Habitat characteristics of skipjack tuna (*Katsuwonus pelamis*) in the Western North Pacific. *Fish. Oceanogr.* 19, 382–396.
- Miyake, M.P., Miyabe, N., Nakano, H., 2004. Historical trends of tuna catches in the world. *FAO Fisheries. Technical Paper* 467, FAO, Rome.
- Millis, C.E and Carlton, J.T., 1998. Diversity Rationale for a system of International Reserves for the open ocean. *Conserv. Biol.* 12, 244-247.

- MRAG Americas Inc., 2002. Review of Ecosystem-Bycatch Issues for the Western and Central Pacific Region. Prepared for the Western and Central Pacific Fisheries Commission, Manila, Philippines, November 18-22, 2002.
- Natih, M.N.N., Anditiya, J.L.G., Endiarso, N., 2010, Spatial distribution of bigeye tuna catches and sea surface chlorophyll concentration in the Indian Ocean (*in Indonesian*). in Indonesian National Seminar Fisheries. 2-3 December 2010, Jakarta, Indonesia. 25-31.
- National Oceanic and Atmospheric Administration (NOAA)., 2007. NOAA's Role in Space-Based Global Precipitation Estimation and Application. Committee on the Future of Rainfall Measuring Missions, National Research Council, 143 pp. Washington, D.C, The National Academic Press.
- Neill, W. H., Chang, R. K. C., and Dizon, A. E., 1976. Magnitude and ecological implications of thermal inertia in skipjack tuna. *Katsuwonus pelamis* (Linneaus). Environment Biology Fisheries. 1, 61–80.
- Nihira, A., 1996. Studies on the behavioral ecology and physiology of migratory fish schools of skipjack tuna (*Katsuwonus pelamis*) in the oceanic frontal area. Bulletin of Tohoku National Fisheries Research Institute. 58, 137–233.
- Ningsih, N.S., Rakhmaputeri, N., Harto, A.B., 2013. Upwelling variability along the southern coast of Bali and in Nusa Tenggara waters. Ocean Science Journal. 48, 49–57.
- Nishikawa, Y., Honma, M., Ueyanagi, S., Kikawa, S., 1985. Average distribution of larvae of oceanic species of scombroid fishes, 1956–1981. S series/Far Seas Fisheries Research Laboratory. 12, 99 p.
- Oceanic Fisheries Programme, Secretariat of the Pacific Community., 2006. Estimates of Annual Catches in the WCPFC Statistical Area. WCPFC Scientific Committee Second Regular session. 2-18 August, 2006, Manila, Philippines.

- Okamoto, K., Iguchi, T., Takahashi, N., Iwanami K., Ushio, T., 2005. The Global Satellite Mapping of Precipitation (GSMaP) project. In 25th IGARSS Proceedings, pp. 3414-3416.
- Okamoto, K., Iguchi, T., Takahashi, N., Ushio, T., Awaka, J., Shige, S., Kubota, T., 2007. High precision and high resolution global precipitation map from satellite data. ISAP 2007 Proceedings, 506-509.
- Oldham, R.S., Keeble, J., Swan M.J.S., Jeffcote M., 2000. Evaluating the suitability of habitat for the Great Crested Newt (*Triturus cristatus*). Herpetol J. 10, 143-155
- Osawa, T., and Julimantoro, S., 2010. Study of Fishery Ground Around Indonesia Archipelago Using Remote Sensing Data. In A. Sumi, K. Fukushi, and A. Hiramatsu (Eds.), Adaptation and Mitigation Strategies for Climate Change (pp. 57–69). Tokyo: Springer.
- Pauwels, V.R.N. and G.J.M. Lannoy. 2005. Improvement of Modeled Soil Wetness Conditions and Turbulent Fluxes through the Assimilation of Observed Discharge. J. Hydrometeor. 7:458-476.
- Perry, R.I. and Smith, S.J., 1994, Identifying habitat associations of the marine fishes using survey data: an application to the northwest Atlantic. Can. J. Fish. Aquat. Sci. 51, 589–602.
- Perez, J.C., Alvarez, M.A., Heikkonen, J., Guillen, J., and Barbas, T., 2013. The efficiency of using remote sensing for fisheries enforcement: Application to the Mediterranean bluefin tuna fishery. Fish. Res. 147, 24-31.
- Polacheck, T., 1991. Measures of effort in tuna longline fisheries: changes at the operational level. Fish. Res. 12, 75–87.

- Polovina, J.J., Howell, E.A., 2005. Ecosystem indicators derived from satellite remotely sensed oceanographic data for the North Pacific. *ICES J. Mar Sci.* 62, 319–327.
- Polovina, J.J., Howell, E., Kobayashi, D.R., Seki, M.P., 2001. The transition zone chlorophyll front, a dynamic global feature defining migration and forage habitat for marine resources. *Prog. Oceanogr.* 49, 469–483.
- Prasetia, R., As-syakur, A.R., Osawa, T., 2013. Validation of TRMM Precipitation Radar satellite data over Indonesian region. *Theor. Appl. Climato.* 112, 575–587.
- Proctor, C.H., Merta, I.G.S., Sondita, M.F.A., Wahuju, R.I., Davis, T.L.O., Gunn, J.S., Andamari, R., 2003. A review of Indonesia's Indian Ocean tuna fisheries. Jakarta-Indonesia: CSIRO Marine Research, Research Institute of Marine Fisheries, and Bogor Agricultural University.
- Qu, T., and Meyers, G., 2005. Seasonal Characteristics of Circulation in the Southeastern Tropical Indian Ocean. *J. Phys. Oceanogr.* 35, 255–267.
- Romaguera, M., Hoekstra, A. Y., Su, Z., Krol, M.S., Salama, M.S., 2010. Potential of using remote sensing techniques for global assessment of water footprint of crops. *Remote Sens.* 2, 1177-1196.
- Saha, S. et al., 2010. The NCEP climate forecast system reanalysis. *Bull. Am. Meteorol. Soc.* 91, 1015–1057 .
- Santos, A.M.P., 2000. Fisheries oceanography using satellite and airborne remote sensing methods: a review. *Fish. Res.* 49, 1–20.
- Scott, J.M., Heglund, P.J., Samson, F., Haufler, J., Morrison, M., Raphael, M., Wall, B., 2002. *Predicting Species Occurrences: Issues of Accuracy and Scale.* Island Press, Covelo, California.

- Setiawati, M.D., Miura, F., Aryastana, P., 2013. Verification of hourly GSMaP rainfall estimates during the flood events in kumamoto prefecture, Japan. 34th Asian Conference on Remote Sensing 2013, ACRS 2013, 7, pp 3542-3549.
- Setiawati, M.D., Sambah, A.B., Miura, F., Tanaka, T., Ass-syakur, A.A ., 2014. Characterization of bigeye tuna habitat in the Southern Waters off Java-Bali using remote sensing data. *Adv. Space Res.* 5, 732-746.
- Seto, S., 2009, An evaluation of overland rain rate estimates by the GSMaP and GPROF Algorithm: the role of lower frequency channels. *J. Meteor. Soc.* 87A, 183-202.
- Shrestha, M. S., Takara, K., Kubota, T., Bajracharya, S. R., 2011. Verification of GSMaP rainfall estimates over the central Himalayas. *J. Hydraul.* 67(4), I37-I42.
- Simorangkir, S., 2003. Status Perikanan Tuna Nasional. Paper presented to workshop: Lokakarya Pengkajian Stok Sumberdaya Ikan Nasional. Jakarta-Indonesia: Indonesian Ministry of Marine Affairs and Fisheries.
- Soman, M.K., Slingo, J., 1997. Sensitivity of the asian summer monsoon to aspects of sea surface temperature anomalies in the tropical pacific ocean. *Q. J. Roy. Meteor. Soc.* 123, 309-336.
- Song, L., Zhou, Y., 2010. Developing an integrated habitat index for bigeye tuna *Thunnus obesus* in the Indian Ocean based on longline fisheries data. *Fish. Res.* 105, 63-74.
- Song, L., Zhou, J., Zhou, Y., Nishida, T., Jiang, W., Wang, J., 2009. Environmental preferences of Bigeye tuna, *Thunnus obesus*, in the Indian Ocean: an application to a longline fishery. *Environ. Biol. Fishes.* 85, 153–171.
- Song, L., Zhang, Y., Xu, L., Jiang, W., Wang, J., 2008. Environmental preferences of longlining for yellowfin tuna (*Thunnus albacares*) in the tropical high seas of the Indian Ocean. *Fish Oceanogr.* 17, 239–253.

- Sprintall, J., Wijffels, S., Molcard, R., and Jaya, I., 2010. Direct evidence of the south java current system in ombai strait. *Dyn. Atmos. Oceans*. 50, 140–156.
- Store, R., Jokimaki, J., 2003. A GIS based multi-scale approach to habitat suitability modeling. *Ecol. Model.* 169, 1-15.
- Stretta, J.M. 1991. Forecasting models for tuna fishery with aerospatial remote sensing. *Int. J. Remote Sens.* 12, 771-779.
- Sund, P.N., Blackburn, M., William, F., 1981. Tunas and their environment in the Pacific Ocean: a review. *Oceanogr. Mar. Biol.* 19, 443–512.
- Sunoko, R., Huang, H.W., 2014. Indonesia tuna fisheries development and future strategy. *Mar. Policy.* 43, 174–183.
- Susanto, R.D., Gordon, A.I., Zheng, Q., 2001. Upwelling along the Coasts of Java and Sumatra and Its Relation to ENSO. *Geophys. Res. Lett.* 28, 1599-1602.
- Susanto, R.D., Moore II, T.S., and Marra, J., 2006. Ocean color variability in the Indonesian Seas during the SeaWiFS era. *Geochem. J. Geochemical Journal.* 7, Q05021.
- Swardika, I.K., Tanaka, T., and Ishida, H., 2012, Study on the characteristics of the Indonesian seas using satellite remote-sensing data for 1998–2007. *Int. J. Remote Sens.* 33, 2378–2394.
- Syamsuddin, M.L., Saitoh, S-I., Hirawake, T., Bachri, S., Harto, A.B., 2013. Effects of El Niño–Southern Oscillation events on catches of Bigeye Tuna (*Thunnus obesus*) in the eastern Indian Ocean of Java. *Fish Bull.* 111, 175–188.
- Takahasi, K., 1955. *Dynamic Climatology*. Iwanami. Tokyo. pp 316. (in Japanese)
- Tezuka, S., Takiguchi, H., Sato, A., Kawagoe, S., Sarukkalige, R., 2014. Estimation of the effects of climate change on flood-triggered economic losses in Japan. *IJDRR.* 9, 58-67.
- Trenberth, K., Hurrell, J., 1997. How accurate are satellite thermometers—Reply. *Nature.* 389, 342–343.

- Turner, W et al., 2015. Free and open-access satellite data are key to biodiversity conservation. *Biol. Cons.* 182, 173-176.
- Uda, M., 1973. Pulsative fluctuation of oceanic fronts in association with the tuna fishing grounds and fisheries. *J. Mar. Sci. Tech.* 7, 245–264.
- Underwood, F.M., 2009. Describing long-term trends in precipitation using generalized additive models. *J. Hydrol.* 364, 285–297. doi:10.1016/j.jhydrol.2008.11.003.
- Ushio T., Sasashige K., Kubota T., Shige S., Okamoto K., Aonashi K., et al., 2009. A Kalman filter approach to the global satellite mapping of precipitation (GSMaP) from combined passive microwave and Infrared radiometric data. *J. Meteor. Soc. Japan.* 87A, 137-151.
- Valavanis, V.D., Pierce, G.J., Zuur, A.F., Palialexis, A., Saveliev, A., Katara, I., and Wang, J., 2008. Modelling of essential fish habitat based on remote sensing, spatial analysis and GIS. *Hydrobiologia.* 612, 5–20.
- Von, V., Huang, S., 2005. The potential of multi-sensor satellite data for applications in environmental monitoring with special emphasis on land cover mapping, desertification monitoring and fire detection. Dissertation. Geo Bio center department. Ludwig-Maximilians University.
- Ward, P., Myers, R.A., 2004. Inferring the depth distribution of catchability for pelagic fishes and correcting for variations in the depth of longline fishing gear. *Can J Fish. Aquat. Sci.* 62, 1130-1142.
- WCPFC (2006a). Estimates of annual catches in the WCPFC statistical area. WCPFC-SC2-2006/ST IP-1. Paper presented to the Second Session of the Scientific Committee (WCPFC), 7-18 August 2006, Manila, Philippines.

- Werdell, P.J., Bailey, S.W., 2005. An improved bio-optical data set for ocean color algorithm development and satellite data product validation. *Rem. Sens. Environ.* 98, 122-140.
- Wilson, C., Morales, J., Nayak, S., Asanuma, I., and Feldman, G., 2008. Ocean-color radiometry and fisheries. In T. Platt, N. Hoepffner, V. Stuart and C. Brown (eds.), *Why Ocean Colour?* (pp. 47–58). Dartmouth-Canada: The Societal Benefits of Ocean-Color Technology. Reports of the International Ocean-Color Coordinating Group 7.
- Wood, S.M., 2006. *Generalized Additive Models, an Introduction with R*. London-UK: Chapman and Hall.
- WWF. 2007. With an eye to the future: addressing failures in the global management of Bigeye Tuna Traffic the wildlife trade monitoring network. http://www.trafficj.org/publication/07_with_an_eye_future.pdf
- Wyrtki, K., 1961. *Physical oceanography of the Southeast Asia waters*. California: NAGA REPORT 2.
- Xie, P., Arkin, P. A., 1995. An intercomparison of gauge observations and satellite estimates of monthly precipitation. *J. Appl. Meteor.* 34(5), 1143–1160.
- Yang, C., Yan, Z., Shao, Y., 2012. Probabilistic precipitation forecasting based on ensemble output using generalized additive models and Bayesian model averaging. *Acta Meteor. Sinica*, 26, 1-12.
- Yang, J., Gong, P., Fu, R., Zang, M., Chen, J., Laing, S., Xu, B., Shi, J., Dickson, R., 2013. The role of satellite remote sensing in climate change studies. *Nature Climate Change: Review Article*. DOI: 10.1038/NCLIMATE1908
- Yee, T.W., Mitchell, N.D., 1991. Generalized additive models in plant ecology. *J. Veg. Sci.* 2, 587-602.

- Yen, K.W., Lu, H.J., Chang, Y., Lee, M.A., 2012. Using remote-sensing data to detect habitat suitability for yellowfin tuna in the Western and Central Pacific Ocean. *Int. J. Remote Sens.* 33, 7507–7522.
- Zagaglia, C.R., Lorenzetti, J.A., Stech, J.L., 2004. Remote sensing data and longline catches of yellowfin tuna (*Thunnus alalunga*) in the Equatorial Atlantic. *Remote Sens. Environ.* 93, 267–281.
- Zainuddin, M., Kiyofuji, H., Saitoh, K., Saitoh, S-I., 2006. Using multi-sensor satellite remote sensing and catch data to detect ocean hot spots for albacore (*Thunnus alalunga*) in the northwestern North Pacific. *Deep-Sea Res. II.* 53, 419–431.
- Zainuddin, M., Saitoh, K., Saitoh, S-I., 2008. Albacore (*Thunnus alalunga*) fishing ground in relation to oceanographic condition in the Western North Pacific Ocean using remotely sensed satellite data. *Fish. Oceanogr.* 17, 61–73.